THE INFLUENCE OF PROCESSING PARAMETERS ON PIEZOELECTRIC AND DIELECTRIC PROPERTIES OF DOME-SHAPED PZT-EPOXY ACTUATORS

BY WANLIN DU

A thesis submitted to the

Graduate School-New Brunswick

Rutgers, The State University of New Jersey

in partial fulfillment of the requirements

for the degree of

Master of Science

Graduate Program in Mechanical & Aerospace Engineering

Written under the direction of

Kimberly Cook-Chennault

and approved by

New Brunswick, New Jersey

May, 2016

ABSTRACT OF THE THESIS

The influence of processing parameters on piezoelectric and dielectric properties of dome-shaped PZT-epoxy actuators

by

WANLIN DU

Thesis Director:

Professor Kimberly Cook-Chennault

Thick film dome-shaped two-phase (lead zirconate titanate ($Pb\left[Zr_xTi_{1-x}\right]O_3(0\leq x\leq 1)$)-Epoxy) structures have been fabricated using a modified sol-gel and spin-coat deposition process. Processing parameters and poling technique (Corona versus contact poling) were studied to elucidate their influences on piezoelectric and dielectric properties. 3 primary studies were carried out in the investigation. To study how time/speed profiles in spin-coating process influence the dielectric and piezoelectric properties of the samples, 4 different time/speed profiles built up form original profile were tested. Poling conditions, such as corona poling and contact poling were studied at the same material structure and compositions. Different poling voltages (45kv/mm and 70kv/mm) with corona poling techniques at low volume fractions of PZT (i.e. 0.1~0.3) were studied on samples fabricated with same techniques to investigate the influences of poling voltage. The combinations of depositing technique and viscosity were studied at low volume fractions such as 0.35 volume fraction of PZT to address the uniformity issue in thickness at lower volume fractions. The piezoelectric strain coefficient d_{33} for this dome structure was 9 times

higher than that previously reported values for a composite PZT-epoxy dome structure of similar structure and composition. The sample morphology was examined with the aid of scanning electron microscopy (SEM) images and the material distribution was studied by energy dispersive x-ray spectroscopy (EDS). The piezoelectric strain coefficients, capacitance and effective dielectric constant increased with increasing PZT content. Samples of all volume fractions of PZT (i.e. 0.1~0.7) that were Corona poled allowed for higher poling voltages (45 kV/mm compared to 2.5kv/mm in contact poling), and exhibited higher values of piezoelectric strain coefficients with same material composition , longitudinal piezoelectric coefficient (@110Hz), effective dielectric constant (@2kHz), and dielectric loss (@2kHz), were 11.1 pC/N, 28.7 and 0.004 respectively for the PZT volume fraction equal to 0.7.. The piezoelectric properties were examined both in terms of piezoelectric effect and converse piezoelectric effect. Piezoelectric strain coefficients and capacitance were measured @110Hz by Piezometer, and displacement of certain volume fractions of PZT were studied by Keyence interferometer. To better examine the polarization-electric field relation, P-E hysteresis loop were measured. Other dielectric properties such as conductance, resistance, and impedance spectrum verse increasing frequency were obtained by Hp impedance analyzer within the frequency range from 2kHz to 20Mhz. Investigation of composite structures such as these may lead to development of actuators with enhanced displacement and sensors with better sensitivity.

Acknowledgement

First of all I want to show my appreciation to my advisor Prof. Kimberly Cook-Chennault, she has been continuously supportive for my research and my personal improvement as well since the first day I joined the research family. She provides invaluable insights and inspiriting point of view when I experienced research difficulties. Without her guidance and persistent help, this thesis would not have been possible.

Besides my advisor I would like to thank my committee members, Prof. Alberto Cuitino and Prof. Shahab Zadeh for their encouragement, time and helpful insight towards my research work.

I would like to thank the formal and present members of HESML, Sankha Banerjee, Udhay Sundar, Andrew Tang, Rui Wang, Eric Bickford and under graduate James Palmer, Niasia Williams, Jordan Hoyt (summer intern) for their support and help. Especially, I want to thank Sankha Barnerjee, as he has been my mentor not only in the research but also my graduate students life and career. Also I want to thank Udhay Sundar, for being so helpful and supportive during these years in research.

Lastly, I want to thank my parents as they have been incredibly patient and supportive, they have always put my happiness on their minds. I would like to thank and show great appreciation to my husband Wenjie, who has been with me for up and downs, good and bad times. He has been so caring and patient, and motivated me gently in my research.

Wanlin du

Rutgers University

May 2016

Table of Contents

Abstract of the thesis ..... **ii**

Acknowledgement ..... **iv**

List of Figures ..... **viii**

List of Tables ..... **xii**

1. Introduction **1**

1.1 Background 1

1.2 Research Goals and Hypotheses 3

1.3 Research Materials and Methodology 4

1.4 Overview of the organization of the thesis 5

2. Definitions, Fundamental Concepts and Literature Review **6**

2.1 Dielectric Materials 6

2.2 Polarization 8

2.3 Piezoelectric material 13

2.4 Ferroelectrics 19

2.5 Polarization Techniques 24

2.5.1 Parallel Plate Contact Poling 24

2.5.2 Corona Poling 25

2.6 Composite Materials 26

2.7 Spin-coating process 31

2.8 Literature review 32

2.8.1 Composite piezoelectric materials 32

2.8.2 Curved/Dome shaped piezoelectric devices 36

3. Methodology 43

3.1 Chapter Organization 43

3.2 Materials 44

3.3 Original and Modified Methodology 44

3.4 Piezoelectric and Dielectric Characterization 48

3.5 Characterization of Surface Morphology and Particle Distribution 50

3.6 Spin-Speed/Time Profile Study 50

3.7 Deposition technique Study 51

3.8 Device displacement 56

3.9 P-E hysteresis 57

4. Results and Discussion 58

4.1 Chapter Organization 58

4.2 Epoxy Dome Device 58

4.3 PZT-Epoxy Dome Results for Optimized Fabrication Method 61

4.4 Spin-speed/time profile study 77

4.5 Deposion technique study 78

4.6 Summary of the Optimized Processing Conditions 81

4.7 Displacement measurement 82

4.8 P-E Hysteresis loop. 83

5. Conclusions and Future work 85

5.1 Conclusions 85

5.2 Future work 87

References **88**

List of Figures

Figure 2.1: (A) Normal state of dielectric material, the dipoles are randomly oriented. (B) Under the influence of external electric field, the dipoles are aligned. 6

Figure 2.2: (A) Example for non-polar dielectrics, no permanent dipole moments possessed. (B) Example for polar dielectrics, permanent dipole moments are randomly oriented. 7

Figure 2.3: Schematic of a dipole pair that is comprised of a positive and negative charged centers..... 8

Figure 2.4: Mechanisms of electronic polarization. In (A) there is no external electric field applied. Thus, there is no permanent dipole moment. In (B) an external electric field is applied, and dipole moments are induced, which results in the alignment of the dipoles within the material. 9

Figure 2.5: Mechanism of ionic polarization: (A) Without the presence of the external electric field, positive and negative's gravity center are coincident, there is no permanent dipole moments. (B) With the externally applied electric field, gravity centers of positive and negative charges are separated; dipole moments are induced and aligned. 10

Figure 2.6: Mechanism of orientation polarization: (A) Permanent dipole moments are facing different directions, over all polarization is zero. (B) With the externally applied electric field, permanent dipole moments are aligned. 10

Figure 2.7: Mechanism of space charge polarization: (A) Without external electric field, the ions are mixed up. (B) At the presence of external electric field, the ions could travel larger distance inside the material..... 11

Figure 2.8: Real part and imaginary part of relative complex permittivity 12

Figure 2.9: Polarization induced by mechanical stress. (A) Without applying the mechanical stress, positive and negative charge centers are in coincidence. (B) After the mechanical stress is applied, the dipole moment is induced. 14

Figure 2.10: Schematic representation of piezoelectric and converse piezoelectric effect. (A) The material after polarization, the polarization direction sis shown in the figure. (B)&(C) explain piezoelectric effect: the polarized material is under stress, and produces voltage. (D)&(E) denotes converse piezoelectric effect, when polarized material is subjected to external electric field the strains are induced**[9]**. 15

Figure 2.11: Illustration of d_{33} measurement. (A)Polarized sample (B) The measurement of d_{33}, the measurement tube would apply the vibration and take the voltage reading at the same time. 18

Figure 2.12: Illustration of d_{31} measurement 18

Figure 2.13: P-E relation of normal dielectrics 20

Figure: 2.14 Hysteresis loop pf ferroelectrics[46] 20

Figure 2.15: Hysteresis loop of ferroelectrics with original polarizing path**[57]** 22

Figure 2.16: Tetragonal perovskite structure below Curie temperature**[9]**..... 23

Figure 2.17: Cubic perovskite structures above Curie temperature**[9]** 23

Figure 2.18: Sketch of conventional contact poling set-up..... 25

Figure 2.19: Sketch of corona poling set-up 26

Figure 2.20: Here shows 10 connectivity pattern families, especially in {0-1}, {0-2}, {0-3}, {1-2},{1-3} and {2-3} families, each of them include 2 connectivity patterns, which makes total number of connectivity pattern16[60]. 28

Figure 2.21: Schematics of typical piezoelectric ceramic composite structures **[23]**..... 29

Figure 2.22: Scheme of spin coating technique 32

Figure 3.1: Overview of the original method used from our previous work. Appropriate amounts of PZT, DEGBA and ethanol were measured and mixed with the aid of a sonicator for 1 hour in the presence of air. The DEGBA binder was then added and the subsequent mixture was sonicated for an additional 30 minutes. The final mixture was spin-coated onto dome shaped substrate and cured at 75C. Samples were subsequently Parallel-Plate Contact poled at~2.2kV/mm [31]..... 46

Figure 3.2: Overview of the method of fabrication used for this work. The appropriate amounts of PZT, DEGBA and ethanol were weighed and then mixed via a sonicator for 2 hours in the presence of air. The mixture was subsequently dessicated for 4 hours to eliminate air bubbles. The mixture was sonicated for an additional hour. The binder was then added to the mixture and sonicated again, for an additional 30 mins. The final mixture is spined coated onto dome-shaped stainless steel substrate, and cured at 75C. Samples were poled via corona discharge. 47

Figure 3.3: The dimensions for the dome shape mold. 47

Figure 3.4: The thickness measurement was taken at five different places, and averaged. 48

Figure 3.5: Speed/Time profiles studied. The datum process has step intervals has 100, 200, 500, 800 rpm for 5s each for both increasing and decreasing process, and the process was held at 1000 rpm for 3mins. Profile 1 followed the similar fashion with the datum except using step intervals of 200, 400, 600, 800 and 1000rpm to maintain the equal spaced speed increment. The holding time is 10s each for 200, 400, 600, 800rpm at both ascending and descending process, and is 140s at 1000rpm. The profile 2 uses the same

speed steps and the descending process as profile 1, but the time held for 200, 400, 600, 800 rpm are 20s each in increasing steps. In this profile, holding time at 1000rpm is 100s. In profile 3 is built on profile 2 by extending the holding time at 800rpm to 1min, and reducing the holding time for 1000rpm to 1min. The profile 4 is built on profile 2 by eliminating the speed step 1000rpm, the top speed in this profile is 800rpm, and is hold for 130s. 51

Figure 3.6: Overview of the deposition layer and sol viscosity study. All of the processes described in this figure incorporated Speed/Interval Profile 3 for the "Deposition" step. Three viscosity settings were used in this study: 150 mPas, 248.7 mPas and 299 mPas. 54

Figure 3.7: Displacement testing set-up..... 56

Figure 4.1: Dielectric constant/loss vs frequency of epoxy single phase samples, the spectrum was measured with small aluminum tape..... 59

Figure 4.2: Conductivity vs frequency of epoxy single phase samples, the spectrum was measured with small aluminum tape..... 59

Figure 4.3: Resistance vs frequency of epoxy single phase samples, the spectrum was measured with small aluminum tape..... 60

Figure 4.4: Impedance/Phase vs frequency of epoxy single phase samples, the spectrum was measured with small aluminum tape. 60

Figure 4.5: Piezoelectric longitudinal coefficient d33 values of this work (without top electrode), this work (with silver paste as top electrodes), previous work, and predicted values by Furukawa are plotted. The d33 values presented in this work, have been 62

Figure 4.6: Piezoelectric coefficient -d31 values of this work and previous work. The samples from previous work were contact poled, and the samples from this work were corona charges poled at 45kv/mm. There was no electrode applied in both cases..... 64

Figure 4.7: Dielectric constant of present work, previous work and predicted values by Furukawa. No electrodes applied in both cases. 64

Figure 4.8: Longitudinal piezoelectric coefficient d_{33} and transverse piezoelectric coefficient d_{31} of previous work, this work (corona poled at 70kv/mm), this work (corona poled at 45kv/mm) and predicted values from Furukawa(only for d_{33}). 66

Figure 4.9: The dielectric spectroscopy (2kHz-20MHz) of previous work and this work, the spectrums were obtained with small triangular aluminum tape as top electrode in both cases. 68

Figure 4.10: Dissipation factor verse frequency (2kHz-20MHz) of previous work and this work, the spectrums were obtained with small triangular aluminum tape as top electrode for both cases. 70

Figure 4.11: Normalized impedance verse frequency (2kHz-20MHz) of previous work and this work, the spectrums were obtained with small triangular aluminum tape as top electrode for both cases. 72

Figure 4.12: Phase verse frequency (2kHz-20MHz) of previous work and this work, the spectrums were obtained with small triangular aluminum tape as top electrode for both cases. 73

Figure 4.13: Resistivity verse frequency (2kHz-20MHz), these samples are fabricated with updated method; the spectrums were obtained with small triangular aluminum tape as top electrode. 74

Figure 4.14: Conductivity verse frequency (2kHz-20MHz), these samples are fabricated with updated method; the spectrums were obtained with small triangular aluminum tape as top electrode. 75

Figure 4.15: Surface of PZT (0.5)-Epoxy 0-3 dome shape structure..... 75

Figure 4.16: Surface of PZT (0.6)-Epoxy 0-3 dome shape structure..... 76

Figure 4.17: EDS images of PZT(0.5)-Epoxy 0-3 dome shape structure. A) SEM images with distribution of Pt, Zr and Ti. B) Distribution of Pb. C) Distribution of Zr. D distribution of Ti. 76

Figure 4.18: EDS images of PZT (0.6)-Epoxy 0-3 dome shape structure. A) SEM images with distribution of Pt, Zr and Ti. B) Distribution of Pb. C) Distribution of Zr. D distribution of Ti. 77

Figure 4.19: Displacement data of 0.5 volume fraction of PZT 82

Figure 4.20: Displacement data of 0.6 volume fraction of PZT. 83

Figure 4.21: Hysteresis loop of PZT(0.5)-Epoxy dome shape structure under 53.9kv/cm.(thickness 0.139mm)..... 84

Figure 4.22: Hysteresis loop of PZT(0.6)-Epoxy dome shape structure under 58.48kv/cm.(thickness 0.188mm)..... 84

List of Tables

Table 2.1 Index transformation 17

Table 2.2 Fabrication techniques of composite thin films 34

Table 2.3: Fabrication techniques and performances of dome-shaped piezoelectric devices 38

Table 3.1: Physical, dielectric and piezoelectric properties of the materials used in the fabrication of piezoelectric dome shaped structures. The values for the PZT are for bulk PZT as published by APC International. The values for the DEGBA were determined from an epoxy dome structure Fabricated using the same steps as defined herein with 0% PZT. 44

Table 4.1 Measurement of viscosity 61

Table 4.2 Comparison between corona poled and contact poled data in 70% PZT 65

Table 4.3 Spin-speed/time profile study 78

Table 4.4 Deposition techniques study's results 79

Chapter 1

Introduction

1.1 Background

Piezoelectric materials generate electric charges when they are subjected to mechanical stress and vice versa [1-3]. Piezoelectric ceramics are widely employed as sensors and actuators because of their ideal electromechanical properties [4-8]. Homogenous ceramic piezoelectric actuators are typically simple in structure and design (disks, rings, plates and cylinders [9]) and are highly reliable with cycle lives that can range from 10^3 to 10^6 [6, 10-12]; render large actuation forces (dynamic force = 128 N @ 120 Volts and static force = 275N to 375N @100 Volts[13]) and high sensitivity ($-1.3\cdot10^{-4}$ to $-1.3\cdot10^{-3}$ $m^2\cdot kg^{-1}\cdot\lambda^{-1}$[14]) rapid response times (response times can range from 5μsec to 50μsec [15]); and consume low power during operation (power ranges 100 μW to 500 mW [16-18]) [8]. Despite these advantages, piezoelectric ceramics are brittle in nature (ultimate strength < 100 MPa [19, 20]) and have low fracture toughness ($0.5\sim2.0 MPa\cdot\sqrt{m}$)[19]. The intrinsic material characteristics limit their operational strains (lead zirconate titanate (PZT)~0.1% at 10kV/cm [4]), operational loading frequency, cycle life and compatibility to applications that require complex shapes. These poor mechanical properties limit their effective and efficient application to devices such as; hydrophones[21, 22], static and vibration based energy harvesting devices[23-25], surgical tactile sensors [8, 26, 27] and synthetic jet actuators[28]. Devices such as these are typically fabricated into complex shapes and structures for enhanced sensitivity, long cycle life reliability and increased displacement and loading. Piezoelectric polymers, such as

polyvinylidene fluoride (PVDF) are flexible, lightweight and have low acoustic and mechanical impedance, but suffer from low piezoelectric properties (d_{31}~6-28 pC/N) [29, 30]. Hence, researchers have begun to investigate piezoelectric composite materials.

Composite piezoelectric materials (CPM), such as 0-3 piezoelectric composites are a category of CPM that has been extensively studied ([3, 31]). Piezoelectric composites with 0-3 connectivity are fabricated so that active piezoelectric filler particles are uniformly distributed within a matrix, where the matrix is self-connected throughout the material while the piezoelectric particles are not self-connected throughout the material. Piezoelectric composites are of interest for many reasons. They offer improved mechanical strength and toughness. For example, P(VDFTrFE)/Ca-modified PbTiO3 composite with 50% volume fraction of ceramic has an elastic stiffness coefficient, $C_{33}^{D}$of a 34.5-40.8 GPa @ 20 MHz [32] juxtapose to PZT whose elastic stiffness is 13.6 GPa [33]. Piezoelectric composites can also be fabricated to have high hydrostatic performance); can offer better electromechanical coupling with host structures; can be less difficult to fabricate and are compatible to mass production techniques.

Over the past decade interest in the dome and curved shaped piezoelectric devices has increased because these structures demonstrate higher deformation (PZT~25.3% at 2.54kv/cm [34]) and electromechanical conversion accuracy (mechanical coupling factor, PZT-5A, K_{eff}~38%[35]) in comparison to planar actuators [36-39]. These materials are typically used in transducers[37, 40], hydrophones[21, 22], actuators[5, 27, 31, 36, 41-48] and sensors[49], but are limited in their functionality and performance due to the electrical/mechanical properties of the materials used. Also, the control of dome height during the manufacture of the structure remains a challenge because most methods em-

ploy the thermal mismatch effect to induce dome shape, which requires more expensive processing parameters, e.g. high temperatures [43, 50, 51] and vacuum [50] .

1.2 Research Goals and Hypotheses

In this work, dome-shaped 0-3 piezoelectric composites comprised of lead zirconate titanate ($Pb(Zr_xTi_{1-x})O_3$ ($0 \leq x \leq 1$)) and epoxy (PZT volume fraction ranged from 0.1 to 0.7) were fabricated using a combination mix, spin coat and cast method. The influences of the viscosity (composite mixture before the spin coat process), the spin-coating time/speed profiles and poling voltage, on the effective composite piezoelectric and dielectric properties, were investigated. This work builds upon the prior work of Banerjee *et al.* and Wei [31], where piezoelectric dome composites were fabricated and analyzed. These devices suffered from the high agglomeration of PZT particles, ununiformed surface morphology and a density of air bubbles which resulted in low piezoelectric coefficients and dielectric properties. The goal of this work was to isolate specific processing parameters that would enhance the piezoelectric and dielectric properties of the dome-shaped structures to make the devices more amenable to actuator applications.

Three research hypotheses were developed to address some of the challenges of the previous devices. The first hypothesis is that the spin speed and the length of time of the coating intervals influenced the dielectric and piezoelectric properties of the composites and that changes in the deposition process time intervals and speed would render different values of dielectric and piezoelectric properties. To test this hypothesis, samples deposited by four separated time/speed profiles, were fabricated and analyzed. This study was done on samples that had 0.50 volume fraction of PZT. The second hypothesis is that the composite dome structures will render higher piezoelectric properties if a Co-

rona polarization process were implemented instead of a contact parallel-plate process. The third hypothesis is that composite gels that there were within an optimal viscosity range prior to deposition would lead to films of uniform thickness and films with higher longitudinal piezoelectric strain values.

1.3 Research Materials and Methodology

The materials of interest are PZT-epoxy composites, where the volume fraction of PZT was varied from 0% to 70% (increments of 10% for each volume fraction). The materials used in the original study and this work were maintained. The lead zirconate titanate used is called PZT – 855 and the two-part epoxy is DGEBA, EpofixTM Cold-setting embedding Resin (purchased from APC International and Electron Microscopy Sciences, respectively).

The samples are fabricated using a combination of sol-gel and spin-coat deposition process where devices were polarized using contact and corona methods. The piezoelectric strain coefficients d_{33} and d_{31} were measured with a Piezo-meter @ 110Hz. The electrically induced displacement was measured by KEYENCE LG-10 interferometer. The dielectric impedance, phase angle, capacitance, conductance, resistance and dielectric loss ($tan\ \delta$) were measured as a function of frequency (2kHz to 20 MHz) on samples that used aluminum tape as the top electrode. The dielectric constant, conductivity and resistivity were calculated from the capacitance, conductance, resistance and geometry of the samples, respectively. The P-E hysteresis loops of PZT-Epoxy 0-3 two-phase dome shaped piezoelectric structure were measured under 750kv and 1000kv by Precision Ferroelectric Tester from Radiant technology Inc. The surface morphology and par-

ticle distribution were examined with the aid of Zeiss Sigma Field Emission Scanning Electron Microscope(SEM) and Energy Dispersive X-Ray Spectroscopy(EDS).

1.4 Overview of the organization of the thesis

This thesis is organized in the following manner. In chapter 1, the research goals and hypotheses are introduced. In Chapter 2, basic definitions for dielectric, piezoelectric and ferroelectric materials, polarization and composite connectivity are provided. In addition, a comprehensive review of the state of the art in the literature on piezoelectric thin films and piezoelectric dome/curved structures is presented in Chapter 2. In Chapter 3, the experimental methodology for fabrication of the devices and the analyses are presented. In particular, studies that examine the influence of the time/speed profiles of spin-coating, polarization technique and viscosity are presented. In Chapter 4, the results of the studies are presented along with an interrogation and discussion of the mechanisms leading to the results. Finally in Chapter 5, the conclusions of the thesis are presented.

Chapter 2

Definitions, Fundamental Concepts and Literature Review

2.1 Dielectric Materials

Dielectric materials are a type of electrical insulator, where when an external electric field is applied the positive and negative charge centers separate. Under the influence of an external electric potential, the positive charges are attracted to the surface with lower electric potential, and the negative charges are attracted to the surface with higher electric potential. The charges accumulate on the surfaces of dielectric material to resist the external electric field, which results in the alignment of the material dipoles in the direction of the applied electric field.

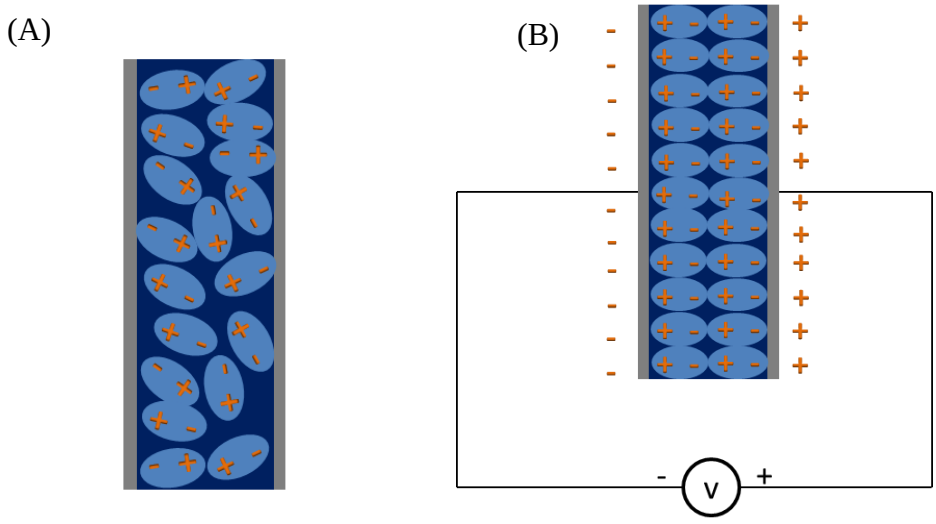

Figure 2.1: (A) Normal state of dielectric material, the dipoles are randomly oriented. (B) Under the influence of external electric field, the dipoles are aligned.

Dielectric materials can be divided into two major groups [52]: Polar and Non-polar dielectrics. Polar dielectrics, such as NH_3, HCl and H_2O are composed of two or more atoms

that have separated positive and negative charge centers. Dielectric polar molecules have permanent polarizations. Without the presence of an electric field, these dipoles are oriented randomly, so even though they possess permanent dipole moments - the overall polarization of the material is zero. The dipoles can be reoriented into a specific direction with the application of an external electric field. Non-polar dielectrics, such as H_2 and O_2, have coincidental positive and negative charge centers, and therefore do not possess a permanent dipole moment. A dipole moment can be induced in non-polar dielectrics, with the application of an external electric field, i.e. the separation of the positive and negative charge centers with the application of an external electric force. Polar and non-polar dielectrics such as HCl and H_2 are shown in Figure 2.2.

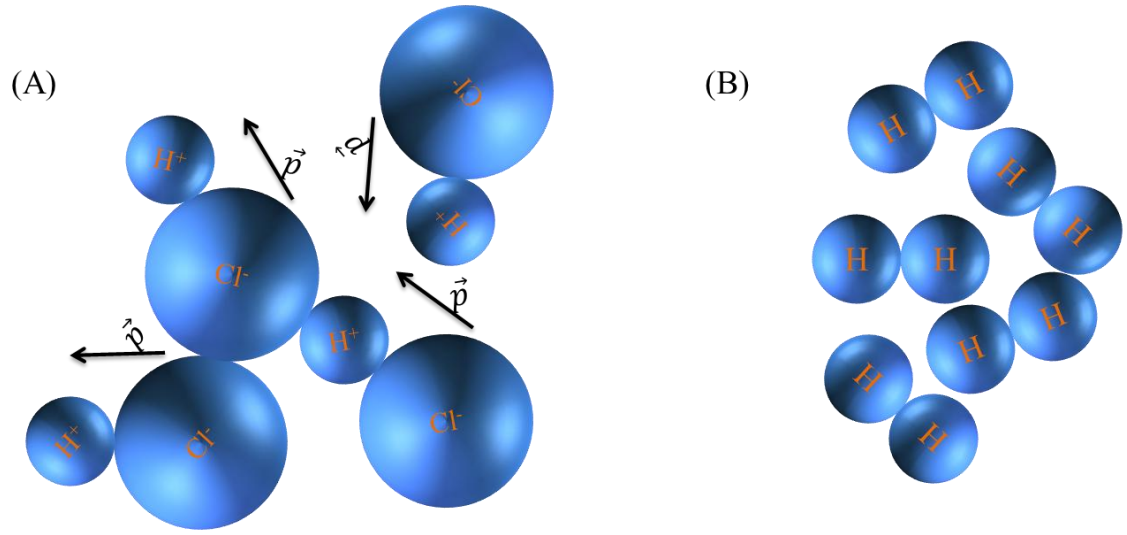

Figure 2.2: (A) Example for non-polar dielectrics, no permanent dipole moments possessed. (B) Example for polar dielectrics, permanent dipole moments are randomly oriented.

2.2 Polarization

Polarization describes the density of permanent or induced electric dipole moments within a material and is expressed as a vector that points in the direction of the alignment of the dipoles within the material. It is an important physical property that distinguishes insulators, dielectrics and conductors from one another. The polarization of a material is the summation of dipole moments per unit volume of the material. An electric dipole is a pair of separated positive and negative electric charges as shown in Figure 2.3.

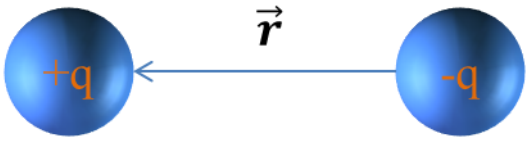

Figure 2.3: Schematic of a dipole pair that is comprised of a positive and negative charged centers.

The dipole moment, $\vec{p}$ of a single pair of charges could be calculated from vector equation 2.1,

$$\vec{p} = q \cdot \vec{r}\ [53], \qquad 2.1$$

where $\vec{p}$ is dipole moment (unit, Coulomb-meter), q is the electricity processed by a single charge (Coulombs) and $\vec{r}$ is the distance between the positive and negative charges (unit, m). The polarization of can be calculated by vector equation 2.2,

$$\vec{P} = \frac{\sum \overrightarrow{p_i}}{V}\ [54], \qquad 2.2$$

where $\vec{P}$ is polarization, $\overrightarrow{p_i}$ is dipole moment of the i^{th} pair of charges per unit volume, V.

A material may be polarized via four mechanisms: electronic polarization, ionic polarization, orientation polarization and space charge polarization. Electronic polarization occurs when an external electric field is applied to a material and the electrons displace relative to their nuclei. In this case, the center of the electron clouds displace in the

direction of lower electric potential. An illustration of the electric polarization of H_2 is provided in Figure 2.4.

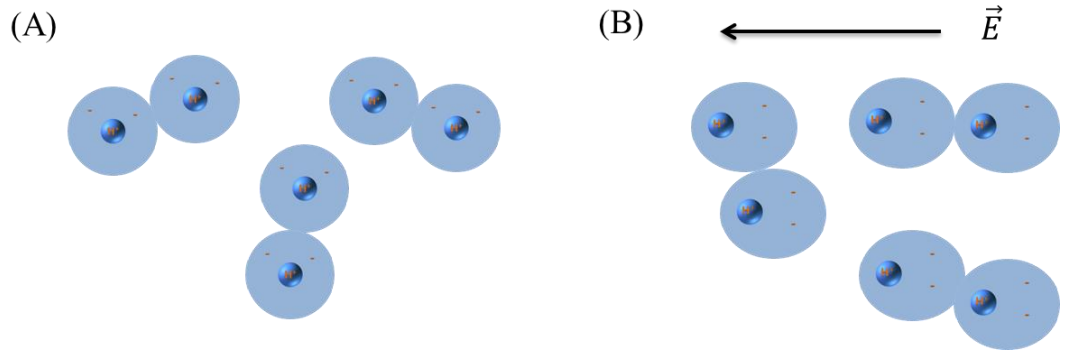

Figure 2.4: Mechanisms of electronic polarization. In (A) there is no external electric field applied. Thus, there is no permanent dipole moment. In (B) an external electric field is applied, and dipole moments are induced, which results in the alignment of the dipoles within the material.

The second type of polarization, ionic polarization is the most common. Ionic polarization occurs when the centers of positive and negative charges (i.e. cations and anions) within molecules are reoriented after the application of an electric field. This reorientation is in the direction of the applied electric field. An example of the ionic polarization of sodium chloride (NaCl) is depicted in Figure 2.5.

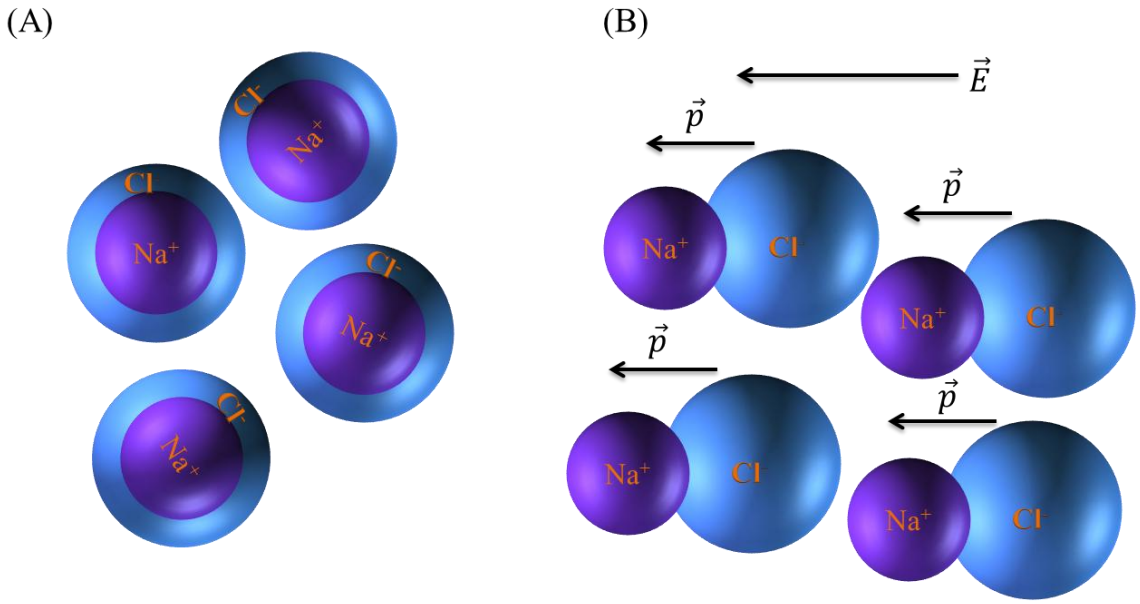

Figure 2.5: Mechanism of ionic polarization: (A) Without the presence of the external electric field, positive and negative's gravity center are coincident, there is no permanent dipole moments. (B) With the externally applied electric field, gravity centers of positive and negative charges are separated; dipole moments are induced and aligned.

When molecules themselves possess a permanent dipole moment, the applied electric field will reorient the molecules so that the permanent dipole moment will be in the opposite direction of the external electric field, this is called orientation polarization. An example of orientation polarization is shown in Figure 2.6.

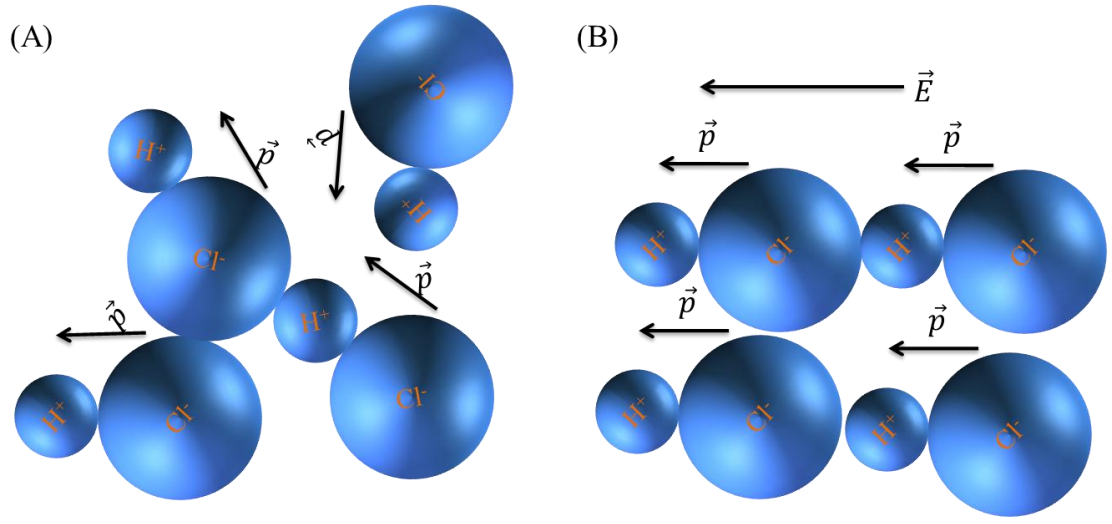

Figure 2.6: Mechanism of orientation polarization: (A) Permanent dipole moments are facing different directions, over all polarization is zero. (B) With the externally applied electric field, permanent dipole moments are aligned.

The forth source of polarization is space charge polarization, which happens when the electrons or the ions migrate larger distances within more conductive phases and accumulate on the surfaces of more resistive phases [54] when subjected to an external electric field. The mechanism of space charge polarization is shown in Figure 2.7.

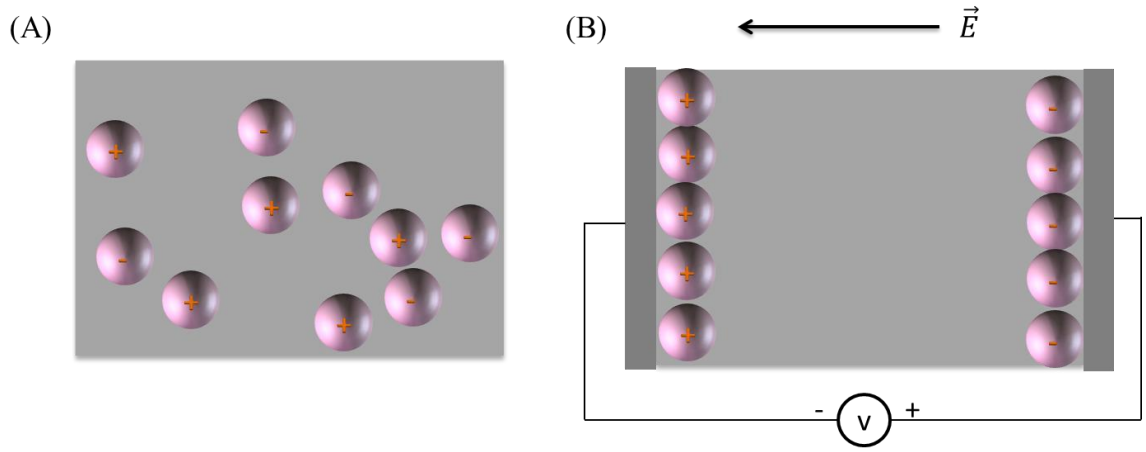

Figure 2.7: Mechanism of space charge polarization: (A) Without external electric field, the ions are mixed up. (B) At the presence of external electric field, the ions could travel larger distance inside the material.

Dielectric materials possess at least one of the four types of polarization mechanisms mentioned above. The degree of polarization within a material is a function of the frequency of the alternating electric field [52].

Dielectric materials store energy in terms of polarization. The relative complex permittivity is an indicator of the effectiveness of the dielectric material in storing energy in comparison to vacuum. The responses of dielectric material under the influences of an alternating current (AC) are very closely related to the frequency of the electric field. The relationship between the complex permittivity and relative complex permittivity is expressed in equation 2.3,

$$\varepsilon_r = {}^{\varepsilon}/_{\varepsilon_0}, \qquad 2.3$$

where ε_r is relative complex permittivity, ε_0 is the dielectric constant of vacuum (8.854×10^{-12}F/m) and ε is the overall complex permittivity of the occupied space. The relative complex permittivity could be further expressed as equation 2.4, where ε_r' is the real part of relative complex permittivity, and ε_r'' is the imaginary part of relative complex permittivity. The relationship between the real and the imaginary parts of the permit-

tivity are shown in Figure 2.8. Both the real and imaginary parts of the complex permittivity vary depending on the given frequency. The real part of the complex permittivity (i.e. ε_r') is a measure of how much energy has been stored in the dielectric material (referred as dielectric constant). The imaginary part of complex permittivity (i.e. $\varepsilon_r^{"}$) is a measure of how dissipative or lossy the material is in facing the alternative electric field. The dissipation factor or loss tangent is a measurement of how dissipative the material is compare to its ability to store energy [55]. could be shown in equation 2.4.

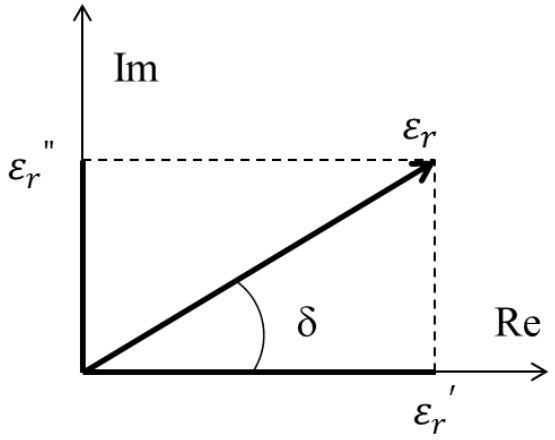

Figure 2.8: Real part and imaginary part of relative complex permittivity

$$\tan\delta = {\varepsilon_r^{"}}/{\varepsilon_r'}, \qquad 2.4$$

Given the frequency of the AC field, the real part of the complex permittivity (mostly referred as dielectric constant) could be calculated through polarization.

Polarization describes how the charges are distributed inside the material, in order to describe the matter without the effect of vacuum, the electric displacement field, denoted as $\vec{D}$ is introduced. Electric displacement field accounts for the effects of free and bound charge within materials. The relation of $\vec{D}$, $\vec{P}$ and dielectric constant of vacuum could be presented as vector equation 2.5,

$$\vec{D} = \vec{P} + \varepsilon_0 \vec{E}\ [54], \qquad 2.5$$

where $\vec{P}$ is polarization, ε_0 is dielectric constant of vacuum and $\vec{E}$ is applied electric field. As the polarization under given electric field is a property of the material itself, so the electric displacement field $\vec{D}$ could be express as equation 2.6as well,

$$\vec{D} = \varepsilon_r \varepsilon_0 \vec{E}\ [54], \qquad 2.6$$

where ε_r is dielectric constant of the material of interest. The mathematical relationship between ε_r and $\vec{P}$ could be expressed in 2.7.

$$P = (\varepsilon_r - 1)\varepsilon_0 E\ [54], \qquad 2.7$$

Dielectric constant, also referred as real part of the relative complex permittivity, is the indicator of how effective of the material behaves as a capacitor, which cannot be measured directly. Usually the capacitance, which accounts for the ability to store charges, area and the thickness of the specimen are measured, and the dielectric constant may be subsequently calculated as a function of Capacitance using equation 2.8.

$$\varepsilon_r = \frac{C \cdot d}{A \cdot \varepsilon_0}, \qquad 2.8$$

where, ε_r is the relative dielectric constant, ε_0 is dielectric constant of vacuum ($\varepsilon_0 \approx 8.854 \times 10^{-12} \mathrm{F \cdot m^{-1}}$), C is capacitance, A is area and d is the thickness of the piezoelectric composite layer.

2.3 Piezoelectric material

Piezoelectric materials are a class of dielectrics, that can not only be polarized by an electric field but also a mechanical stress [52]. This special property arises from the crystal structure of piezoelectric material. Some of the piezoelectric materials have permanent dipole moments; some of them have their positive and negative charge center coinci-

dence. Due to piezoelectric materials' natural non-centrosymmetric crystal structure, when stress is applied, the distortion of the crystal structure will further separate or induce the separation of positive and negative charge centers, this phenomenon is shown in Figure 2.9.

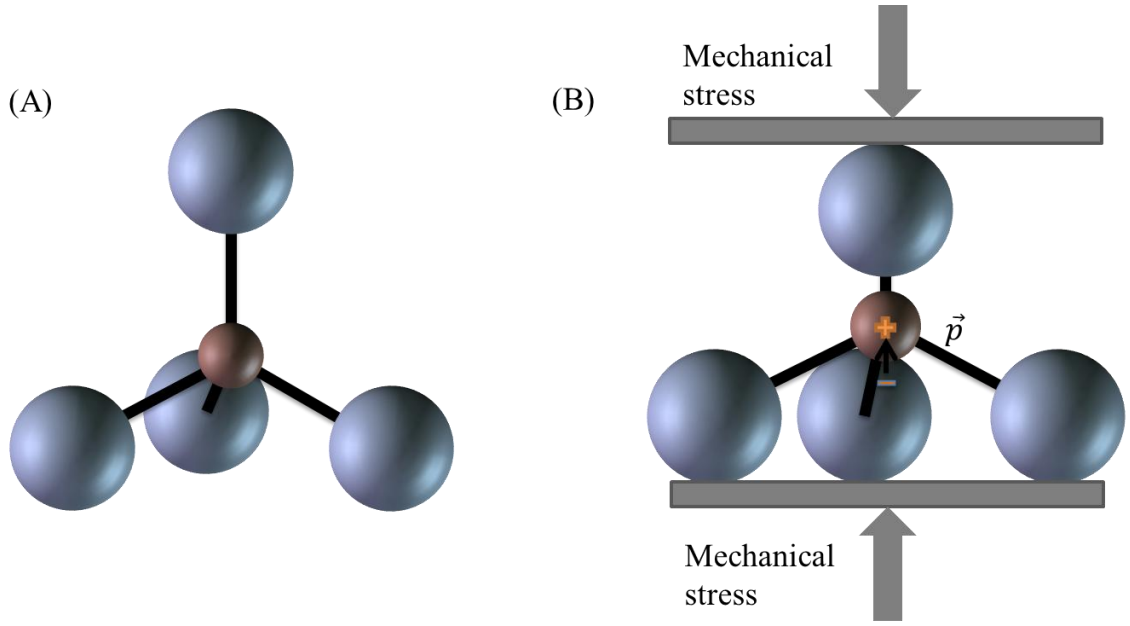

Figure 2.9: Polarization induced by mechanical stress. (A) Without applying the mechanical stress, positive and negative charge centers are in coincidence. (B) After the mechanical stress is applied, the dipole moment is induced.

There are many materials in our everyday life that have piezoelectricity, such as quarts and bones. Polarization is developed when a piezoelectric material is subjected to mechanical stress. Similarly, the converse piezoelectric effect occurs when an external electric field is applied to the material and it develops a strain in response to the applied stress. Both piezoelectric and converse piezoelectric effects are shown in Figure 2.10.

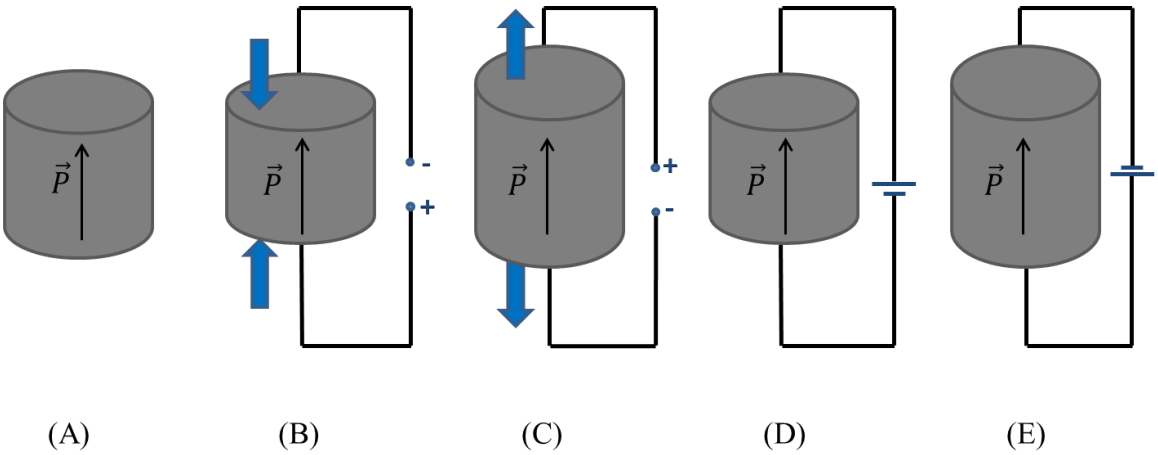

Figure 2.10: Schematic representation of piezoelectric and converse piezoelectric effect. (A) The material after polarization, the polarization direction sis shown in the figure. (B)&(C) explain piezoelectric effect: the polarized material is under stress, and produces voltage. (D)&(E) denotes converse piezoelectric effect, when polarized material is subjected to external electric field the strains are induced**[9]**.

Within the 7 crystal system, there are 32 points groups in total that have the possible combinations of symmetries, 11 of them are centrosymmetric point groups, 21 of them are non-centrosymmetric groups. Since Neumann's Principle[56] is applied, the piezoelectricity is limited to materials have non-centrosymmetric structures. Point group 432 is special because the dipole moments generated along axis <111> cancels each other, left this point group similar to centrosymmetric point groups. However, the non-centrosymmetric structure is only necessary to piezoelectricity but not sufficient, as only a few thousand materials exhibit meaningful piezoelectric effect compared to several hundred thousand materials with non- centrosymmetric structures.

The critical measurement of piezoelectricity are the piezoelectric coefficients, e.g the piezoelectric charge coefficients. The linear piezoelectric constitutive equations for the converse and direct piezoelectric effects are expressed in equation 2.9 and equation 2.10, respectively,

$$S_{ij} = d_{kij} \cdot E_k \text{ (Converse piezoelectric effect),} \quad 2.9$$

$$D_k = d_{kij} \cdot \delta_{ij} \text{ (Piezoelectric effect),} \quad 2.10$$

where d_{kij} is the piezoelectric charge coefficient tensor, S_{ij} is corresponding strain tensor, and δ_{ij} is the stress tensor, where $i, j = 1,2,3$. The first index indicates the direction of polarization, the second index denotes the normal to the surface where the stress acts, and the third index is the actual direction on specific surface. As E_k and D_k are both first order tensors, and S_{ij} and δ_{ij} are both second order tensors, d_{kij} is the third order tensor, which have 3^3=27 elements in total. Owing to the symmetric property of strain and stress tensor ($S_{ij} = S_{ji}$, $\delta_{ij} = \delta_{ji}$) so $d_{kij} = d_{kij}$ and the total number of piezoelectric coefficients reduces to 18 [52].

The lowest symmetry point group is point group 1, from the triclinic crystal system, which only has 1 fold of rotation. So the crystals in this point group will not have further reduction in the number of piezoelectric charge coefficients like other point groups who have more symmetry elements. The piezoelectric coefficient tensor are expressed in equations 2.11, 2.12 and 2.13,

$$d_{1jk} = \begin{bmatrix} d_{111} & d_{112} & d_{113} \\ d_{112} & d_{122} & d_{123} \\ d_{113} & d_{123} & d_{133} \end{bmatrix}, \quad 2.11$$

$$d_{2jk} = \begin{bmatrix} d_{211} & d_{212} & d_{213} \\ d_{212} & d_{222} & d_{223} \\ d_{213} & d_{223} & d_{233} \end{bmatrix}, \quad 2.12$$

$$d_{3jk} = \begin{bmatrix} d_{311} & d_{312} & d_{313} \\ d_{312} & d_{322} & d_{323} \\ d_{313} & d_{323} & d_{333} \end{bmatrix}. \quad 2.13$$

As we can see from those equations, all three tensors are symmetric, so the last two indexes may be rearranged as shown in Table 2.1.

Table 2.1 Index transformation

11	1
22	2
33	3
23/32	4
31/13	5
12/21	6

Then after rearranging, the new piezoelectric charge coefficient tensor may be expressed as,

$$d = \begin{bmatrix} d_{11} & d_{12} & d_{13} & d_{14} & d_{15} & d_{16} \\ d_{21} & d_{22} & d_{23} & d_{24} & d_{25} & d_{26} \\ d_{31} & d_{32} & d_{33} & d_{34} & d_{35} & d_{36} \end{bmatrix}. \quad 2.14$$

The crystal structures are centrosymmetric, by multiplying inverse transformation matrix $\begin{bmatrix} -1 & 0 & 0 \\ 0 & -1 & 0 \\ 0 & 0 & -1 \end{bmatrix}$ on the left, the piezoelectric charge coefficient tensor will be $-d$, and at the same time Neumann's Principle requires that $d = -d$, all elements in piezoelectric charge coefficient tensor will be cancelled. So non-centrosymmetric is necessary for piezoelectricity. The increasing number of symmetries possessed by crystal structure reduces the number of remaining piezoelectric charge coefficient elements. Piezoelectric charge coefficient d_{33} and d_{31} are most commonly measured. They are often measured as charges accumulated when subjected to vibrations. The frequency of vibration should be within 25-300Hz[54]. For piezoelectric charge coefficients mentioned here, the polarization direction is both in 3rd direction, the stress applied when measuring d_{33} is also in 3rd direction, however, the stress applied when measuring d_{31} is in 1st direction. The directions of polarization and stress for both cases are indicated in Figure 2.11 and Figure 2.12.

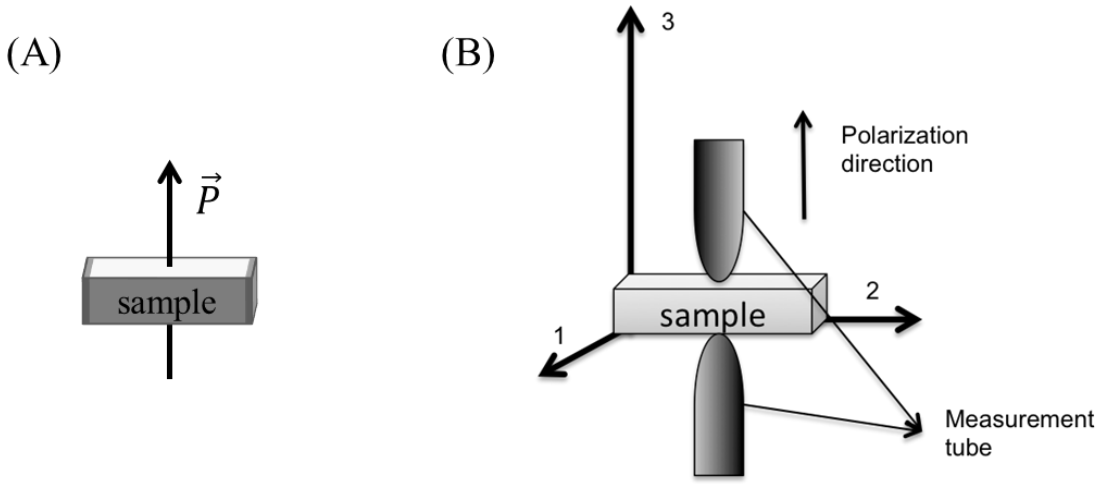

Figure 2.11: Illustration of d_{33} measurement. (A)Polarized sample (B) The measurement of d_{33}, the measurement tube would apply the vibration and take the voltage reading at the same time.

In Figure 2.11, in measuring the $d_{33,}$ the polarization direction is in 3rd direction, when stress in terms of vibration is applied also in 3rd direction, the measurement tube will measure the polarization along the same direction.

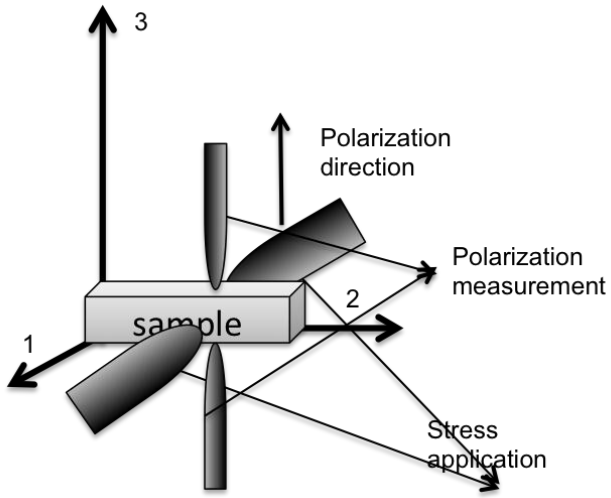

Figure 2.12: Illustration of d_{31} measurement

In Figure 2.12, to measure $d_{31,}$ the polarization direction is still in the 3rd direction; however, the vibration is applied in 1 direction. Once the measurement started, the tubes will measure the polarization along the 3rd direction.

2.4 Ferroelectrics

Ferroelectrics are crystals with a spontaneous polarization that can be switched from one orientation to another by an externally applied electric field[52]. All ferroelectrics are piezoelectric and ferroelectrics are different from normal piezoelectric materials. First, they possess spontaneous polarization, and their polarization can be switched from one orientation to another when an external electric field is applied. Second, the phase transition can also affect the spontaneous polarization, when temperature keeps increasing, the crystal structure becomes more symmetric. Beyond a critical temperature called the Curie temperature, the current crystal structure will become a centrosymmetric cubic shape structure, which is the temperature at which a ferroelectric material will loose its spontaneous polarization. When the temperature is reduced these materials experience a phase transaction to a lower symmetric structure, and the spontaneous polarization emerges again. Third, all ferroelectric materials have domains, as when they are cooled from a higher temperature above the Curie temperature, the permanent dipole moments are generated and aligned in different directions. The units aligned in the same direction will form a domain, and will be separated from adjacent domains whose polarization is in a different direction. These properties come from their crystal structures.

The most important property of ferroelectric is reversible spontaneous polarization, which lead to the Polarization-Electric field (P-E) hysteresis loop. P-E hysteresis loop, as its name indicates, is measuring the polarization accumulated versus the increas-

ing strength of externally applied electric field. Dielectrics except ferroelectrics have a linear polarization-electric field relation as shown in Figure 2.13, where when the external electric field is removed, the polarization will no longer exist.

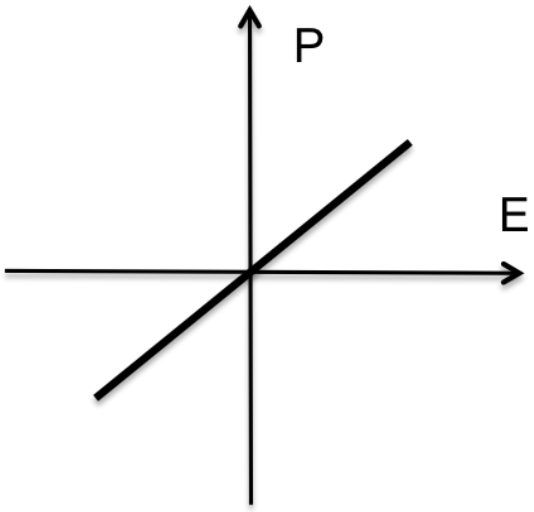

Figure 2.13: P-E relation of normal dielectrics

Ferroelectrics' P-E relations could be presented as a hysteresis loop, as shown in Figure 2.14. The actual P-E hysteresis loop includes line AB, BC and CD, however, we could only observe lines of AB, BB', CC' and CD[57].

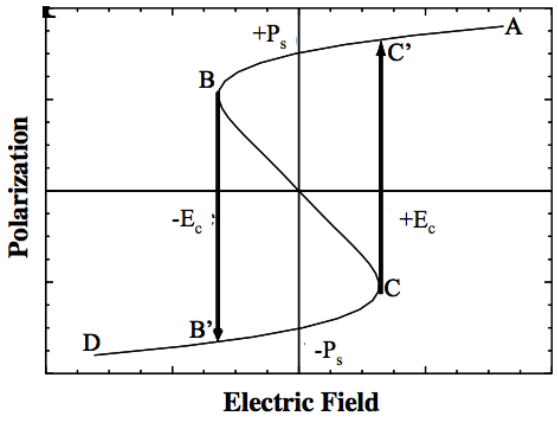

Figure 2.14: Hysteresis loop pf ferroelectrics[46]

The whole hysteresis loop is explained more clearly in Figure 2.15. Even though ferroelectrics have spontaneous polarization in their initial state, their overall net polarization is equal to zero because of the existence of multiple domains with different spontaneous polarization directions. Once the external electric field is applied, the polarization is increased with the strength of the electric field until saturated; this is OB line in Figure 2.15. The saturation point of polarization means that all possible switchable domains are aligned in the direction of the electric field. Increasing the strength of the electric field beyond this point will not increase polarization anymore. As shown in this figure, the gradual reduction in the external electric field to zero results in a net overall polarization called the remnant polarization, which is denoted as P_r. The higher the remnant polarization value, the more domains of spontaneous polarization that are aligned in the electric field's direction. If the electric field continues to increase in the opposite direction, the polarization will be compensated eventually. The strength of the external applied electric field applied required to achieve zero polarization is called coercive field, denoted as E_c. E_c indicates the resistance to reverse the direction of the polarization. This process is shown in Figure 2.15 as line CF. If the external electric filed increases further, the ferroelectrics would be polarized in the opposite direction until saturated, which is shown as line FG. Then the line GHB is describing the similar phenomenon just in opposite direction.

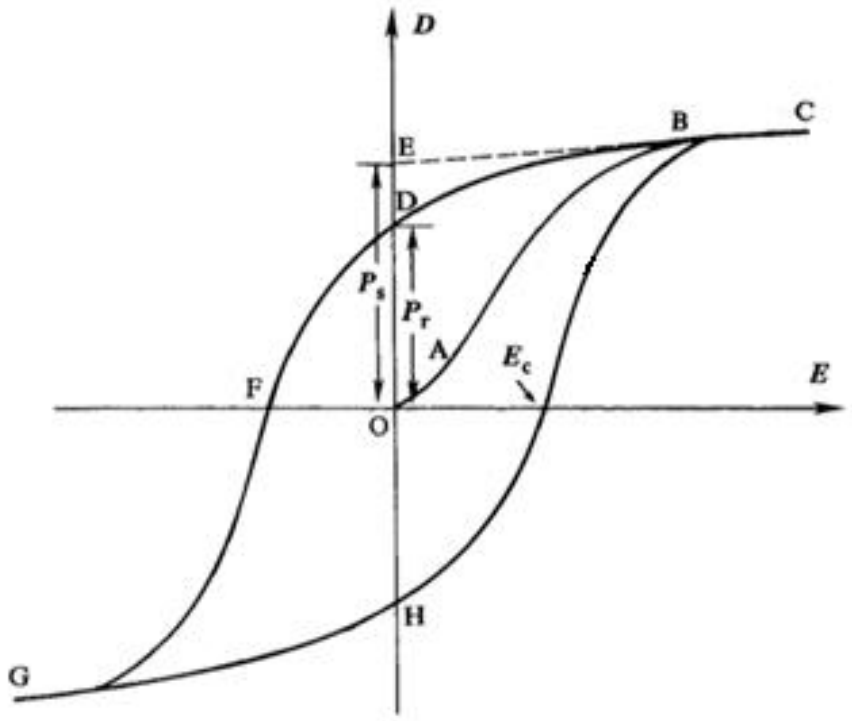

Figure 2.15: Hysteresis loop of ferroelectrics with original polarizing path**[57]**

Ferroelectric materials exist in different conditions such as single crystal, poly-crystalline ceramic and fine grain ceramic will have hysteresis loop in different shape[57]. In measuring hysteresis loops, programmed changing electric field is applied, and the polarization information will be collected.

There are different types of piezoelectric such as Bi-layer structured systems, Tungsten bronze structures and most common one--perovskite structures. Most ferroelectrics adopt the ABO_3 perovskite structure, and we will mainly focus on this group of ferroelectrics. General chemical formula of materials with perovskite structure is ABO_3, depending on the size of A atom and B atoms (there could be more than one type of B atoms), they could mostly belong to tetragonal, orthorhombic, rhombohedral and cubic crystal systems. Along the increasing of the temperature, the structure will gradually gain

more symmetry element until reach the cubic shape. The tetragonal perovskite structure below Curie temperature is shown in Figure 2.16, blue bigger atoms are A^{2+}, red big atoms are O^{2+} and the smallest black atom is B^{4+}. If we take PZT as an example, the blue atoms will be Pb^{2+}, the red big atoms will be O^{2+} and the smallest black atom will be Zr^{4+}. From Figure 2.16 we could also see that the positive and negative charge centers are not coincident, this leaves the ferroelectrics permanent dipole moment.

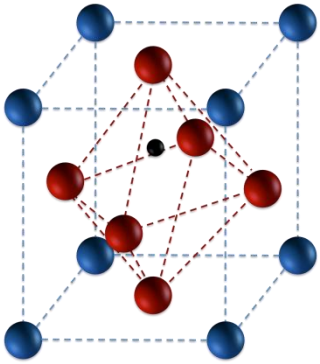

Figure 2.16: Tetragonal perovskite structure below Curie temperature**[9]**

When the temperature is increased beyond Curie temperature, the perovskite structure will experience a phase change and become centrosymmetric. The crystal structure above Curie temperature is shown in Figure 2.17, the positive and negative charge centers are at the same place, and piezoelectricity is lost.

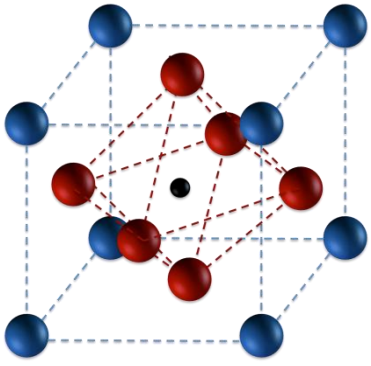

Figure 2.17: Cubic perovskite structures above Curie temperature**[9]**

As domains with polarization in different direction, before ferroelectrics present piezoelectricity, we need to apply external DC electric file to align dipoles in favorable direction. Aligning spontaneous polarization in one favorable direction by applying external DC electric field is called poling. Depending on different crystal structure, there could be many polarization directions, for examples, rhombohedral crystal class could have as many as 8 polarizations directions, orthorhombic crystal class could have 12 polarizations directions, and tetragonal crystal structure will have 6 polarizations directions. When crystals are cooled from Curie temperature, multiple domains are formed, and domains next to each other develop spontaneous polarizations in different directions, so the overall net polarization is zero. By applying DC electric field, mostly two effects could be observed: (1) Upon applying the electric field, the spontaneous polarization could be switched, as mentioned above that all different crystal systems have more than one polarization direction. (2) The externally applied electric field would induce domain wall motion. The applied electric field supply the energy that B^{4+} requires to jump from one equilibrium state to another, i.e. flip the polarization to the opposite direction by B^{4+} atom moving correspondingly. The elevated temperature is also required to help overcome the energy barrier.

2.5 Polarization Techniques

2.5.1 Parallel Plate Contact Poling

As sufficient polarization is important for ferroelectrics, different poling techniques are developed. Conventional contact poling, as shown Figure 2.18, usually employs two metal electrodes connected to a DC voltage source, and sample will be sandwiched in be-

tween, the two electrodes will direction contact the surface of the sample, and the whole set up is bath in heated silicon oil.

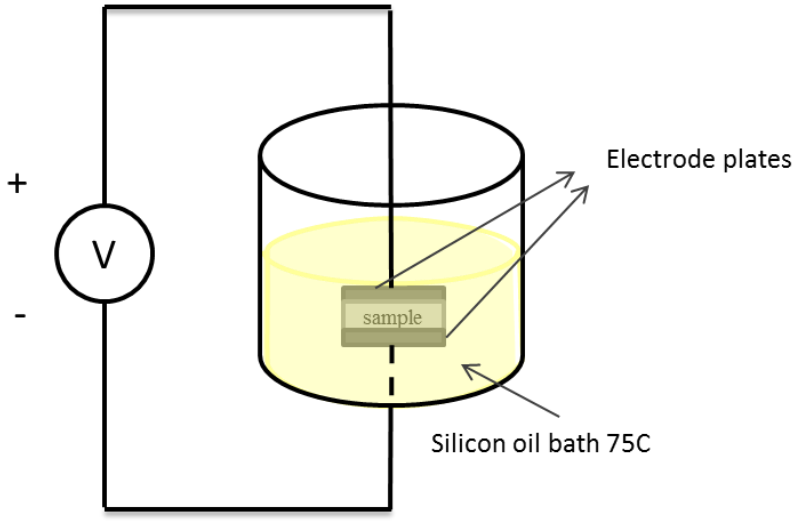

Figure 2.18: Sketch of conventional contact poling set-up

During the fabrication, deficient points and voids would commonly occur on samples, when poled by conventional contact poling, once the charges find one pathway to go through, not only the electric field over that deficient point will be lost but the whole electric field will be vanished, so the sample will not be properly poled, this is called dielectric breakdown in poling process. So contact poling requires high quality of samples and also possibly could not offer electric field enough to sufficiently polarize samples.

2.5.2 Corona Poling

Corona poling, as indicated by its name, employs corona charges to create electric field. The scheme figure of corona poling set up is shown in Figure 2.19. The sample will be heated on a heat source, and only contact with ground. The needle right on top of the

sample will be connected to high voltage. One turned on, the tip of the needle will ionize surrounding air, and the electric field generated by ionized air will align the dipoles.

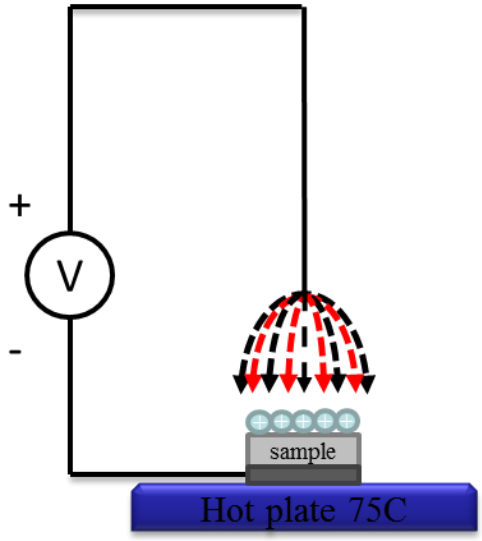

Figure 2.19: Sketch of corona poling set-up

In corona poling process, the deficient points where charges could leak through, will not affect the overall electric field except the deficient point itself since the 'top electrodes' are ionized air. Thus, by employing corona poling much higher poling voltage can be achieved.

2.6 Composite Materials

According to the broadest definition, a composite is any material consisting of two or more distinct phases[58]. Composites viewed as an intermediate, could inherit the advantages of all materials have been employed. Composite piezoelectric materials (CPM) possess several characteristics that distinguish them from their single-phase ceramic counterparts: few spurious modes (less noise associated with resonant modes), high com-

pliance/flexibility (less brittle), and flexibility in processing - moldable (can be easily fabricated into synclastic and anticlastic shapes).

Composite's electromechanical and all other properties are based on arrangement of the phases comprising the composites[59]. The connectivity was first brought up by Skinner[60] and Newnham[61], based on in how many directions the material is self-connected. For example, if material A is embedded in material B, if A is self-connected in 3 directions then A has connectivity of 3, and if material B only self-connected in 1 direction then B has connectivity of 1, the composite will be called as A-B 3-1 two-phase composite. Even with more than two phases, the expressions should follow the same fashion.

For two-phase composite, there are 10 established connectivity patterns, such as (0-0), (0-1), (0-2), (0-3), (1-1), (1-2), (2-2), (1-3), (2-3), and (3-3) [59]. The patterns could be illustrated better by Figure 2.20.

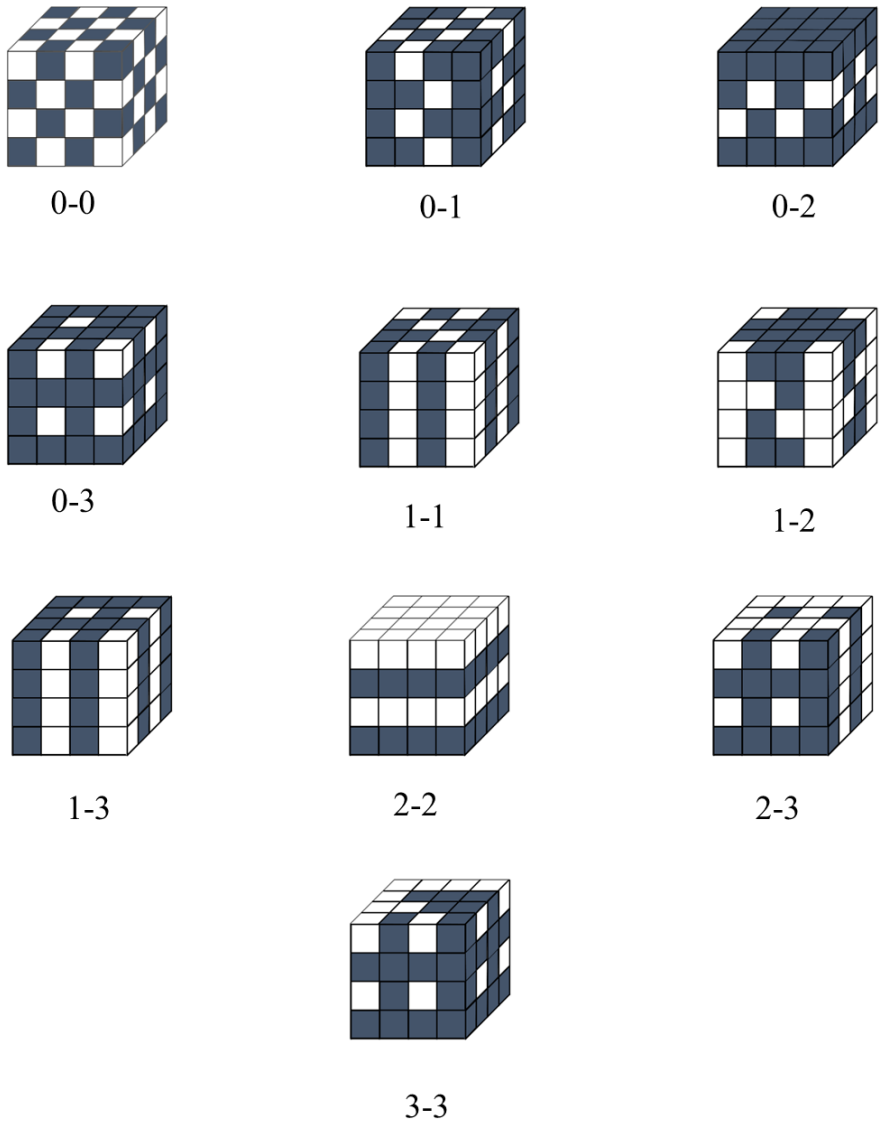

Figure 2.20: Here shows 10 connectivity pattern families, especially in {0-1}, {0-2}, {0-3}, {1-2},{1-3} and {2-3} families, each of them include 2 connectivity patterns, which makes total number of connectivity pattern16[60].

Based on connectivity concept, lots of piezoelectric/polymer has been developed[60, 61], such as particles in a polymer (0-3), ceramic rods in a polymer (1-3), diced composite (1-3), ceramic air composite (3-0), sheet composite (2-2), ladder composite (3-

3), more composites developed are shown in Figure 2.21.

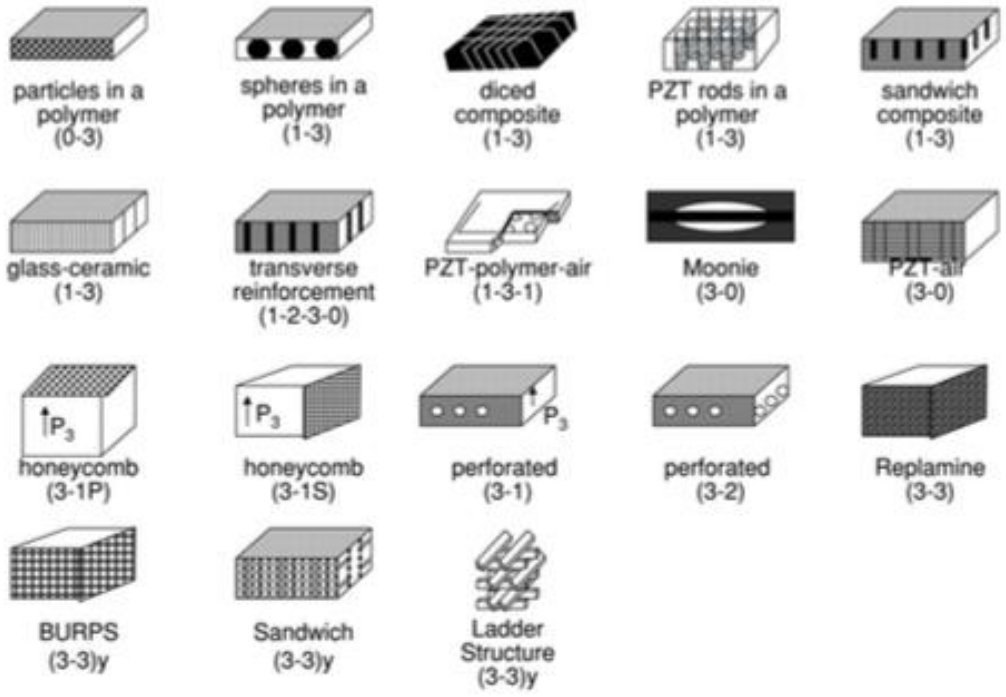

Figure 2.21: Schematics of typical piezoelectric ceramic composite structures **[23]**

As desirable as piezoelectric, their brittle nature limits them from being suitable for applications that require flexibility and particular shapes. Ferroelectric composites, embedding ferroelectric into matrixes, offer improved mechanical properties compared to ferroelectric ceramics, and inherit the excellent electromechanical and dielectric properties.

Embedding in matrix with different properties opens many opportunities for CPMs in varied applications. Cement-based piezoelectric composites, could be used as sensors and transducers in buildings with smart structures[62]. Polymer-based CPMs are well suitable for actuator and sensor applications. Polymer-based CPMs have electromechanical coupling factors (K_t~60%-92%[63]) that are comparable and higher to single-phase ceramic (K_{33}~40%-94%[59]) and polymer piezoelectric materials (K_t~11%-30%

[59, 64]), respectively. CPMs also demonstrate enhanced fracture toughness and high mechanical shock resistance, which renders them amenable to high quality thin and thick film applications[59].

Among all connectivity patterns introduced above, 0-3 piezoelectric composite standout as one of the easiest to produce and highly compatible to massive production. In 0-3 composite, the piezoelectric ceramic powders are not self-connected in any direction while the host material (i.e. polymer) is three-dimensional connected (Figure 2.20). Polymer based 0-3 composite offers good compatibility with various acoustic couplings such as castor oil[65]. Moreover, its properties are independent of pressure and frequency. Polymer based 0-3 composite are also attractive for power harvesting applications because of their ability to withstand large amounts of strain[1]. The larger the strain the device could take, the more energy could be possibly converted to electrical energy. The polymer based piezoelectric composites are also suitable to transducers such as hydrophones[65-67], air sensors, vibration sensors, pressure and stress sensors[68], underwater acoustic transducer[65] and medical diagnostic applications since they can be fabricated in suitable thin and flexible forms to provide enhanced hydrostatic piezoelectric properties (low in dielectric constant) and improved acoustic impedance[69].

Despite all favorable features 0-3 composites could offer, the relatively low piezoelectric coefficient limits this type of composites to be employed in applications need larger electromechanical responses. This could be result from difficulties in evenly distributing the fillers into the matrix, especially in high concentrations. Voids might be creates during the process could contribute to lower the dielectric breakdown strength, which may result in insufficient polarization for the ceramic phase. Besides all issues

mentioned above, as the nature of this composites (strong dielectrics embedded in weak dielectrics) the severally distinction in ability to be polarized between two phases makes the composite harder to be poled, as the electric filed will not come through the polymer phase easily[59].

So in order to be compatible to wider applications, processing techniques to increase homogeneity and poling techniques to improve polarizations of the active fillers are needed.

2.7 Spin-coating process

Spin coating combined with sol-gel processing is one of most common techniques to apply thin films onto substrates, as the process could quickly and easily produce very uniform films from a few nano-meters to a few microns in thickness[70]. Spin coating was first studied experimentally and analytically by Dietrich Meyerhofer [71]. This process has been widely used in the manufacture of integrated circuits[70], microelectronic applications[72], optical devices , coating color in TV screens, magnetic storage disk, fabrication of polymer and other Newtonian fluid based thin films[73].

Spin coating techniques use centrifugal force to dispense the solvent to a substrate. Thickness and uniformity of the samples fabricated are sensitive to speed, gas conditions, and rheology of concentrating, solidifying liquid[74]. The scheme of the spin coating process could be shown in Figure 2.22.

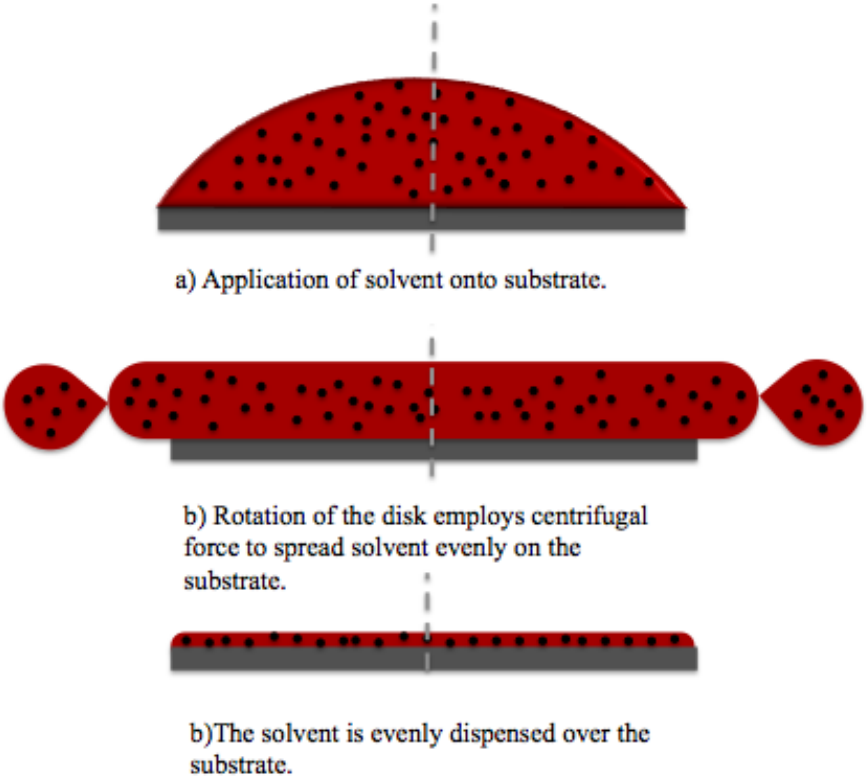

Figure 2.22: Scheme of spin coating technique

2.8 Literature review

2.8.1 Composite piezoelectric materials

0-3 piezoelectric composites are a category of CPM that has been extensively studied ([3, 31]). A summary of thin and thick film CPM piezoelectric and dielectric properties, and fabrication methods is presented in Table 2.2. As indicated in Table 2.2, the majority of the thick and thin composite films were fabricated using solvent casting[75, 76], spin-coating[77], screen printing[78], mode injecting[79], combination of spin-coat and sol-

gel[80, 81]and combination of solvent casting and compressed mode methods for deposition of the precursor composite material onto planar substrates.

Table 2.2 Fabrication techniques of composite thin films

Processing & materials [Ref]	**Substrate**	**Dielectric constant, ε**	**d_{33} [pC/N]**	**tanδ**	**Poling condition**	**Coercive field (Remnant polarization)**	**Remnant Polarization**	**Actuation performance**
Screen printed (200μm) PZT-PVDF-TrFE (50% PZT) [78]	ITO coated glass substrates	71@1 kHz	7.1pm/V	0.0231	Corona discharge at DC voltage of 17.5kV for 2h, followed by poling at room temperature for 1h			
Screen printed (200μm) PZT-PVDF-TrFE (30% PZT)		45@1 kHz	9.5pm/V	0.032		0.3MV/cm	10.5μC/cm^2	
Spin coat-Sol gel (5μm) PZT (100% PZT) [80]	Gold-coated alumina substrate	558@1 kHz	340pm/V	0.022	Corona poled at 15kV for 20min at 150C			d=5.2nm (@1 kHz, 40V$_{pp}$) d=0.4nm (@2 kHz, 40V$_{pp}$)
Solvent casting (30-150μm, free standing) PZT-P(VDF-HFP) (50%PZT) [75]	Glass plates	Permittivity=65	24.8 pC/N (Corona poled)		Corona poled at 20kV for 30 min @110C			
			22.1 pC/N (Direct-contact)		Contact poled at 20MV/m for 30 min @120C			
Solvent casting (100μm, free standing) PZT-P(VDF-HFP) (41%PZT) [82]	Glass plate	Permittivity=50	10.5pC/N		Corona poled at 20kV for 3 min @RT	1.5MV/cm -1.6MV/cm	±41MC/m^2	
			9pC/N		Contact poled by bipolar and unipolar @RT			
Solution cast and compression mold (30μm) PT-P (VDF-TrFE) (70/30% vol.) [83]			13.7pC/N		Contact poling 50MV/m at 120C		0.5C/m^2	
Injection mold at 270C (200μm) PZT –liquid crystalline polyester thermoset (40/60%vol) [79]		32 @100Hz	9pC/N @800C		Contact poling 15kV/mm for 1 h at 180C			
Spin coat PZT-P(VDF-TrFE) (5μm) (30% PZT)	Gold-coated silicon wa-	34@1 kHz	4pm/V	0.036	Corona discharge at DC voltage of 17.5kV for 2h,			

[77]	fers				followed by poling at room temperature for 1h			
Sol gel-spin coat and infiltration (5μm) PZT (100% PZT) [81]	Standard $Si/SiO_2/Ti/Pt$ substrate	2270@0.1V 1kHz	88pm/V	0.035		40kV/cm -80kV/cm	35 $\mu C/cm^2$ @480V_{pp}	

2.8.2 Curved/Dome shaped piezoelectric devices

Over the past decade interest in dome and curved shaped piezoelectric devices has increased because dome/curved shaped structures demonstrate higher deformation (~25.3% at 2.54kv/cm[34]) and electromechanical conversion accuracy (mechanical coupling factor K_{eff}~38%[35]) in comparison to planar actuators [36-39]. A summary of work performed in dome-shaped piezoelectric devices is presented in Table 2.3. Dome-shaped piezoelectric actuators can also achieve large loading [84] and large electro-induced displacements [35] in comparison to planar bimorph and multilayer actuators, as indicated in Table 2.3. Primarily three strategies have been investigated towards production of high performance dome-shaped piezoelectric structures. The first of these approaches achieves a curved structure via a thermal mismatch effect between device layers. Devices such as these include the RAINBOW (reduced and internally biased oxide wafer)[4, 42, 46, 85-87], THUNDER (thin layer unimorph driver) [34, 43, 84, 88] and LIPCA (lightweight piezo-composite actuator)[43-45, 47, 89-92]. These devices generally incorporate a co-firing technique, which enables exceptionally high displacement (ε~4.77%-162% [4, 34, 43, 45, 46, 48, 85, 86, 88-91]) and enhanced loading ability as shown in Table 2.3. However, the arch height of these structures is difficult to modify. Hence, [89] proposed a method to control the arch height of the piezoelectric actuator by electroplating nickel film on metal substrate of the actuator, wherein the arch height of the piezoelectric actuator was controlled by the thickness of the nickel layer and/or the time used for electroplating.

The second approach used to produce dome/curved piezoelectric structures includes the use of molds, such as those that adhere to the standard MEMS [37-39, 93]

technology and powder injection molding (PIM) techniques [28, 36, 41]. These techniques allowed for accurate control of the arch heights, and were compatible with batch processing techniques.

The last category of fabrication methods investigated, employed a pressure difference [40, 49, 94] or DC bias [35] to achieve the dome-shaped structure. This approach also enabled better control of the arch height and was compatible with batch processing techniques. However, this approach was most appropriate for application to piezoelectric thin film membranes.

Table 2.3: Fabrication techniques and performances of dome-shaped piezoelectric devices

Application - Processing & materials [Ref]	**ε / tan δ / k_{eff}**	**d_{33} /d_{31}**	**BC/LC**	**Geometry /layer**	**Poling Condi-tions**	**Resonant Frequency**	**Max. Displacement (Strain induced)**
Unimorph (PZT)/spin-coating [This work]	56@110 Hz	d_{33}=11.106 pC/N d_{31}=3.9 pC/N (effective)			Corona poled a@ 45kv/mm (30min)		
Actuator - Unimorph (70% PZT)/spin-coating [31]	76.1 @110Hz	d_{33}=425-500pC/N (material) d_{33}=1.06 pC/N d_{31}=0.74 pC/N (effective)	-- Dome-down No-load	r_{open}=25.4mm h=5.08 mm t_{total}=310μm	Contact poled 2.2kv/mm @ 75C for 15mins	--	--
Actuator - Three layers (Nd2O3 & ZrO2 doped Ba-TiO3)/co-firing [4]	2000-3000 @1kHz / Of the order 0.01-0.02	d_{33}=526pC/N d_{31}=325pC/N (effective)	Unclamped Dome-down No load	r_{open}=0.28cm h_{inner}=0.04cm t_{total}=0.066cm	--	--	d=8μm (op ,Ep-p=20kv/cm @0.1 Hz)
Actuator - Single layer (0.04Pb(Sb0.5Nb0.5)O3–0.46PbTiO3–0.5PbZrO3)/PIM (powder injection mold) [36, 41]	k_{33T}=1950 / k_p=0.7 (material)	d_{33}=550pC/N (material)	Clamped Dome- horizontal point load (weight of the device only)	r_{open}=4.93mm R=4.53mm t_{total}=0.4mm	Contact poled 2.5kv/mm @ 150C in silicon oil for 40mins	*f*=52kHz/51.4kHz/50.8kHz (first,60Vp-p, geometry #1) *f*=68.2kHz/61.6kHz /98.3kHz (first,60Vp-p, geometry #2)	d=7.48μm (--,60Vp-p @50kHz,10g)
LIPCA-C2 - Multi-layer (PZT, Carbon/Epoxy, Glass/Epoxy)/Thermally induced [48]		d31= -190x10-12 m/V d33= 390x10-12 m/V (material)	Simply supported Dome-down No load	L=71mm/100mm B=23mm/24mm t_{piezo}=0.25mm t_{total}=0.62 mm	--	--	d=1.1552mm (--,400Vp-p @1Hz, no load)
Actuator - Single layer (0.04Pb(Sb0.5Nb0.5)O3–0.46PbTiO3–0.5PbZrO3)/PIM (powder injection mold) [36]	ε= 1450 / Kp= 0.7 (material)	d33=550pC/N (material) (effective: 700nm/0.5mm=d*	-- Dome-horizontal Load unclear	r_{open}=8mm R=10mm t_{total}=0.5mm	Contact poled 2.5kv/mm @ 150C in silicon oil for 40mins	*f*=0.5Hz (first,50Vo-p, device)	d=700nm (op,50Vo-p @1Hz-0.33Hz)

		25V/0.5mm)					
Actuator - Single layer (ZnO)/MEMS [38]	--	(effective: 1.6μm/10μm=d*40v/410μm)	Clamped(fixed at circular edge) -- --	r_{open}=5.5mm R=3mm t_{piezo}=10μm	--	*f* =16kHz (first,80Vp-p,device)	d=1.6 μm (--,80Vp-p @0-300kHz)
Transducer - Single layer (ZnO)/MEMS [39]	80pF @1kHz Keff2=0.08	--	Clamped(fixed at circular edge) Dome-down No load	r_{open}=5mm t_{piezo}=13μm t_{total}=13.5μm	--	*f* = 215MHz	--
Actuator - Multi-layer (PZT-5H,Epoxy as glue, stain-less steel) /Thermally induced [84]	--	--	Fixed at four corners Dome-down Tip point loading	a=37mm b=37mm t_{piezo}=0.3mm t_{total}=0.4516mm h=10.68mm	Contact poled 1.5kv/mm @ 60C for 10mins	--	d=115 μm (V=200v, no loading) D=-11.79μm/Nt*load+115 μm @ V=200v (DC/AC unclear)
Transducer - Single layer membrane (PZT-5A) /DC bias [35]	k_{33}=826 (material, calculat-ed) K_{eff}^2=0.15	d33=329.8pC/N d31=-154pC/N (material, calculat-ed)	Clamped (fixed at circular edge) Dome-down No load	r_{open}=2mm t_{total}=13.6μm h=16μm	--	--	d_{DC} =3.5μm(V_{DC}=10v)
PCA - Multi-layers (PZT, carbon-epoxy, glass-epoxy)/ Thermally induced [45]	--	d_{31}= d_{32}=-320x10^{-12} m/V(material)	Simple supported Dome-down Central line loading	a=32mm b=32mm t_{piezo}=250μm t_{total}=655 μm h=970μm	--	$f_{resonance}$=13.25Hz (--,200 $V_{p-p,}$ device)	d_{DC}=0.35mm (V_{DC}=150v, no load) 0.14mm/100g (V_{DC}=150v) d_{AC}=0.42 mm (op, V_{p-p}=200 @1Hz, no load) d_{AC}=1.62mm (op, V_{p-p}=200 @13.25Hz, no load)
			Fixed-free boundary Dome-down			*f*=32.5Hz (--,200 $V_{p-p,}$ device)	d_{DC}=2.25mm (V_{DC}=150v, no load)

			Central line loading				0.85mm/100g (V_{DC}=150v) d_{AC}=2.62mm (op, V_{p-p}=200 @1Hz, no load)
Actuator - Single layer (PLZT 5.5/56/44 (La/Zr/Ti))/RAINBOW [85]	20.8nF / 2.5%	d_{33}=312pC/N (effective)	-- -- No-load	h=305µm t_{piezo}=0.635mm t_{total}=635.5 µm r_{open}=31.75mm	Three times of coercive filed strength	600-1000 Hz and 8-50 kHz (--,--,device) They think this is bending mode	d=125 µm (DC: E=9.5kV/cm or V=450v)
Actuator - Monolithic bilayer composite(piezo:0.65PMN-0.35PT; electrostrictive: 0.9PMN-0.1PT)/co-fire [86]	k_{33}=20000 (material, electro-strictive) k_{33}=630 (material, piezoe-lectric)	d33=630pC/N (material, piezoe-lectric)	Unclamped Dome-down Tip-load	h=0.5mm r_{open}=7.5mm t_{piezo}=490µm t_{total}=986µ m	Contact poled 2.5kv/mm @ 150C in silicon oil for 10mins	--	d=15µm (--,bipolar 10kV/cm @--, 0.5N) d=14µm (--,unipolar 10kV/cm @--, 0.5N)
Actuator - Single layer (PLZT)/RAINBOW [87]	--	--	--	h=30µm r_{open}=20mm t_{total} =t_{piezo}=0.5mm	--	--	--
Sensor - Multi-layers (PZT-5A, Aluminum, LaRC-SI adhesive film)/THUNDER [34]	80-95nF @(10^{-3} Hz-100Hz)	--	Fixed at four corners Dome-down No-load	t_{piezo}=0.1778mm t_{total}=0.3937 mm R=157.48mm	Re-poling: 420v for 5mins	$f_{resonance}$=250Hz (--,--, device) They have stated that resonance frequency is independent on thickness and driving voltage	d_{AC}=0.642 mm (--,V_{p-p}=200 @1Hz & 10Hz, no load)
LIPCA - Multi-layer (PZT, Carbon/Epoxy ,Glass /Epoxy)/ Thermally induced [43]	--	d_{31}= -176x10^{-12} m/V(material)	Screw-fixed Dome-down Point load	L=71mm/100mm B=23mm/24mm t_{piezo}=0.1778mm t_{total}=0.25 mm R=308.8mm h=2.03mm	--	--	d_{AC}=0.34mm (--,400V_{p-p} @1Hz, no load) 0.17mm /1N(--,100V_{p-p} @1Hz) 0.34mm /1N(--,200V_{p-p} @1Hz)

LIPCA - Multi-layer (PZT-3195HDs, Carbon/Epoxy UD(0°), Glass/Epoxy)/ Thermally induced [89]	--	d_{31}= -190x10^{-12} m/V(material)	Simply-supported -- Point load	L=71mm B=23mm t_{piezo}=0.25mm t_{total}=0.53mm	--	--	d_{AC}=0.69mm (--, 400V_{p-p}@1Hz, no load) d_{DC}=0.4mm (V_{DC}=200V, no load) D=0.55mm/N*load+0.4 mm (V_{DC}=200V)
LIPCA - Multi-layer (Piezoelectric ceramic, Carbon/Epoxy ,Glass/Epoxy)/ Thermally induced [90]	--	d_{31}= d_{32}=-190x10^{-12} d_{33}=374x10^{-12} m/V(material)	Screw-fixed -- --	L=70mm B=23mm R=308.8mm t_{piezo}=0.25mm t_{total}=0.53mm	--	--	d=80μm (--,100V_{p-p},--,--)
LIPCA - Multi-layer (PZT-3195HDs, Carbon/Epoxy Fabric, Glass/Epoxy,)/ Thermally induced [91]	--	d_{31}= -190x10^{-12} m/V(material)	Simply-supported -- Point load	L=71mm B=23mm t_{piezo}=0.25mm t_{total}=0.68mm	--	--	$d_{no\ load}$=0.25mm D=-0.35mm/N*load+0.25mm (V_{DC}=200V)
LIPCA - Multi-layer (PZT, UD Carbon/Epoxy , Woven Glass/Epoxy)/ Thermally induced [92]	--	--	Grip on shorter edge Dome-down No load	L=72mm/100mm B=24mm t_{piezo}=0.25mm t_{total}=0.62mm h=0.92mm	--	$f_{resonance}$=11.5Hz (--,±200 $V_{p-p,}$ device)	d_{AC}=20mm (--,±200V_{p-p} @11.5Hz, no load)
LIPCA - Multi-layer (PZT, Carbon/Epoxy ,Glass/Epoxy)/ Thermally induced [44]	--	d_{31}= -190x10^{-12} m/V d_{33}= 390x10^{-12} m/V (material)	Simply-supported Dome-down No-load	L=71mm/100mm B=23mm/24mm t_{piezo}=0.25mm t_{total}=0.62 mm	--	--	d_{AC}=0.0852mm (op, 400V_{p-p}@1Hz, no load)
Sensor - Single layer (PVDF-TrEE) Mold/Spin-coating [93]	--	Sensitivity 0.0108V/N @5Hz	Clamped (fixed at circular edge) Dome-down Surface load	r_{open}=1.5mm t_{total} =t_{piezo}=30 μm h=30 μm	Contact poled 70kv/mm @90C for 30min	--	V_{p-p}=10.8mV (@1000mN, 5Hz)
Sensor- Single layer (PVDF)/air inflation technique [49]	--	Sensitivity =8.83V/N(total) or =0.55V/N(individual) t_{piezo}=56μm	Clamped (fixed at circular edge) Dome-down Point load	r_{open}=1mm t_{piezo}=56μm t_{total}=54-66μm h=1mm	80C	--	Output voltage $V_{p-p\ total}$=4.45v $V_{p-p\ single}$=0.27v (@300mN,5Hz)

Acoustic transducer - Single layer (PVDF)/static pressure difference (50mbar) [40]	--	d=5pC/N (material)	Clamped(fixed at circular edge) Dome-up --	r_{open}=40mm R=219.17mm (calculated value) t_{piezo}=25μm h=3.65mm (50mbar)	--	$f_{resonance}$=1.8kHz (first, 50mbar, device) $f_{resonance}$=1.8kHz (second, 100mbar, device)	--
Actuator - Double layer (PZT 53/47 doped with La^{3+}, Nb^{5+}, and PZT doped with Fe3+, Ni^{2+})/conventional ceramic processing & pressing [42]	--	d_{31}=108pC/N—donor doped PZT d_{31}=42pC/N—acceptor doped PZT (material)	-- Dome-down No load	r_{open} = or R= 14mm t_{piezo}=1mm	Contact poled 30kV/mm @ 120 C in silicon oil. (Poling direction is perpendicular to thickness direction)	$f_{resonance}$=5.3kHz (First, flexural mode, 400V/mm E_{p-p}, device) $f_{resonance}$=77kHz (Second, 400V/mm $E_{p-p,}$ radial mode, device) $f_{resonance}$=near 2MHz (Third, thickness mode, 400V/mm $E_{p-p,}$ device)	d_{AC}=30μm (op, 400V/mm E_{p-p} @--, no load)
Ultrasonic transducer - Single layer (PVDF)/Deep drawing process (negative pressure) [94]	--	--	Clamped (fixed at circular edge) -- --	r_{open} =1/2/3mm	Contact poled (combination of unipolar & bipolar electric field)	$f_{resonance}$=65kHz/73kH/93kH (--,--, device)	D=1.5nm/V @65kHz or 73kHz or 93kHz (3 samples – max. displacement of the 3) Polarization (-1/0.75 a.u. @ -1500/1500v)
Acoustic resonator - Monolithic (4 thin PZNT films)/Micro machined, elliptical [76]	--	--	Clamped (fixed at circular edge) -- --	r_{open}=25.26μm R=16.84μm (calculated) h=13.68μm	--	--	--

Chapter 3

Methodology

This work focuses on examination (and subsequent modification) of the processing parameters used to produce piezoelectric dome structures from our previous work [31]. A thorough parametric study was designed to relate the device processing parameters to the surface morphology, device thickness, distribution of PZT and air pocket density within the matrix. In addition, higher volume fractions of PZT (in comparison to our previous work) were included in this study (from 0.1 to 0.7). These higher volume fractions of PZT were achieved because of the change from Contact Parallel-Plate to Corona polarization.

3.1 Chapter Organization

In this section an overview of the organization of Chapter 3 is presented. In Section 3.2, physical, dielectric and piezoelectric properties of the materials are described. In Section 3.3, the procedure implemented in our prior work [31] is presented along with the optimized fabrication methodology for PZT volume fractions that are greater than 0.40. This methodology includes the optimized spinning speed profile (Profile 3) that was obtained from the Spin-Speed/Time Profile Study that is described in Section 3.6. In Sections 3.4 and 3.5, the equipment and analytical techniques used to perform piezoelectric and dielectric characterization are described. In Section 3.6, the study to understand the influences of spin speed and timing is presented. In Section 3.7, the Layer Deposition Study

is described. This study was developed when it was discovered that the methodology that was ideal for higher volume fractions of PZT, was not appropriate for lower volumes of PZT (less than 0.40 PZT). In Section 3.8, the experimental method used to obtain the device displacement is described. In Section 3.9, further study was presented to investigate relationship between polarization and applied electric field.

3.2 Materials

In Table 3.1, the physical, dielectric and piezoelectric properties of the lead zirconate titanate ($Pb\left(Zr_xTi_{(1-x)}\right)O_3$– 855, Navy VI) and the two-part epoxy - DGEBA, EpofixTM Cold-setting embedding resin (purchased from APC International and Electron Microscopy Sciences, respectively) are presented.

Table 3.1: Physical, dielectric and piezoelectric properties of the materials used in the fabrication of piezoelectric dome shaped structures. The values for the PZT are for bulk PZT as published by APC International. The values for the DEGBA were determined from an epoxy dome structure Fabricated using the same steps as defined herein with 0% PZT.

Property	PZT 855[95] (Navy VI)	DEGBA
Relative dielectric constant, ε_r	3300	3.7-3.9
Dielectric dissipation, $tan\delta$	≤ 2.50%	~0.002-0.004
Yong's Modulus, Y_{11}^E / Y_{33}^E	5.9/5.1	2.21~2.7 [96]

3.3 Original and Modified Methodology

The materials used in the original study and this work were maintained. An overview of the fabrication process from our original work is presented in Figure 3.1. Several modifications were made to the original fabrication methodology: 1) a desiccation step was added to eliminate air bubbles; 2) the spin coat deposition process was modified based on a study described herein (Section 3.6); 3) sol gel viscosity was maintained within a range

of 150-200mPas; and 4) Corona poling was used instead of the Contact Parallel Plate Poling.

An overview of the fabrication methodology used for this work is provided in Figure 3.2. The volume fraction of PZT was varied from 0.0 to 0.7. First, the PZT powder (purchased from APC International) was ball milled for 24 hours, where the mean diameter of the PZT after the ball mill step was observed to be 0.97 microns. Next, adequate amounts of the PZT and the epoxy were weighed and mixed with ethanol (15ml) by hand. The subsequent mixture was then subjected to sonication for 2 hours, desiccated for 4 hours, and then subjected to sonication for an additional hour. In this process, the sonication and desiccation steps were used to distribute the PZT particles within the matrix, enhance the evaporation of the ethanol and reduce the presence of air bubbles. The dynamic viscosity of the mixture was then measured using a Brookfield DV-E viscosity meter. Samples that had initial viscosity values less than 150mPas were subjected to additional sonication until the final viscosity was within the range of 150 to 200 mPas @100rpm. The resulting mixture was spin coated (using Speed/Time Profile 3 in Figure 3.5) onto a dome shaped Type 304, stainless steel substrate (purchased from Alfa Aesar, Ward Hill, MA, USA). The dimensions for the dome structure are provided in Figure 3.3. Once deposited, the dome shaped composite thick films were cured over a hot plate at 75° C for 8 h. A minimum of three samples were prepared for each volume fraction of PZT (PZT volume fraction was varied from 0.0 –0.70). These measurements were averaged to obtain the nominal thickness for each film. The dome shaped stainless steel substrate was made by pressing the stainless steel substrate into a mold at a pressure of 500 psi for 15 minutes at room temperature.

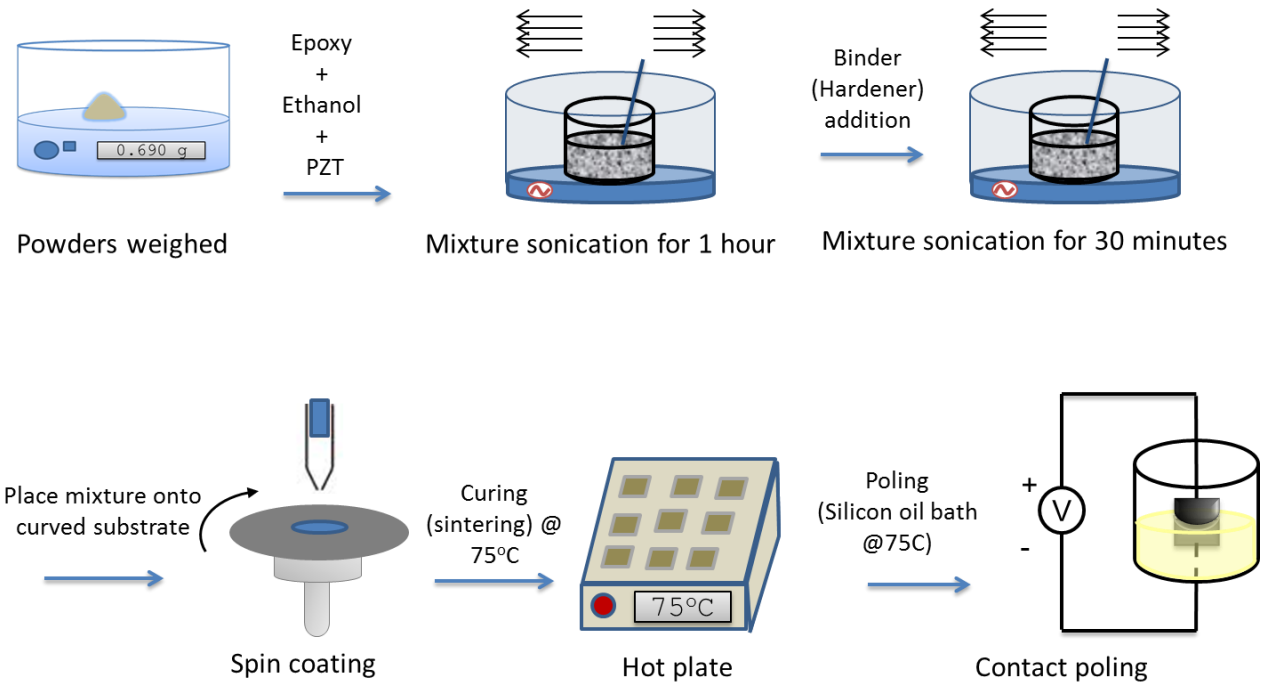

Figure 3.1: Overview of the original method used from our previous work. Appropriate amounts of PZT, DEGBA and ethanol were measured and mixed with the aid of a sonicator for 1 hour in the presence of air. The DEGBA binder was then added and the subsequent mixture was sonicated for an additional 30 minutes. The final mixture was spin-coated onto dome shaped substrate and cured at 75C. Samples were subsequently Parallel-Plate Contact poled at~2.2kV/mm [31].

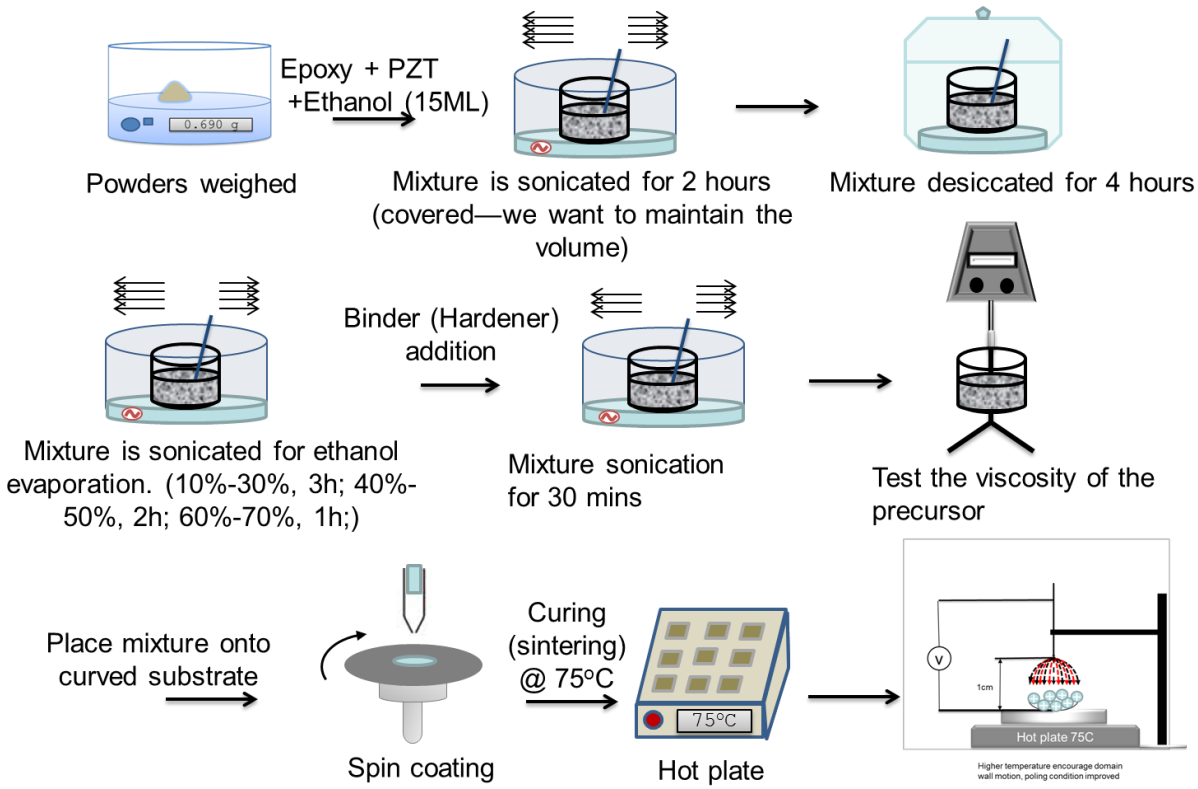

Figure 3.2: Overview of the method of fabrication used for this work. The appropriate amounts of PZT, DEGBA and ethanol were weighed and then mixed via a sonicator for 2 hours in the presence of air. The mixture was subsequently dessicated for 4 hours to eliminate air bubbles. The mixture was sonicated additional time. The binder was then added to the mixture and sonicated again, for an additional 30 mins. The final mixture is spined coated onto dome-shaped stainless steel substrate, and cured at 75C. Samples were poled via corona discharge.

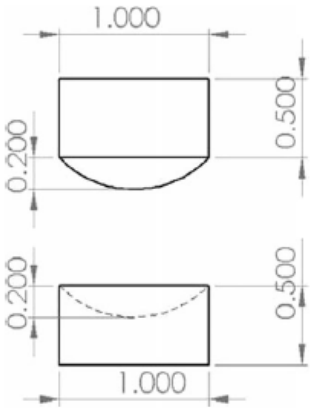

Figure 3.3: The dimensions for the dome shape mold.

The piezoelectric dome structures were heated using a hot plate for 10 minutes at 75 ° C prior to application of the poling electric field. A Corona polarization approach was used to align the dipoles of the PZT phase along the thickness of the samples, using a SL Rack Mount Power supply from Spellman Inc. One set of samples (that were comprised of 10%-70% volume fraction of PZT) was poled at 45kV/mm at a temperature of 75° C in air for 30 minutes. Another set of samples (samples comprised of 0.10, 0.20 and 0.30 volume fractions of PZT) were poled at 70kV/mm at 75° C for 30 minutes. The former set of samples could be poled at a higher poling voltage due to the smaller amount of PZT, while the others could not be poled at the higher voltage. No top electrodes were used during the poling process. The samples were wrapped in aluminum foil to remove residual charges for 24 hours after the poling process. The film thickness was measured at 5 locations on the dome structure in positions that are illustrated in Figure 3.4. The final thickness was the average of the 5 measurements.

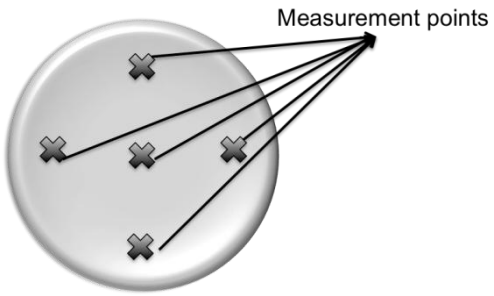

Figure 3.4: The thickness measurement was taken at five different places, and averaged.

3.4 Piezoelectric and Dielectric Characterization

The piezoelectric strain coefficients, d_{33} and d_{31} were measured at the frequency of 110Hz using the PiezoMeter PM300. Frequency dependent capacitance, dielectric loss, resistance, conductance, impedance and phase spectra were measured with an impedance

analyzer, HP 4194, and used to calculate the dielectric constant, resistivity, conductivity and normalized impedance. The impedance was normalized with the area and thickness. The piezoelectric strain coefficients and the capacitance were initially measured without a top electrode. Then, electrically conductive silver paste was added to some samples for the top electrode, and the d_{33} values were recorded again and compared to the values where no top electrode was used (still at 110Hz). The dielectric impedance, phase angle, capacitance and dielectric loss ($tan\ \delta$) were measured as a function of frequency (2kHz to 20 MHz) on samples that used aluminum tape as the top electrode. The aluminum tape electrode was triangular in shape with an average area equal to 18.5 mm^2. Aluminum tape was used instead of silver paste because the paste caused some samples to short circuit. The dielectric constant was calculated using equation 1;

$$\varepsilon_r = \frac{C \cdot d}{A \cdot \varepsilon_0}, \qquad 3.15$$

where, ε_r is the relative dielectric constant, ε_0 is dielectric constant of vacuum ($\varepsilon_0 \approx 8.854 \times 10^{-12} \mathrm{F \cdot m^{-1}}$), C is capacitance (measured by both PiezoMeter PM300 (@110Hz) and HP 4194 impedance analyzer(2kHz-20MHz)), *A* is area; *d* is the thickness of the piezoelectric composite layer. The empirical dielectric constants were compared to those predicted by an analytical model proposed by Furukawa [97] model, expressed in equation 3.16,

$$\varepsilon = \frac{2\varepsilon_1 + \varepsilon_2 - 2\emptyset(\varepsilon_1 - \varepsilon_2)}{2\varepsilon_1 + \varepsilon_2 + \emptyset(\varepsilon_1 - \varepsilon_2)} \varepsilon_1, \qquad 3.16$$

where ε, ε_1 and ε_2 are the effective dielectric constant of the composite and dielectric constants of the epoxy matrix and PZT particle inclusions. In this equation, $\emptyset$, represents the volume fraction of the inclusions.

The measured piezoelectric strain coefficient, d_{33} was compared to the coefficients predicted by another model developed by Furukawa [18],

$$d_{33} = \frac{1}{c} \cdot \emptyset L_s L_E d_2 c_2. \qquad 3.17$$

In equation 3.17, d_{33} is the piezoelectric coefficient; the subscripts 1 and 2, denote the matrix and PZT inclusions respectively. Also, in this equation, $L_s = \frac{1}{\emptyset}\frac{c_1 - c}{c_1 - c_2}$ and $L_E = \frac{1}{\emptyset}\frac{\varepsilon_1 - \varepsilon}{\varepsilon_1 - \varepsilon_2}$ are parameters, where c, c_1 and c_2 are the Young's Moduli of the composite, matrix and PZT inclusions.

3.5 Characterization of Surface Morphology and Particle Distribution

The surface topology, morphology and distribution of the particles within the polymer matrix were observed with the aid of scanning electron microscope (SEM) and Energy Dispersive Spectroscopy (EDS) micrographs obtained from a Zeiss Sigma Field Emission Microscope.

3.6 Spin-Speed/Time Profile Study

A spin coat speed and time increment study was performed to ascertain the ideal characteristics for the spin coat and deposition step in the fabrication procedure. An overview of the spin coat speed and time interval profiles examined are provided in Figure 3.5. This study was done on samples that were comprised of 0.50 volume fraction of PZT, where the viscosity of the sol gel was maintained at ~164.5 mPas @100 rpm. The amount of sol gel and *total* spin coat time was maintained at 2 mL and 220 seconds, respectively.

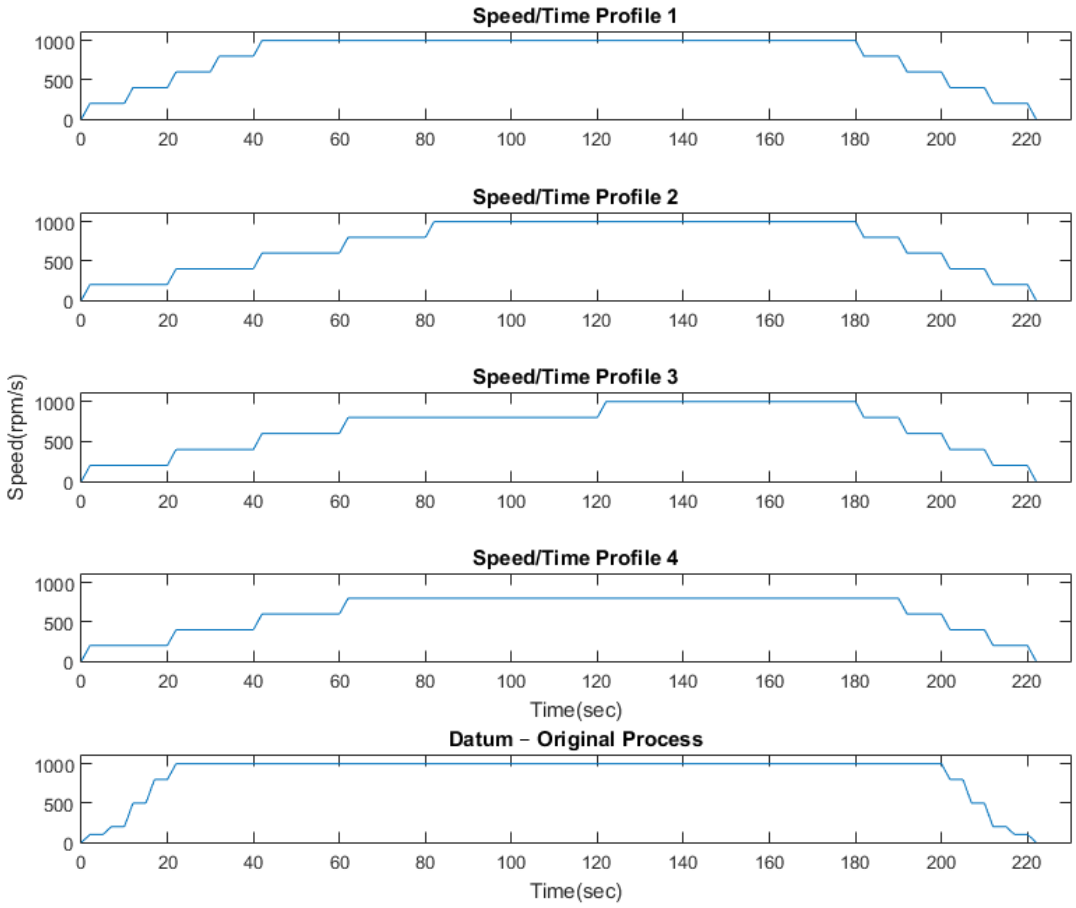

Figure 3.5: Speed/Time profiles studied. The datum process has step intervals has 100, 200, 500, 800 rpm for 5s each for both increasing and decreasing process, and the process was held at 1000 rpm for 3mins. Profile 1 followed the similar fashion with the datum except using step intervals of 200, 400, 600, 800 and 1000rpm to maintain the equal spaced speed increment. The holding time is 10s each for 200, 400, 600, 800rpm at both ascending and descending process, and is 140s at 1000rpm. The profile 2 uses the same speed steps and the descending process as profile 1, but the time held for 200, 400, 600, 800 rpm are 20s each in increasing steps. In this profile, holding time at 1000rpm is 100s. In profile 3 is built on profile 2 by extending the holding time at 800rpm to 1min, and reducing the holding time for 1000rpm to 1min. The profile 4 is built on profile 2 by eliminating the speed step 1000rpm, the top speed in this profile is 800rpm, and is hold for 130s.

3.7 Deposition technique Study

Since the sample thickness values of the samples with less than 0.40 volume fraction of PZT (poled at 45kv/mm) had inconsistent thickness and d_{33} values, a deposition layer study was performed. The of volume fraction 0.35 PZT was chosen because at volume fractions of PZT at and below 0.40, no piezoelectric strain coefficient was detected after

polarization at 45kV/mm when the sol viscosity was between 150 to 200 mPas. The influences of the number of deposition layers, time interval between layer deposition and sol gel viscosity were examined in this study to understand how they influenced the final thickness of the samples.

An overview of the deposition layer process studies is provided in Figure 3.6. The steps before deposition were kept the same as those depicted in Figure 3.2. For each sample fabricated, the amount of sol gel was maintained at 2ml. Sample were fabricated at viscosities equal to 150, 248.7 and 299mPas (equipment operated at 100rpm).

The films were deposited in one, two or three layers as shown in Figure 3.6. The overall amount of sol gel was maintained for each process and the same speed/interval profile was maintained for each layer deposition step. The Datum sample included one deposition layer, where the measured viscosity prior to application of the single layer was 150mPas. Process A included two data sets, where the first set of samples was fabricated with one deposition layer at a measured viscosity equal to 248.7mPas and the second data set had a viscosity of 299mPas. Processes B, C and D incorporated two layers of deposition. Three sets of samples were prepared using Process B where the measured viscosities for each data set were equal to 150, 248.7 and 299 mPas, respectively. The time interval between the deposition of the first and second layers (for Process B) was three minutes. Similarly, three sets of samples were prepared using Processes C and D, and the viscosities were measured to be equal to 150, 248.7 and 299 mPas, respectively. The time intervals between the deposition of the first and seconds layers were 9 and 3 minutes for Process C, and 18 and 5 minutes for Process D. Three layers of deposition were used for

Processes E and F, and three sets of samples were prepared at viscosity values equal to 150, 248.7 and 299 mPas, respectively.

The time increments between the deposition of the layers for Process E were equal to 29, 3 and 3 minutes, respectively, and equal to 44, 5 and 5 minutes, respectively for Process F. Process G was implemented for the fabrication of two data sets of samples at viscosities equal to 248.7 and 299 mPas, respectively. A single time interval of 63 minutes was taken prior to the deposition of the first and only layer.

The piezoelectric dome shaped composites underwent polarization following the process described in Figure 3.2 after the layer(s) were deposited onto the stainless steel substrate and pressed. The devices were Corona polarized at 45kV/mm, and were allowed to age one day before the measurement of the piezoelectric strain coefficients, thicknesses and dielectric properties.

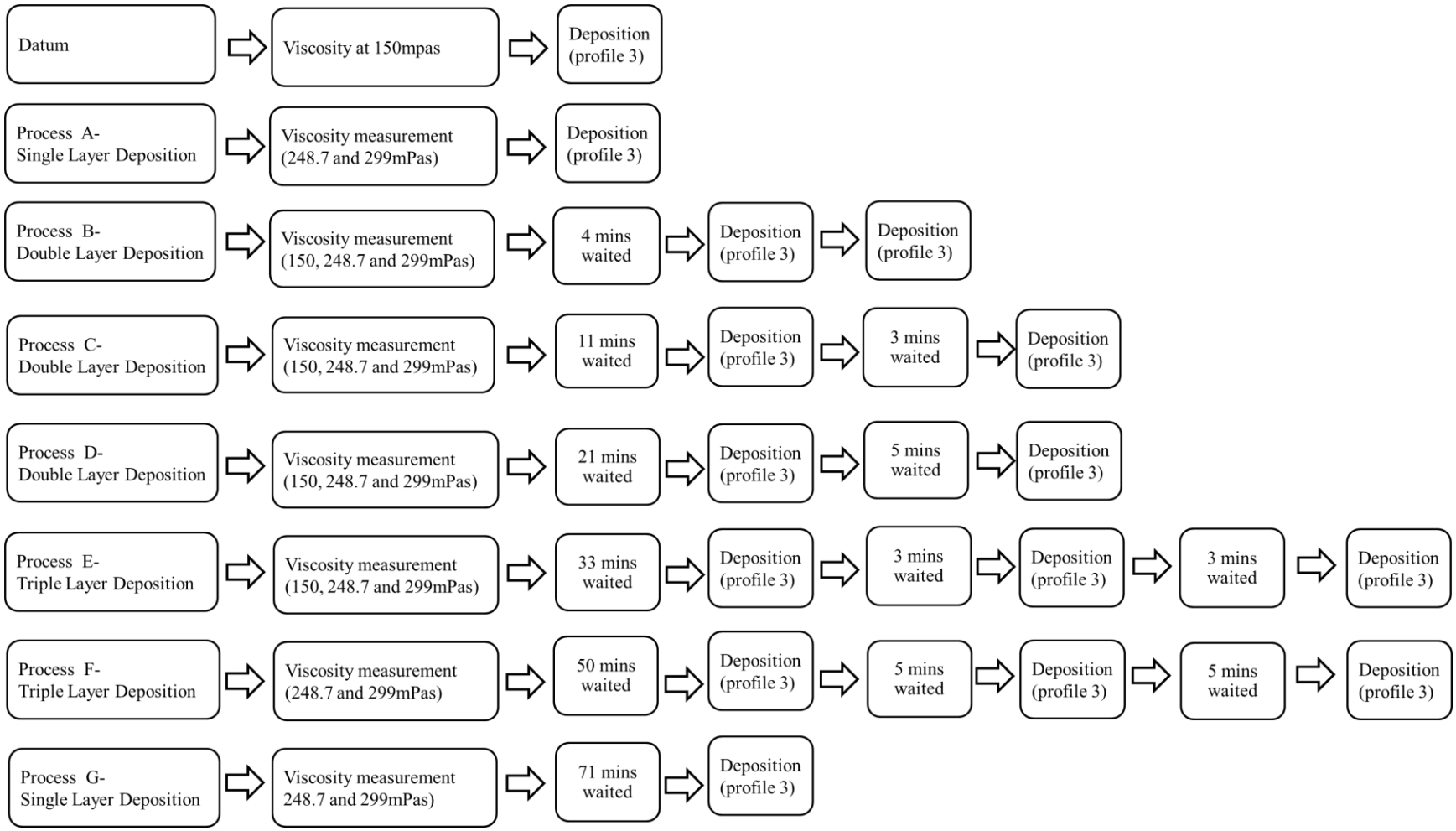

Figure 3.6: Overview of the deposition layer and sol viscosity study. All of the processes described in this figure incorporated Speed/Interval Profile 3 for the "Deposition" step. Three viscosity settings were used in this study: 150 mPas, 248.7 mPas and 299 mPas.

3.8 Device displacement

The displacement was a measured as a function of applied electrical voltage using a laser interferometer (KeyenceLK-G10). An overview of the experimental set-up is provided in Figure 3.7. The sample was placed on an insulated plate with the curved face (dome) facing down. The laser light from the interferometer was focused on the highest point on the dome-shaped device. The electrical voltage was applied using a Corona charge set-up, where the voltage was delivered from a needle connected with high voltage. The voltage applied was linearly increased from 1kV/mm to 20kV/mm in increments of increases 0.2kV every 200 seconds.

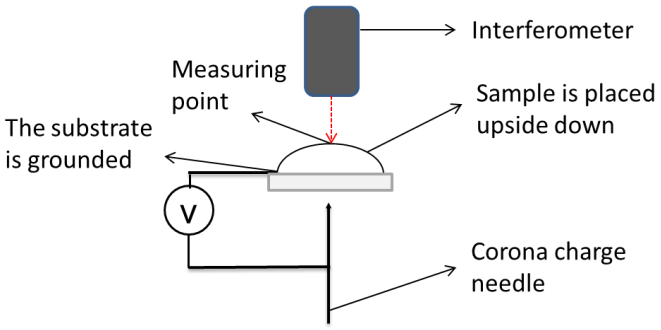

Figure 3.7: Displacement testing set-up

The surface topology, morphology and distribution of the particles within the polymer matrix were observed with the aid of scanning electron microscope (SEM) and Energy Dispersive Spectroscopy (EDS) micrographs obtained from a Zeiss Sigma Field Emission Miscroscope.

3.9 P-E hysteresis

The P-E hysteresis loop of (50%)PZT and (60%)PZT were measured by Precision Ferroelectric Tester from Radiant technology Inc.

Chapter 4

Results and Discussion

4.1 Chapter Organization

In this chapter, the results from our prior work[31], are compared to the results obtained from a parametric study of processing parameters. In section 4.2, electrical properties of epoxy single phase are presented. In Section 4.3 the results from optimized processing procedure are presented and compared to the results from our prior work[31]. In order to achieve the optimized processing steps described in Chapter 3, Section 4.4, a parametric study was performed to identify the influence of spin-speed/time profiles on the resulting piezoelectric and dielectric properties of the dome-shaped devices. In Sections 4.5, a study on deposition technique was performed to investigate the influence of several parameters in deposition on 0.1-0.35 volume fraction of PZT. In section 4.6, the optimized processing conditions are summarized. In section 4.7 and 4.8, the device displacements and hysteresis were measured on selected composites.

4.2 Epoxy Dome Device

The epoxy single-phase dome-shaped samples were fabricated with exactly same procedure with other samples (0.1-0.7 PZT), so that the composite samples could be to this base study.

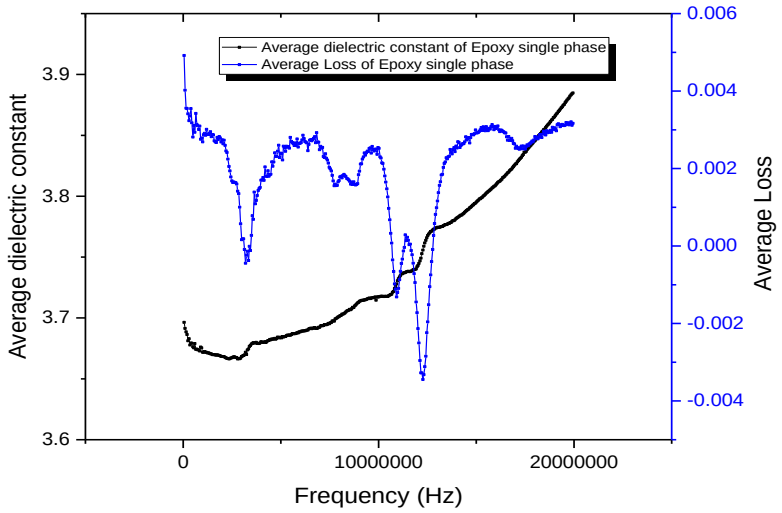

Figure 4.1: Dielectric constant/loss vs frequency of epoxy single phase samples, the spectrum was measured with small aluminum tape.

In Figure 4.1, the loss of epoxy single phase is mostly between 0.002-0.004, the negative values could be equipment's error. .

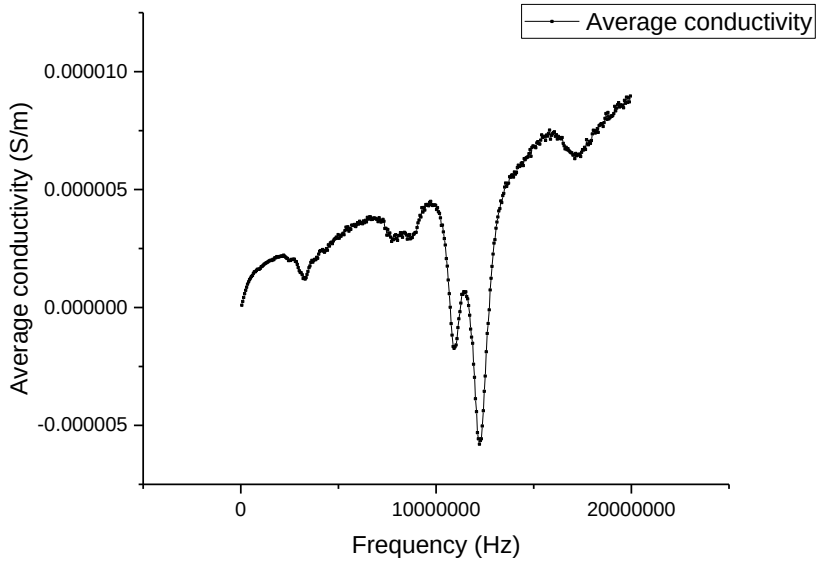

Figure 4.2: Conductivity vs frequency of epoxy single phase samples, the spectrum was measured with small aluminum tape.

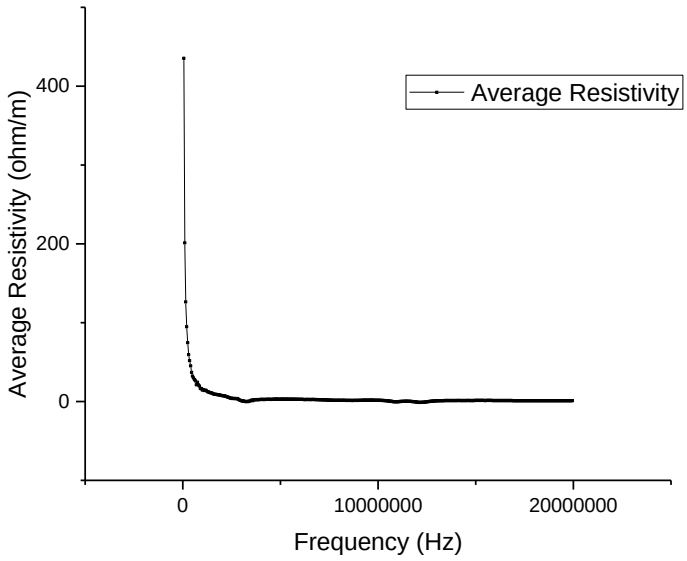

Figure 4.3: Resistance vs frequency of epoxy single phase samples, the spectrum was measured with small aluminum tape.

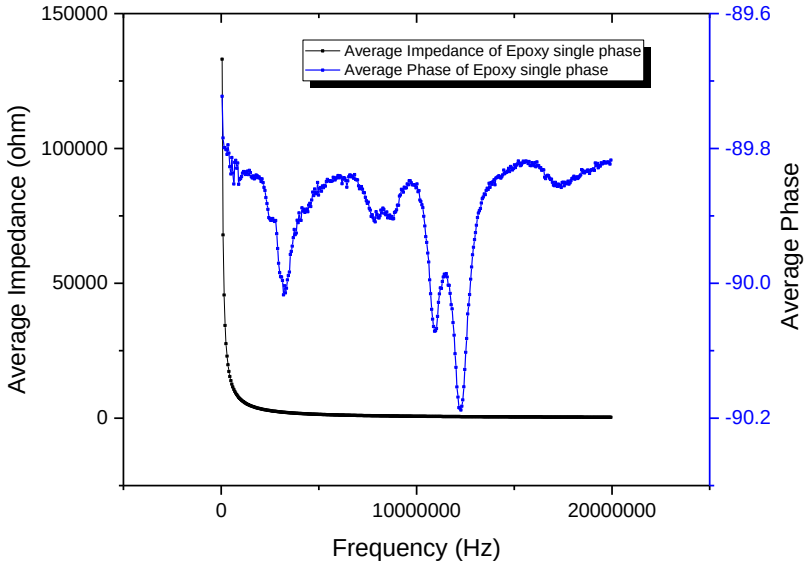

Figure 4.4: Impedance/Phase vs frequency of epoxy single phase samples, the spectrum was measured with small aluminum tape.

4.3 PZT-Epoxy Dome Results for Optimized Fabrication Method

To address the issues such as air bubbles and agglomerations of PZT, the sonication time was increased in order to achieve better dispersion of PZT particles within the sol gel prior to deposition of the layer. Also a desiccation step is also added to reduce the air trapped in the sol. PZT volume fractions that ranged from 0.10 to 0.70 were fabricated, and polarized Corona charges at 45kv/mm. All the viscosities prior to deposition were maintained in 150mpas~200mPas range. The viscosity values are shown in Table 4.1. (To meet the viscosity requirement, sols of lower volume fractions required longer curing times ~2-3hours longer during the last sonication step), all sample are fabricated with spin-speed/time profile 3.

Table 4.1 Measurement of viscosity

Volume fraction of PZT	Average thickness (Microns)	Viscosity (mPas @100rpm)
0.7	0.178	158.4
0.6	0.188	175.5
0.5	0.139	159.5
0.4	0.136	194.7

As in all four volume fractions presented in Table 4.1, the viscosities were within range 150mPas-200mPas, but the thickness were not similar. Especially for 0.5 volume fraction of PZT, the viscosity is similar to the viscosity of 0.7 volume fraction of PZT, but the thickness is 39μm lower when compared to 0.7 volume fraction of PZT.

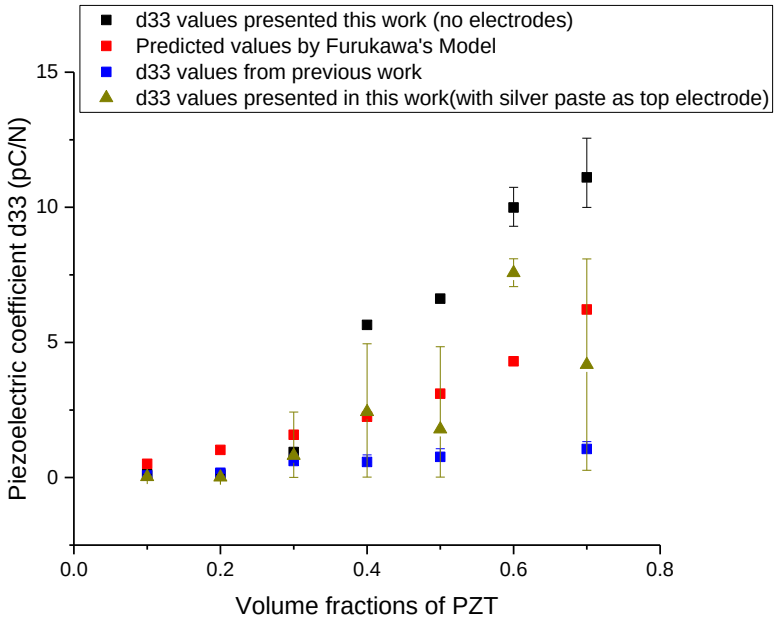

Figure 4.5: Piezoelectric longitudinal coefficient d33 values of this work (without top electrode), this work (with silver paste as top electrodes), previous work, and predicted values by Furukawa are plotted. The d33 values presented in this work, have been

The longitudinal piezoelectric coefficient d_{33} values obtained by this work with and without electrodes, the previous d_{33} values and d_{33} values predicted by Furukawa's analytical model[97] are shown in Figure 4.5. When tested without top electrodes, d_{33} values from this work and previous work both are increasing with the volume fractions of PZT, similar trend has been found in other PZT-polymer composite[97, 98]. B Satish et al[99] fabricated PZT-PVDF 0-3 composites; the piezoelectric coefficient d_{33} they reported also shown a positive correlation with the increasing volume fractions of PZT, the highest d_{33} they reported was 25pC/N, from 0.7 volume fraction of PZT. It is comparable with our present results which is 11.106 pC/N @70% PZT as they use PVDF, which also has piezoelectric coefficient d_{33} around 28 pC/N[99], as the matrix.

d_{33} values obtained by this work is one magnitude higher than values obtained from previous work. This could because (1) we increased the sonication time, which will result in better dispersion of PZT particles. (2) The corona poling allowed us to pole the samples at a higher voltage, which will improve the efficacy of the polarization process.

The experimental values obtained in present work are in agreement with theoretical values; in higher volume fractions of PZT the experimental values are even higher than predicted values. Also a sharp drop in d_{33} at 0.3 volume fraction of PZT could be observed in our present work. The d_{33} measured with silver paste as top electrode is similar or smaller than original measurement (i.e. measurement captured on same samples but no electrodes were applied), this could because during the process of applying the silver paste on top of the film, some silver paste found its way through the film and eventually connected to the bottom stainless steel substrate causing the sample to short cuircuit.

The transvers piezoelectric coefficients -d31 values of this work and previous work are shown in Figure 4.6, the values of our present work are also comparable to others, 4pC/N @(0.21) PZT-PVDF 0-3 composites fabricated by Furukawa et al[100].

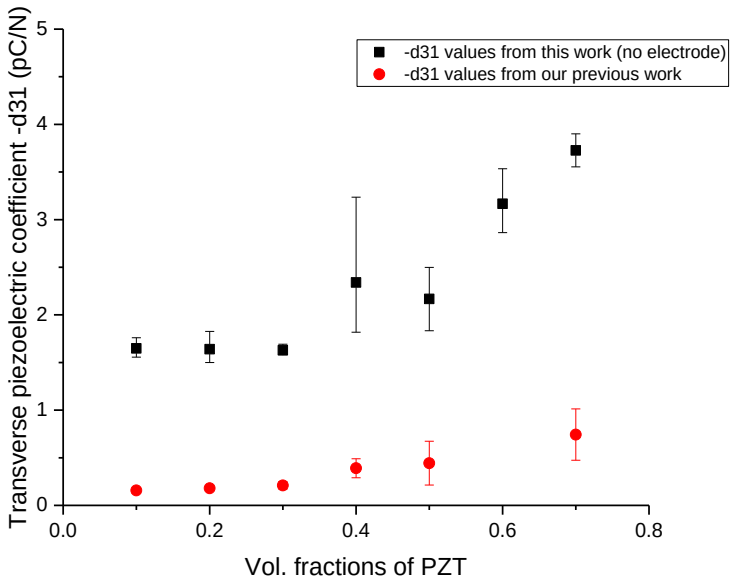

Figure 4.6: Piezoelectric coefficient -d31 values of this work and previous work. The samples from previous work were contact poled, and the samples from this work were corona charges poled at 45kv/mm. There was no electrode applied in both cases.

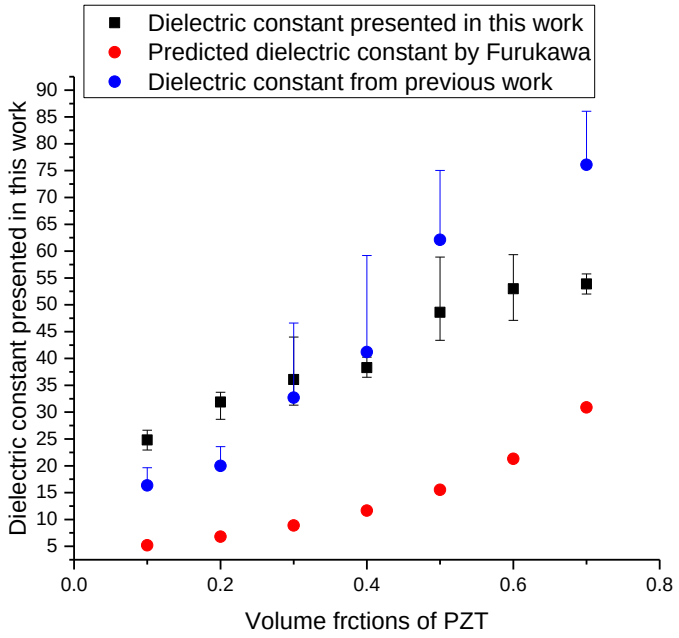

Figure 4.7: Dielectric constant of present work, previous work and predicted values by Furukawa. No electrodes applied in both cases.

Dielectric constant is tested under the room condition @110Hz. In both previous work and this work, the dielectric constants are increasing with the volume fractions of PZT. The dielectric constant of this work is smaller than previous work, this could because of the reduction of the agglomeration of PZT. As in Figure 4.7, the experimental values and the predicted values have similar trends, and experimental values and predicted values are comparable.

Comparison in important properties between previous work and this present work at 0.7 volume fraction of PZT are shown in Table 4.2 Comparison between corona poled and contact poled data in 70% PZTTable 4.2

Table 4.2 Comparison between corona poled and contact poled data in 70% PZT

	Contact poled 0.7 PZT	**Corona poled 0.7 PZT**
Piezoelectric strain coefficient, d_{33}	1.18pC/N	11.11pC/N
Piezoelectric strain coefficient, d_{31}	0.75pC/N	3.73pC/N
Dielectric constant	76.10048	53.87

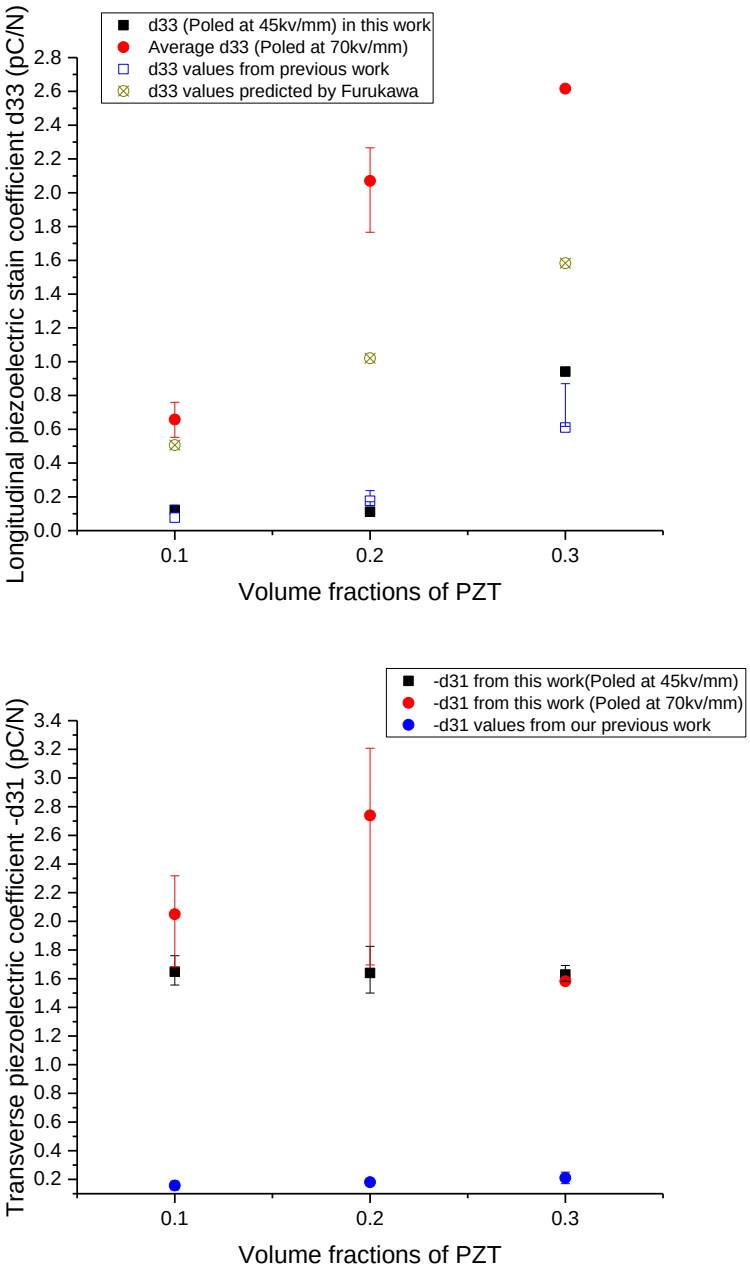

Figure 4.8: Longitudinal piezoelectric coefficient d_{33} and transverse piezoelectric coefficient d_{31} of previous work, this work (corona poled at 70kv/mm), this work (corona poled at 45kv/mm) and predicted values from Furukawa(only for d_{33}).

From Figure 4.8, the d_{33} values of samples poled under 70kv/mm are substantially higher than samples poled with 45kv/mm, with same volume fractions of PZT. The pie-

zoelectric coefficient d_{33} captured from samples poled at 70kv/mm are more in agreement with the predicated values than samples poled with 45kv/mm. But d_{31} values are similar in both sets of samples, both sets of corona poled samples have higher - d_{31} values than previous work.

Frequency spectrums of properties of samples fabricated by updated methods are shown below.

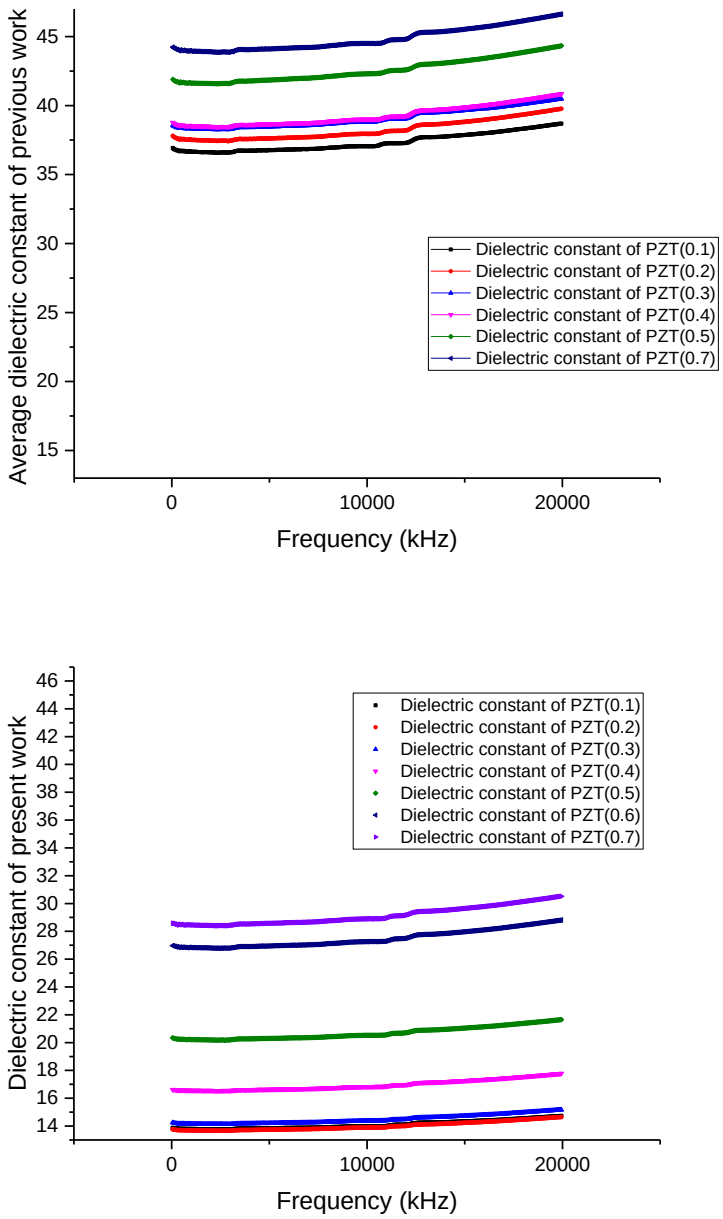

Figure 4.9: The dielectric spectroscopy (2kHz-20MHz) of previous work and this work, the spectrums were obtained with small triangular aluminum tape as top electrode in both cases.

The capacitance was measured, and then the dielectric constant was calculated for both previous work and present work. As our frequency range is 2kHz-20MHz, space charge polarization that mostly responsible for lower frequencies could not be clearly ob-

served in Figure 4.9 (this is because due to the equipment, the second measurement frequency is 50kHz). Within 2kHz~1MHz, the spectrums show mostly dipolar polarizations and since space charge polarizations could not follow the frequencies, the dielectric constant shows a decreasing trend versus the increasing frequency. Within 1MHz~10MHz, the frequency dependence of the dielectric constant is very low and this polarization is mostly the result of ionic mechanism. The increasing dielectric constant with frequency above 10MHz could be resulted from the epoxy phase, since in Figure 4.1, epoxy single phase samples show a substantial positive correlation with the increasing frequency.

In corona poled samples and contact poled samples' spectrums, dielectric constants are increasing with the volume fractions of PZT. The dielectric constant of present work is smaller than previous work; this could because the reduction of the sample thickness, as there was less dielectric material. The dielectric constants are less dependent on frequencies too.

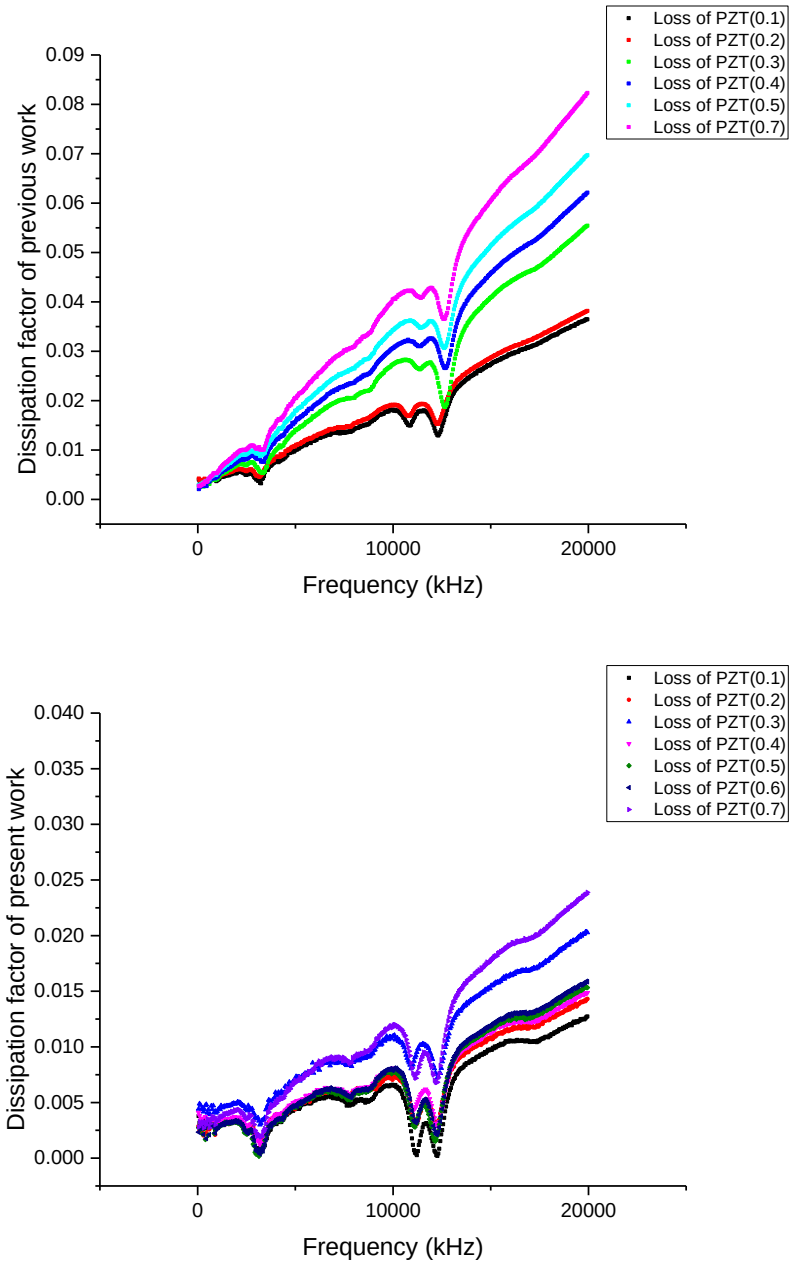

Figure 4.10: Dissipation factor verse frequency (2kHz-20MHz) of previous work and this work, the spectrums were obtained with small triangular aluminum tape as top electrode for both cases.

Figure 4.10 shows the dissipation factors of both contact poled corona poled samples; in both cases the dissipation factors increase with the volume fractions of PZT. The dissipation factor of PZT (~2.5%) is relatively higher than epoxy matrix (0.002~0.004).

The spectrums also show a substantial increase with the frequency, as epoxy's dissipation factor is relatively stable, this increase is largely due to PZT inclusions. The dissipation factors of present work are smaller than previous work as the samples fabricated by up-dated methods this could because the reduction of air trapped in samples and better distribution of PZT in the epoxy matrix.

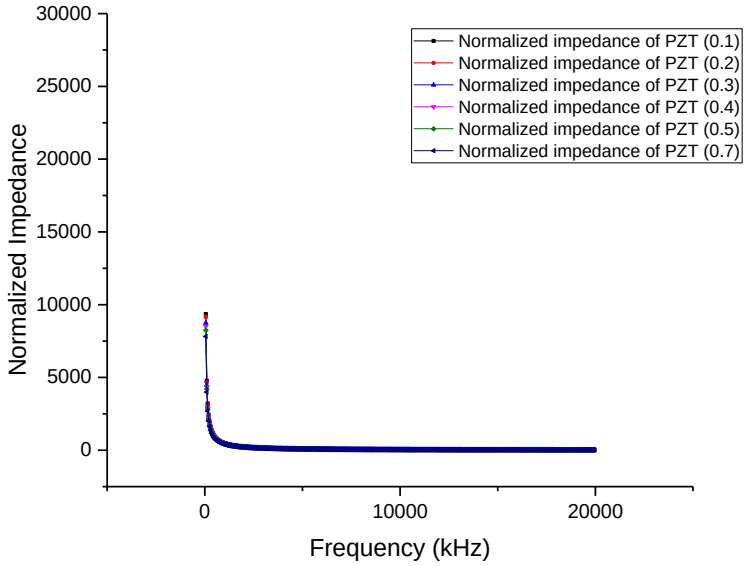

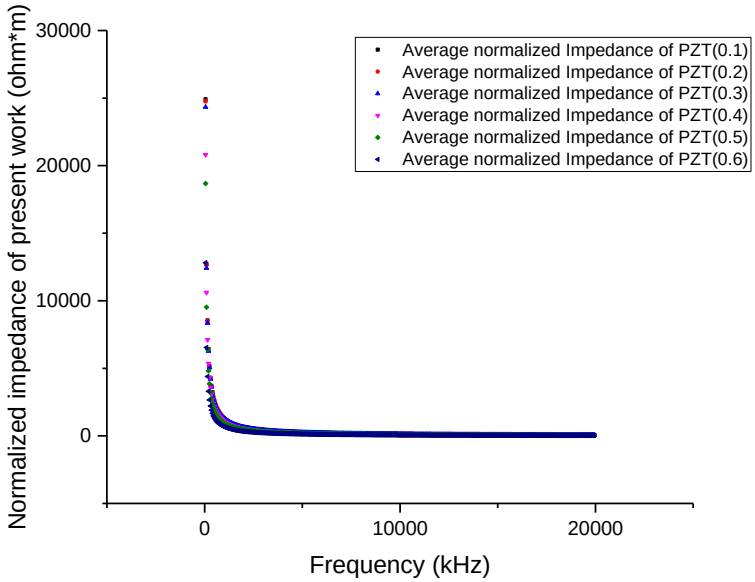

Figure 4.11: Normalized impedance verse frequency (2kHz-20MHz) of previous work and this work, the spectrums were obtained with small triangular aluminum tape as top electrode for both cases.

Shown in Figure 4.11, the impedance in both previous work and present work decrease with the volume fractions of PZT. Compared to previous work, the impedances are higher in present work.

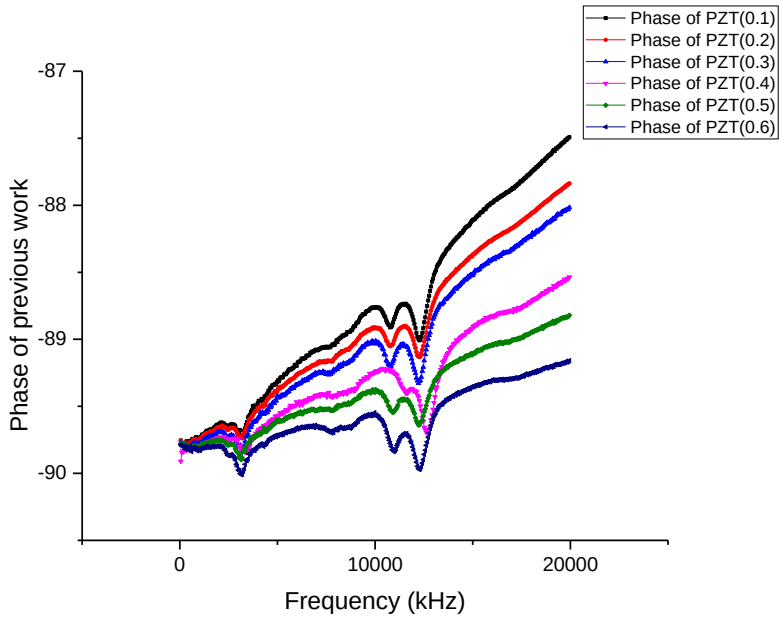

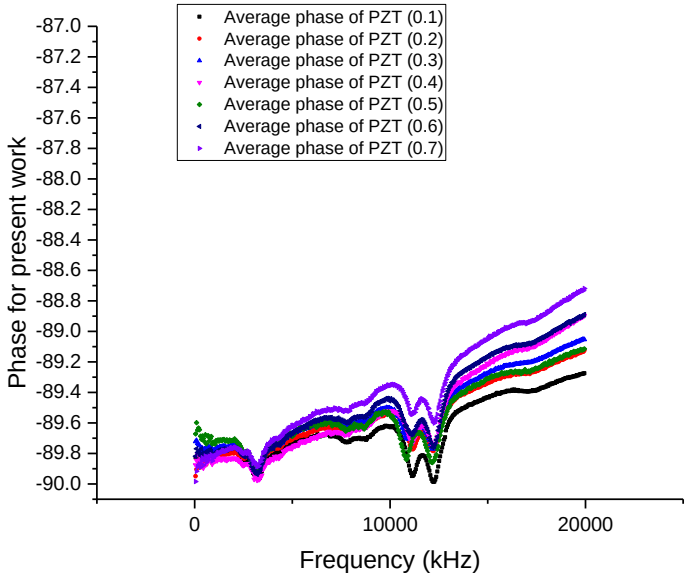

Figure 4.12: Phase verse frequency (2kHz-20MHz) of previous work and this work, the spectrums were obtained with small triangular aluminum tape as top electrode for both cases.

In a pure capacitive circuit, the phase of voltage will be 90° behind the alternative current. As seen in Figure 4.12 in both previous and present work, the phases increase with frequency, as the materials will be less dielectric in high frequency region. Phase increases are also increase with volume fractions of PZT. Phases in each volume fractions in present work are lower than the corresponding part in previous work, this could indicate that the updated method has better capacitive property.

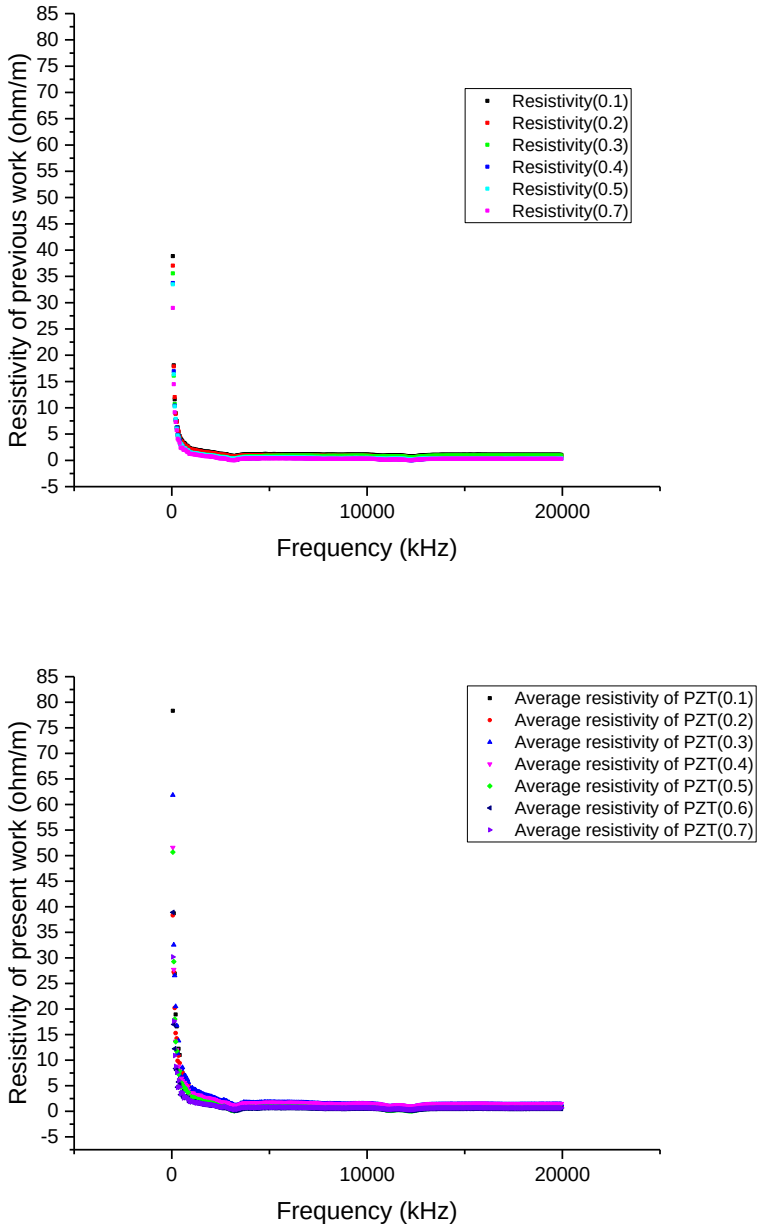

Figure 4.13: Resistivity verse frequency (2kHz-20MHz), these samples are fabricated with updated method; the spectrums were obtained with small triangular aluminum tape as top electrode.

Similar to impedance spectrum, Figure 4.11 shows that resistivity decreases with the increasing PZT volume fractions. And the resistivity of previous work is lower than

present work, together with impedance spectrum, could indicated that the samples fabricated with updated method could have lower leakage current.

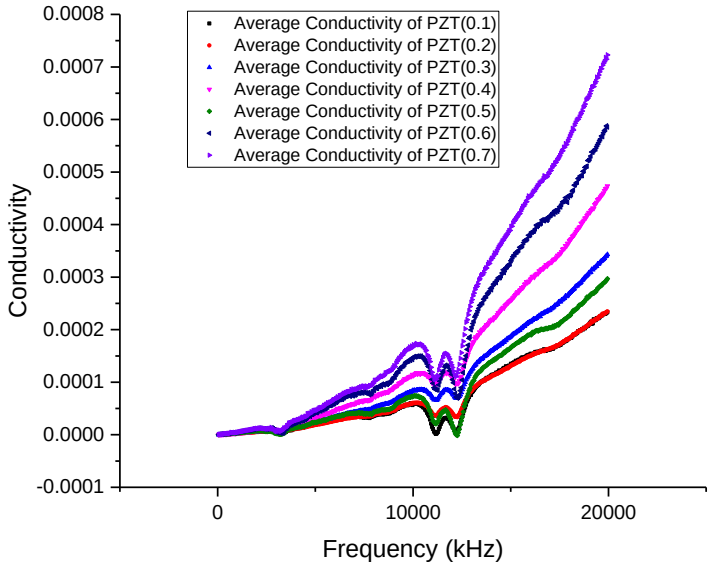

Figure 4.14: Conductivity verse frequency (2kHz-20MHz), these samples are fabricated with updated method; the spectrums were obtained with small triangular aluminum tape as top electrode.

The conductivity of the present work is found to be increasing with the increase of volume fractions of PZT and the frequency, similar as A. Seema et al[98].

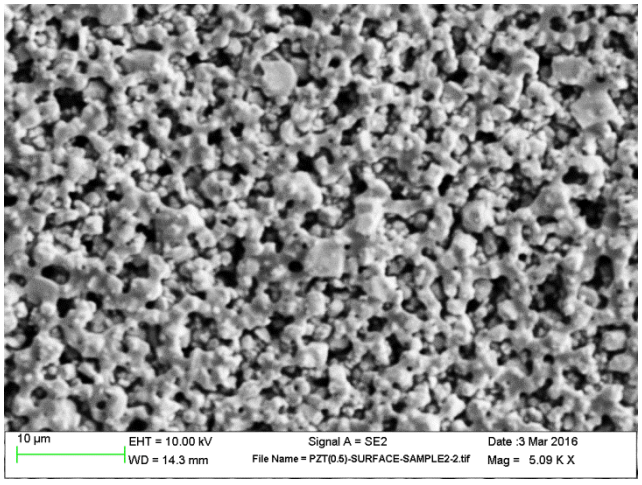

Figure 4.15: Surface of PZT (0.5)-Epoxy 0-3 dome shape structure.

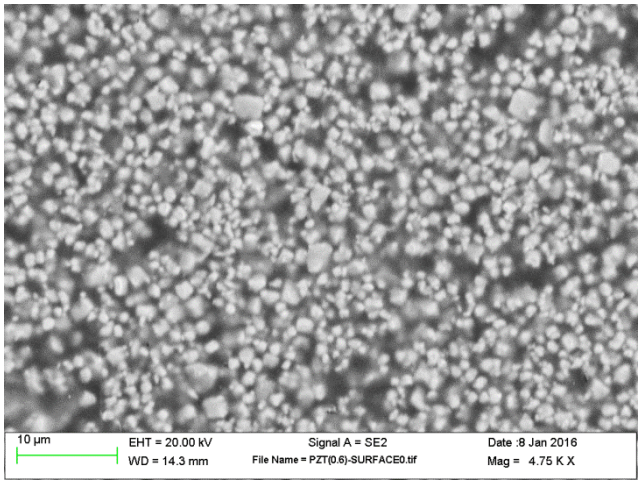

Figure 4.16: Surface of PZT (0.6)-Epoxy 0-3 dome shape structure.

Figure 4.15 and Figure 4.16 shows the surface morphology of 50%PZT and 60%PZT composites. PZT particles haven been using in the study has mean diameters as 0.97µm, has comparable size to the clusters shown in Figure 4.15 and Figure 4.16, this indicated that PZT particles are well distributed in epoxy matrix, no significant agglomerations are observed. There were no pores observed in both SEM images.

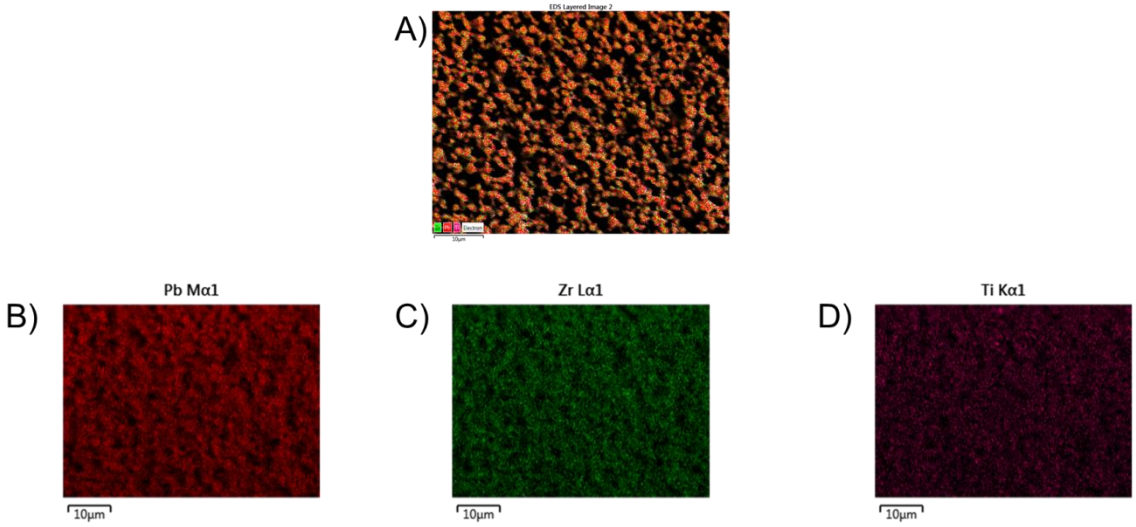

Figure 4.17: EDS images of PZT(0.5)-Epoxy 0-3 dome shape structure. A) SEM images with distribution of Pt, Zr and Ti. B) Distribution of Pb. C) Distribution of Zr. D distribution of Ti.

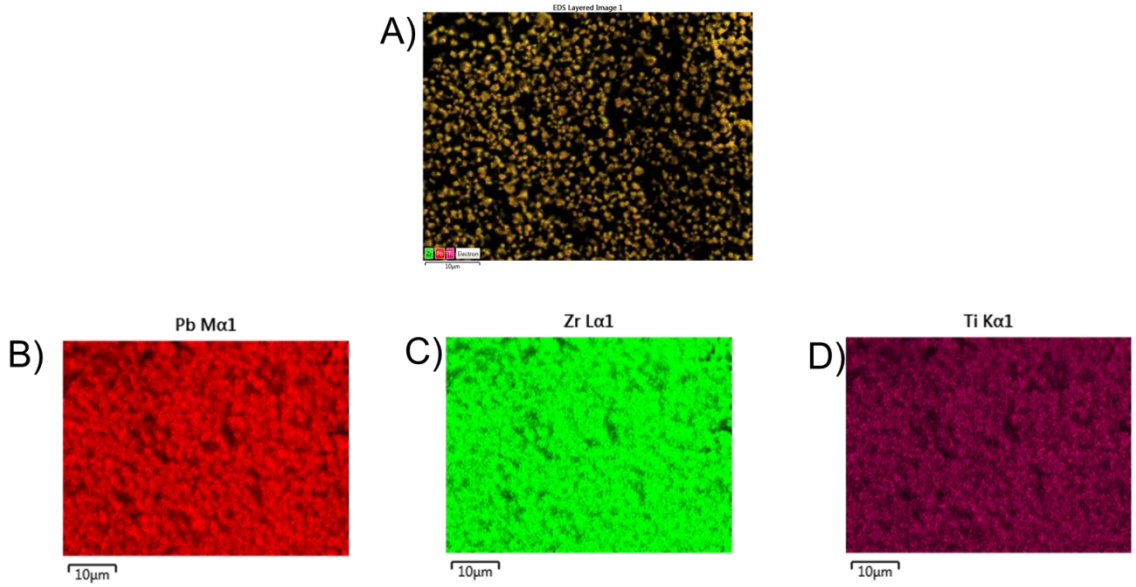

Figure 4.18: EDS images of PZT (0.6)-Epoxy 0-3 dome shape structure. A) SEM images with distribution of Pt, Zr and Ti. B) Distribution of Pb. C) Distribution of Zr. D distribution of Ti.

Figure 4.17 and Figure 4.18 shows EDS images of 50%PZT and 60%PZT composites, further indicate the distribution of PZT in epoxy matrix.

4.4 Spin-speed/time profile study

Originally we used the spin coat speed and time intervals describe in the previous paper, however since a few changes are made in fabrication methods (Fixed the ethanol usage in this study, increase the amount of time in the original sonication and adding desiccation and sonication steps) the sample fabricated could not present electromechanical responses. The spin coat speed and time intervals are designed by experiments described in Table 4.3. All steps before spin coating are maintained as main procedure. And in the spin coating process, 4 combinations of spin coating speeds and time intervals are studied. This study was done on 50% of PZT in volume fractions, the viscosity prior to deposition is 164.5mPas @100rpm.

We studied how the spin-coating time intervals and speed will affect the thickness of the sample, and eventually affect the piezoelectric and dielectric properties. This study was performed at 50%PZT.

Table 4.3 Spin-speed/time profile study

	Average piezoelectric layer thickness (mm)	**Planned Poling voltage (kv)**	**Planned Poling electric field (kv/mm)**	**d33(pC/N)**	**Capacitance (pF)**	**Calculated dielectric constant**	**comment**
Profile (1)	0.105	4.7	45	-0.04	10.5	25.36	The d_{33} values here shown is within the margin of the equipment
Profile (2)	0.141	6.3	45	7.26	13.9	45.08	Higher at center where is thicker
Profile (3)	0.177	8	45	7.52	15	61.07	
Profile (4)	0.241	10.8/7.8	45	4.27	18.3	101.44	Short circuit @45kv/mm
Datum	0.089	4.1	45	0.02	9.8	20.06	

As we could see from Table 4.3 the first sample which was fabricated with profile 1 shown no piezoelectric response.

Samples fabricated through profile 2 and 3 presents reasonable d_{33} value, but the center of the sample fabricated through profile 2 appears to be thicker than elsewhere. Samples fabricated through profile 3 have uniform thickness throughout the whole sample, and presents reasonable piezoelectric response.

4.5 Deposion technique study

The deposing techniques study was done on 0.35 PZT, this volume fraction of PZT was chosen because of discontinuity in piezoelectric property at volume fractions of PZT below 0.4. There were 3 starting viscosities, 150mPas, 248.7mPas and 299mPas respective-

ly, chosen from 150-200mPas, 200-250mPas, and 250-300mPas ranges to investigate the influence of viscosity on piezoelectric and dielectric properties.

There were 8 processes including our datum study are employed, this allows us to investigate the influence of time between depositions and the numbers of layer on piezoelectric and dielectric properties.

Table 4.4 Deposition techniques study's results

Profile	Viscosity tested	d33	Average capacitance (pF)	Piezoelectric layer thickness (mm)	Calculated dielectric constant	Corona poling electric field
Datum study	150mPas	-0.02	22.9	0.065	34.23953	45kv/mm
Process A	248.7mPas	0.01	21.7	0.087	43.42681	45kv/mm
	299.3mPas	0.02	22.4	0.115	59.25498	45kv/mm
Process B	150mPas	0.02	20.8	0.085	40.66879	45kv/mm
	248.7mPas	0.02	20.8	0.127	60.76396	45kv/mm
	299.3mPas	4.32	20.08	0.147	67.89848	45kv/mm
Process C	150mPas	0.02	23.22	0.093	49.67343	45kv/mm
	248.7mPas	0.01	22.3	0.113	57.96453	45kv/mm
	299.3mPas	5.45	20.94	0.149	71.76983	45kv/mm
Process D	150mPas	0.03	24	0.103	56.8627	45kv/mm
	248.7mPas	5.78	19.9	0.141	64.5433	45kv/mm
	299.3mPas	5.51	19.25	0.167	73.94796	45kv/mm
Process E	150mPas	5.51	20.5	0.129	60.83066	45kv/mm
	248.7mPas	5.74	18.43	0.173	73.35487	45kv/mm
	299.3mPas	5.37	18.42	0.179	75.84407	45kv/mm
Process F	248.7mPas	4.62	15.4	0.217	76.87045	Dielectric break down @45kv/mm
	299.3mPas	4.02	15.76	0.227	82.29265	Dielectric break down @45kv/mm
Process G	248.7mPas	0.04	19.45	0.118	52.79352	45kv/mm
	299.3mPas	4.34	19	0.143	62.49836	45kv/mm

As we can see in the table, the sample fabricated with our datum process shown no piezoelectric response, neither do samples fabricated through process A, which have elevated viscosities.

Process B, C and D are involved with two times deposition. Samples with all viscosity fabricated through process B experience no piezoelectricity. Sample has viscosity as 299mPas, fabricated through process C, shows longitudinal piezoelectric coefficient after poled by 45kv/mm, the value captured here is comparable to 0.4 volume fraction of PZT sample, which is 5.6pC/N respectively. Samples fabricated though the same process but with lower viscosity still shown no piezoelectric response. Fabricated though process D, samples fabricated with higher viscosity (i.e. 248.7mPas and 299mPas) experience piezoelectricity.

Process E and F are involved with three times deposition. Fabricated through E, samples with all viscosities tested shown reasonable longitudinal piezoelectric coefficient. Only two samples were fabricated through process F, and both them experienced dielectric break down during the poling process, there d_{33} values are lower compared to other sample with same volume fraction.

And when the starting viscosity is high enough, and waited for a longer time, 1h, respectively, the samples fabricated through Process G, similar to datum process could also have piezoelectric charge coefficients measurement, as the container was covered during the whole experiment period which avoided the evaporation of ethanol, this could come from the viscosity increase by the epoxy hardener.

All these studies show that, within the range of viscosity we decided for higher PZT volume fractions (0.4~0.7), lower volume fractions of PZT (0.1~0.3) requires multiple depositions to achieve the favorable thickness. And with the increasing viscosity and right technique, the samples of lower volume fractions of PZT (0.1~0.3) could also be possible to fabricate with single deposition. If the thickness is to maintain, we should ei-

ther increase the viscosity reading to 300mPas-350mPas or fabricate through profile 5 when the viscosity is maintained in 150-200mPas.

4.6 Summary of the Optimized Processing Conditions

The spin/speed profile 3 offers most uniform surface, and reasonable longitudinal piezoelectric d_{33} was observed, the d_{33} value is 7.52pC/N at 05 volume fraction of PZT. Compared to contact poling, samples poled by corona charges experience stronger piezoelectric effect. For volume fractions 0.4-0.7 of PZT, the original deposition method was sufficient to achieve reasonable piezoelectric response, the values for d_{33} and $-d_{31}$ were 11.11pC/N and -4pC/N respectively at 0.7 volume fraction of PZT. For volume fractions 0.1-0.35 of PZT, the process D (when the viscosity is within 200mPas-250mPas) should be employed, the d_{33} value is 5.78pC/N at 0.35 volume fraction of PZT.

The agglomeration may be attributed to several mechanisms of agglomeration: Brownian, gravitational, turbulent, and electrostatic, where the gravitational form is mitigated by the spin coating process. This can be validated through Figure 4.15 and Figure 4.16, where minimal coagulation of particles is observed at the interface of the substrate and the composite. The as-received PZT powders tend to naturally form clusters that vary between 5-20 μm in the case of aluminum and 10-25 μm in the case of PZT, where these agglomerations are most likely attributed to electrostatic agglomeration. Addition of ethanol to the mixture did not effectively change the pH of the solution to negate the surface charge on the all of the particles which most likely diminished its effectiveness in counteracting the electrostatic forces between particles. The extent of the effectiveness of the

ethanol on the pH of the solution was also a function of the number of particles within the colloidal sol gel.

4.7 Displacement measurement

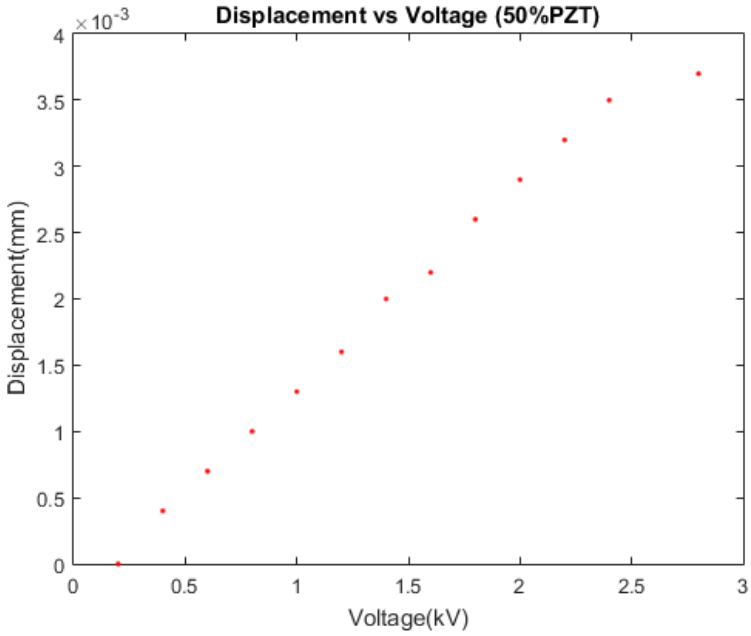

Figure 4.19: Displacement data of 0.5 volume fraction of PZT .

Figure 4.19 shows the displacement of 0.5 volume fraction of PZT composites. The displacement is increasing with the incremental voltage; the largest displacement is 3.7μm, highest strain rate is 2.7%, found @20kV/mm.

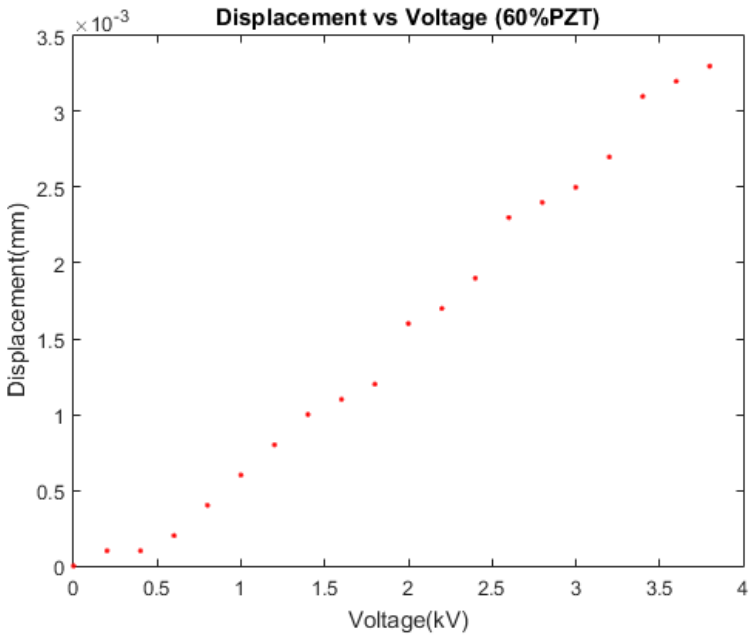

Figure 4.20: Displacement data of 0.6 volume fraction of PZT.

Figure 4.20 shows the displacement of 0.6 volume fraction of PZT composites. The displacement is also increasing with the incremental voltage; the largest displacement is 3.2μm, highest strain rate is 1.7%, found @20kV/mm.

4.8 P-E Hysteresis loop.

The P-E hysteresis loos of 0.5volume fraction and 0.6 volume fraction are presented below.

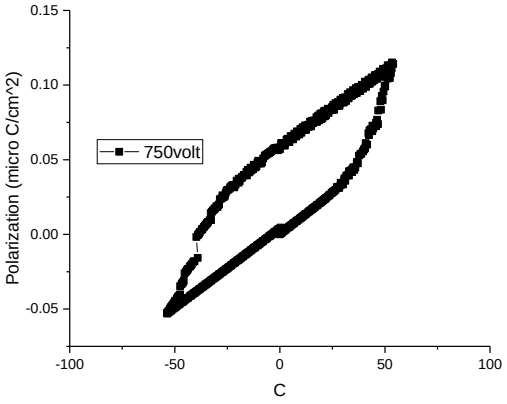

Figure 4.21: Hysteresis loop of PZT(0.5)-Epoxy dome shape structure under 53.9kv/cm.(thickness 0.139mm)

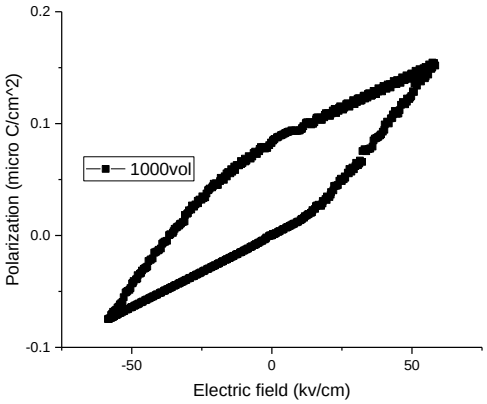

Figure 4.22: Hysteresis loop of PZT(0.6)-Epoxy dome shape structure under 58.48kv/cm.(thickness 0.188mm)

Chapter 5

Conclusions and Future work

5.1 Conclusions

Piezoelectric 0-3 composites PZT-Epoxy with PZT's volume fractions 0%-70% are fabricated using a combination of solvent and spin coat deposition technique. In the presented work, the fabrication methods are updated to improve longitudinal and transverse piezoelectric coefficients in PZT-Epoxy 0-3 composites. Both longitudinal and transverse piezoelectric coefficients are increasing with the volume fractions of PZT. Compared to previous work, the piezoelectric characteristic is enhanced largely. This could because of the employment of corona poling technique, and better mixing of the two phases. The longitudinal piezoelectric coefficient d_{33} and dielectric constant are in agreement with values predicted by Furukawa's analytical model. Specifically, the values for $d_{33,}$ d_{31} and dielectric constant were 11.11pC/N, -4pC/N and 56 respectively at 79% volume fraction of PZT. Similar and lower values of the longitudinal piezoelectric coefficient d_{33} were observed with silver paste as top electrode, this could because the silver pastes could create electric pathway to cause samples to short circuit. Based on SEM images and EDS micrographs obtained the agglomerations of PZT in the composite are largely reduced, and the distribution of PZT in the composite are uniform. Dielectric constant is increasing the volume fractions of PZT, this due to the increase in the effective dipole moment of the piezoelectric component. The dielectric constant of the present work is smaller than

previous work in corresponding volume fractions, this could be a result of the reduction of agglomeration of PZT. These results indicate that devices such as these may have potential applications as energy harvester, actuator and capacitors. Corona poling with different voltages in lower volume fractions of PZT were studied additionally, the piezoelectric response in longitudinal mode was improved; however there was no significant improvement in transverse mode observed. There was clear dependence of impedance, phase, dielectric constant, loss, conductivity and resistivity on the frequency. Like previous results, impedance, and phase are reducing with the increasing volume fractions of PZT, and dielectric constant, conductivity and loss are increasing with the increasing volume fractions of PZT. The impedance and resistivity are increased compare to the corresponding volume fractions in the previous work, this indicate less leakage current could occur when subjected to alternative currents.

The spin-speed/time profiles were studied at 0.5 volume fractions of PZT ,sample fabricated through profile 3 had largest piezoelectric coefficient d_{33} value, 7.52pC/N respectively.

The discontinuity in longitudinal piezoelectric coefficient d_{33} was observed in lower volume fractions of PZT (i.e. 0.1-0.3). To address the issue, a depositing technique study at 0.35 volume fraction of PZT was carried out. The results shown that samples fabricated with Process D (viscosity~200mPas~250mPad) had most optimized d_{33} value, 5.78pC/N respectively.

The displacement of 50% and 60% volume fraction of PZT were studied, the devices were subjected to step increasing electric file. The largest electric field applied as 20kv/mm, half of the poling electric filed. The largest displacement of 50% and 60% vol-

ume fraction of PZT were observed as 3.7μm and 3.2μm, and the strain rate corresponding were 2.7% and 1.7% respectively.

Lastly, the P-E hysteresis loops of 50% and 60% volume fraction of PZT are presented.

5.2 Future work

To further enhance the piezoelectric characteristics, the future work will include a conductive third phase. The influence of the conductive third phase on piezoelectric behavior will be further investigated by fabrication and analysis of three phase composites by variation of the PZT volume fraction and the volume fractions of the conductive third phase. Dome shaped thick film composites will be fabricated to understand both the d33 and d31 piezoelectric strain characteristics. The dependence if impedance, dielectric constant, resistivity and conductivity will be further studied. Devices displacement and P-E hysteresis will also be investigate.

References

[1] S. R. Anton and H. A. Sodano, "A review of power harvesting using piezoelectric materials (2003–2006)," *Smart materials and Structures*, vol. 16, p. R1, 2007.

[2] J. Baker, S. Roundy, and P. Wright, "Alternative geometries for increasing power density in vibration energy scavenging for wireless sensor networks," in *Proc. 3rd Int. Energy Conversion Engineering Conf.(San Francisco, CA, Aug.)*, 2005, pp. 959-70.

[3] S. Banerjee, "An experimental and theoretical analysis of two and three phase epoxy based piezoelectric composites," Rutgers University-Graduate School-New Brunswick, 2013.

[4] R. C. Buchanan, E. Park, R. Surana, H. Tennakone, and K. Tennakone, "High piezoelectric actuation response in graded Nd2O3 and ZrO2 doped BaTiO3 structures," *Journal of electroceramics*, vol. 26, pp. 116-121, 2011.

[5] O. Delas, A. Berry, P. Masson, and Y. Pasco, "Optimizing the thickness of piezoceramic actuators for bending vibration of planar structures," *Journal of Intelligent Material Systems and Structures*, vol. 18, pp. 1191-1201, 2007.

[6] G. H. Haertling, "Ferroelectric ceramics: history and technology," *J. Am. Ceram. Soc.*, vol. 82, pp. 797-818, 1999.

[7] C.-H. Nguyen, S. Pietrzko, and R. Buetikofer, "The influence of temperature and bonding thickness on the actuation of a cantilever beam by PZT patches," *Smart materials and structures*, vol. 13, p. 851, 2004.

[8] A. Nisar, N. Afzulpurkar, B. Mahaisavariya, and A. Tuantranont, "MEMS-based micropumps in drug delivery and biomedical applications," *Sensors and Actuators B: Chemical*, vol. 130, pp. 917-942, 2008.

[9] L. APC International, *Piezoelectric Ceramics: Principles and Applications*: APC International, 2002.

[10] D. Wang, Y. Fotinich, and G. P. Carman, "Influence of temperature on the electromechanical and fatigue behavior of piezoelectric ceramics," *Journal of Applied Physics*, vol. 83, pp. 5342-5350, 1998.

[11] S. Mall and T. Hsu, "Electromechanical fatigue behavior of graphite/epoxy laminate embedded with piezoelectric actuator," *Smart Materials and Structures*, vol. 9, p. 78, 2000.

[12] D. P. Wang and G. P. Carman, "Combined electrical and mechanical fatigue of piezoelectric ceramics undergoing polarization switching for large displacement actuation," 1998, pp. 210-221.

[13] J. E. Frank, G. H. Koopmann, W. Chen, and G. A. Lesieutre, "Design and performance of a high-force piezoelectric inchworm motor," 1999, pp. 717-723.

[14] C. Caliendo, S. Sait, and F. Boubenider, "Love-Mode MEMS Devices for Sensing Applications in Liquids," *Micromachines,* vol. 7, p. 15, 2016.

[15] A. Dogan, K. Uchino, and R. E. Newnham, "Composite piezoelectric transducer with truncated conical endcaps" Cymbal"," *Ultrasonics, Ferroelectrics, and Frequency Control, IEEE Transactions on,* vol. 44, pp. 597-605, 1997.

[16] S. Shahab, D. Tan, and A. Erturk, "Hydrodynamic thrust generation and power consumption investigations for piezoelectric fins with different aspect ratios," in *ASME 2015 Conference on Smart Materials, Adaptive Structures and Intelligent Systems*, 2015, pp. V002T06A011-V002T06A011.

[17] H. Shen, F. S. Zhang, H. L. Ji, J. H. Qiu, and Y. X. Bian, "Self-powered semi-passive vibration damping system based on self-sensing approach," in *Seventh International Symposium on Precision Mechanical Measurements*. vol. 9903, L. Yu, Ed., ed Bellingham: Spie-Int Soc Optical Engineering, 2016.

[18] Y. Jia, C. D. Do, X. D. Zou, and A. A. Seshia, "A Hybrid Vibration Powered Microelectromechanical Strain Gauge," *Ieee Sensors Journal,* vol. 16, pp. 235-241, Jan 2016.

[19] M. Kuna, "Fracture mechanics of piezoelectric materials – Where are we right now?," *Engineering Fracture Mechanics*, vol. 77, pp. 309-326, 1// 2010.

[20] H. J. Hwang, M. Yasuoka, M. Sando, M. Toriyama, and K. Niihara, "Fabrication, Sinterability, and Mechanical Properties of Lead Zirconate Titanate/Silver Composites," *Journal of the American Ceramic Society,* vol. 82, pp. 2417-2422, 1999.

[21] S. Choi, H. Lee, and W. Moon, "A micro-machined piezoelectric hydrophone with hydrostatically balanced air backing," *Sensors and Actuators A: Physical,* vol. 158, pp. 60-71, 2010.

[22] H. Lee, S. Choi, and W. Moon, "A micro-machined piezoelectric flexural-mode hydrophone with air backing: Benefit of air backing for enhancing sensitivitya)," *The Journal of the Acoustical Society of America,* vol. 128, pp. 1033-1044, 2010.

[23] K. Cook-Chennault, N. Thambi, and A. Sastry, "Powering MEMS portable devices—a review of non-regenerative and regenerative power supply systems

with special emphasis on piezoelectric energy harvesting systems," *Smart Materials and Structures,* vol. 17, p. 043001, 2008.

[24] K. A. Cook-Chennault, N. Thambi, M. A. Bitetto, and E. Hameyie, "Piezoelectric energy harvesting a green and clean alternative for sustained power production," *Bulletin of Science, Technology & Society,* vol. 28, pp. 496-509, 2008.

[25] H.-S. Yoon, G. Washington, and A. Danak, "Modeling, optimization, and design of efficient initially curved piezoceramic unimorphs for energy harvesting applications," *Journal of Intelligent Material Systems and Structures,* vol. 16, pp. 877-888, 2005.

[26] F. Amirouche, Y. Zhou, and T. Johnson, "Current micropump technologies and their biomedical applications," *Microsystem technologies,* vol. 15, pp. 647-666, 2009.

[27] M. M. Teymoori and E. Abbaspour-Sani, "Design and simulation of a novel electrostatic peristaltic micromachined pump for drug delivery applications," *Sensors and Actuators A: Physical,* vol. 117, pp. 222-229, 2005.

[28] J. P. Choi, K. S. Kim, Y. H. Seo, and B. H. Kim, "Design and fabrication of synthetic air-jet micropump," *International Journal of Precision Engineering and Manufacturing,* vol. 12, pp. 355-360, 2011.

[29] J. Harrison and Z. Ounaies, *Piezoelectric polymers*: Wiley Online Library, 2002.

[30] J. Dargahi, "Piezoelectric and pyroelectric transient signal analysis for detection of the temperature of a contact object for robotic tactile sensing," *Sensors and Actuators A: Physical,* vol. 71, pp. 89-97, 1998.

[31] S. Banerjee, W. Du, L. Wang, and K. Cook-Chennault, "Fabrication of dome-shaped PZT-epoxy actuator using modified solvent and spin coating technique," *Journal of Electroceramics,* vol. 31, pp. 148-158, 2013.

[32] S. P. Marra, K. T. Ramesh, and A. S. Douglas, "The mechanical properties of lead-titanate/polymer 0–3 composites," *Composites Science and Technology,* vol. 59, pp. 2163-2173, 11// 1999.

[33] S. N. Zhu, B. Jiang, and W. W. Cao, "Characterization of piezoelectric materials using ultrasonic and resonant techniques," in *Ultrasonic Transducer Engineering: Medical Imaging 1998*. vol. 3341, K. K. Shung, Ed., ed, 1998, pp. 154-162.

[34] K. M. Mossi, G. V. Selby, and R. G. Bryant, "Thin-layer composite unimorph ferroelectric driver and sensor properties," *Materials Letters,* vol. 35, pp. 39-49, 1998.

[35] J. Peng, C. Chao, and H. Tang, "Piezoelectric micromachined ultrasonic transducer based on dome-shaped piezoelectric single layer," *Microsystem technologies,* vol. 16, pp. 1771-1775, 2010.

[36] Y. Man-Soon, H. Sung-Moo, and U. Soon-Chul, "A newly designed chopper for pyroelectric infrared sensor by using a dome-shaped piezoelectric linear motor (DSPLM)," *Journal of electroceramics,* vol. 23, pp. 242-247, 2009.

[37] G.-H. Feng, "A piezoelectric dome-shaped-diaphragm transducer for microgenerator applications," *Smart Materials and Structures,* vol. 16, p. 2636, 2007.

[38] G.-H. Feng and E. S. Kim, "Piezoelectrically actuated dome-shaped diaphragm micropump," *Microelectromechanical Systems, Journal of,* vol. 14, pp. 192-199, 2005.

[39] G.-H. Feng, C. C. Sharp, Q. Zhou, W. Pang, E. S. Kim, and K. Shung, "Fabrication of MEMS ZnO dome-shaped-diaphragm transducers for high-frequency ultrasonic imaging," *Journal of Micromechanics and Microengineering,* vol. 15, p. 586, 2005.

[40] B. Gazengel, P. Hamery, P. Lotton, and A. Ritty, "A dome shaped pvdf loudspeaker model," *Acta Acustica United with Acustica,* vol. 97, pp. 800-808, 2011.

[41] M.-S. Yoon, N. H. Khansur, K.-S. Lee, and Y. M. Park, "Compact size ultrasonic linear motor using a dome shaped piezoelectric actuator," *Journal of electroceramics,* vol. 28, pp. 123-131, 2012.

[42] H. Chen, C. Fan, and Z. Meng, "Preparation and electromechanical properties of a piezoelectric ceramic dome-like actuator with d 31 gradients," *Current Applied Physics,* vol. 11, pp. S324-S327, 2011.

[43] K. J. Yoon, S. Shin, H. C. Park, and N. S. Goo, "Design and manufacture of a lightweight piezo-composite curved actuator," *Smart Materials and Structures,* vol. 11, p. 163, 2002.

[44] K. Yoon, K. Park, H. Park, and D. Perreux, "Thermal deformation analysis of curved actuator LIPCA with a piezoelectric ceramic layer and fiber composite layers," *Composites science and technology,* vol. 63, pp. 501-506, 2003.

[45] S.-C. Woo, K. H. Park, and N. S. Goo, "Influences of dome height and stored elastic energy on the actuating performance of a plate-type piezoelectric composite actuator," *Sensors and Actuators A: Physical,* vol. 137, pp. 110-119, 2007.

[46] X. Ruan, B. Cheeseman, A. Safari, S. C. Danforth, and T.-W. Chou, "Design optimization of dome actuators," *Ultrasonics, Ferroelectrics, and Frequency Control, IEEE Transactions on,* vol. 46, pp. 1489-1496, 1999.

[47] G. Lee, K. You, T. Kang, K. J. Yoon, J. O. Lee, and J. K. Park, "Modeling and design of h-infinity controller for piezoelectric actuator LIPCA," *Journal of Bionic Engineering,* vol. 7, pp. 168-174, 2010.

[48] K. Kim, K. Park, H. Park, N. Goo, and K. Yoon, "Performance evaluation of lightweight piezo-composite actuators," *Sensors and Actuators A: Physical,* vol. 120, pp. 123-129, 2005.

[49] M.-S. Kim, H.-R. Ahn, S. Lee, C. Kim, and Y.-J. Kim, "A dome-shaped piezoelectric tactile sensor arrays fabricated by an air inflation technique," *Sensors and Actuators A: Physical,* vol. 212, pp. 151-158, 2014.

[50] Y. Kim, L. Cai, T. Usher, and Q. Jiang, "Fabrication and characterization of THUNDER actuators—pre-stress-induced nonlinearity in the actuation response," *Smart Materials and Structures,* vol. 18, p. 095033, 2009.

[51] S. Chandran, V. Kugel, and L. Cross, "Characterization of the linear and non-linear dynamic performance of RAINBOW actuator," in *Applications of Ferroelectrics, 1996. ISAF'96., Proceedings of the Tenth IEEE International Symposium on*, 1996, pp. 743-746.

[52] R. S. Dahiya and M. Valle, *Robotic tactile sensing: technologies and system*: Springer Science & Business Media, 2012.

[53] P. A. Tipler and G. Mosca, *Physics for scientists and engineers*: Macmillan, 2007.

[54] A. Safari, "Polarization-Dilectircs," 2014.

[55] C. Dervos, C. Paraskevas, P. Skafidas, and P. Vassiliou, "A Complex Permittivity Based Sensor for the Electrical Characterization of High-Voltage Transformer Oils," *Sensors,* vol. 5, p. 302, 2005.

[56] F. E. Neumann, "Vorlesungen über die Theorie der Elastizität der festen Körper und des Lichtäthers, edited by O. E. Meyer. Leipzig, B. G. Teubner-Verlag," 1885.

[57] A. Safari, "Ferroelectric Polarization VS. Applied Electric Field," *Presentation: Ferroelectricity I in Advance electronic ceramics class, Rutgers,* 2014.

[58] C. Dias and D. Das-Gupta, "Inorganic ceramic/polymer ferroelectric composite electrets," *Dielectrics and Electrical Insulation, IEEE Transactions on,* vol. 3, pp. 706-734, 1996.

[59] E. K. Akdogan, M. Allahverdi, and A. Safari, "Piezoelectric composites for sensor and actuator applications," *Ultrasonics, Ferroelectrics, and Frequency Control, IEEE Transactions on,* vol. 52, pp. 746-775, 2005.

[60] R. Newnham, D. Skinner, and L. Cross, "Connectivity and piezoelectric-pyroelectric composites," *Materials Research Bulletin,* vol. 13, pp. 525-536, 1978.

[61] R. E. Newnham, "Composite electroceramics," *Ferroelectrics,* vol. 68, pp. 1-32, 1986.

[62] Z. Li, D. Zhang, and K. Wu, "Cement-Based 0-3 Piezoelectric Composites," *Journal of the American Ceramic Society,* vol. 85, pp. 305-313, 2002.

[63] B. Jadidian, *Design and fabrication of a flexible large area fabric transducer for bone healing application,* 1998.

[64] L. F. Brown, "Ferroelectric polymers: current and future ultrasound applications," in *Ultrasonics Symposium, 1992. Proceedings., IEEE 1992*, 1992, pp. 539-550.

[65] X.-D. Chen, D.-B. Yang, Y.-D. Jiang, Z.-M. Wu, D. Li, F.-J. Gou, *et al.*, "0–3 Piezoelectric composite film with high d 33 coefficient," *Sensors and Actuators A: Physical,* vol. 65, pp. 194-196, 1998.

[66] H. Banno and S. Saito, "Piezoelectric and dielectric properties of composites of synthetic rubber and PbTiO3 or PZT," *Japanese Journal of Applied Physics,* vol. 22, p. 67, 1983.

[67] J. Giniewicz, K. Duscha, R. Newnham, and A. Safari, "(Pb 1-x, Bi x)(Ti 1-x (Fe 1-y Mn y) x) O 3-Polymer 0-3 Composites for Hydrophone Applications," in *Applications of Ferroelectrics. 1986 Sixth IEEE International Symposium on*, 1986, pp. 323-327.

[68] Y. Lee, M. Ham, A. Safari, and R. Newnham, "Preparation of PbTiO 3 Powder for a Flexible 0-3 Piezoelectric Composite," in *Applications of Ferroelectrics. 1986 Sixth IEEE International Symposium on*, 1986, pp. 318-322.

[69] X. Cai, C. Zhong, S. Zhang, and H. Wang, "A surface treating method for ceramic particles to improve the compatibility with PVDF polymer in 0-3 piezoelectric composites," *Journal of materials science letters,* vol. 16, pp. 253-254, 1997.

[70] N. Sahu, B. Parija, and S. Panigrahi, "Fundamental understanding and modeling of spin coating process: A review," *Indian Journal of Physics,* vol. 83, pp. 493-502, 2009.

[71] D. Meyerhofer, "Characteristics of resist films produced by spinning," *Journal of Applied Physics,* vol. 49, pp. 3993-3997, 1978.

[72] R. Yonkoski and D. Soane, "Model for spin coating in microelectronic applications," *Journal of applied physics,* vol. 72, pp. 725-740, 1992.

[73] C. Lawrence, "The mechanics of spin coating of polymer films," *Physics of Fluids (1958-1988),* vol. 31, pp. 2786-2795, 1988.

[74] L. E. Scriven, "Physics and Applications of DIP Coating and Spin Coating," *MRS Online Proceedings Library Archive,* vol. 121, pp. null-null, 1988.

[75] K. Arlt and M. Wegener, "Piezoelectric PZT/PVDF-copolymer 0-3 composites: aspects on film preparation and electrical poling," *Dielectrics and Electrical Insulation, IEEE Transactions on,* vol. 17, pp. 1178-1184, 2010.

[76] A. Hajati, D. Latev, D. Gardner, M. Ottosson, D. Imai, M. Torrey, *et al.*, "Monolithic ultrasonic integrated circuits based on micromachined semi-ellipsoidal piezoelectric domes," *Applied Physics Letters,* vol. 103, p. 202906, 2013.

[77] M. Dietze, J. Krause, C.-H. Solterbeck, and M. Es-Souni, "Thick film polymer-ceramic composites for pyroelectric applications," *Journal of Applied Physics,* vol. 101, p. 054113, 2007.

[78] M. Dietze and M. Es-Souni, "Structural and functional properties of screen-printed PZT–PVDF-TrFE composites," *Sensors and Actuators A: Physical,* vol. 143, pp. 329-334, 2008.

[79] D. A. van den Ende, W. A. Groen, and S. van der Zwaag, "The effect of calcining temperature on the properties of 0-3 piezoelectric composites of PZT and a liquid crystalline thermosetting polymer," *Journal of electroceramics,* vol. 27, pp. 13-19, 2011.

[80] M. Es-Souni, M. Kuhnke, A. Piorra, and C.-H. Solterbeck, "Pyroelectric and piezoelectric properties of thick PZT films produced by a new sol–gel route," *Journal of the European Ceramic Society,* vol. 25, pp. 2499-2503, 2005.

[81] J. Pérez, N. Vyshatko, P. Vilarinho, and A. Kholkin, "Electrical properties of lead zirconate titanate thick films prepared by hybrid sol–gel method with multiple infiltration steps," *Materials chemistry and physics,* vol. 101, pp. 280-284, 2007.

[82] M. Wegener and K. Arlt, "PZT/P (VDF-HFP) 0? 3 composites as solvent-cast thin films: preparation, structure and piezoelectric properties," *Journal of Physics D: Applied Physics,* vol. 41, p. 165409, 2008.

[83] Y. Or, C. Wong, B. Ploss, and F. G. Shin, "Modeling of poling, piezoelectric, and pyroelectric properties of ferroelectric 0–3 composites," *Journal of applied physics,* vol. 94, pp. 3319-3325, 2003.

[84] C. Cheng and S. Tu, "Fabrication of a novel piezoelectric actuator with high load-bearing capability," *Sensors and Actuators A: Physical,* vol. 141, pp. 160-165, 2008.

[85] S. Lang and G. Li, "Rainbow ceramics: Processing techniques; Piezoelectric, dielectric and pyroelectric properties; and polarization distributions as determined with SLIMM," *JOURNAL OF THE KOREAN PHYSICAL SOCIETY,* vol. 32, pp. S1268-S1270, 1998.

[86] P. Ngernchuklin, E. Akdogan, A. Safari, and B. Jadidian, "Electromechanical displacement of piezoelectric-electrostrictive monolithic bilayer composites," *Journal of Applied Physics,* vol. 105, p. 4102, 2009.

[87] S. Xing, "Preparation and structure of rainbow piezoelectric ceramics," *Journal of Wuhan University of Technology-Mater. Sci. Ed.,* vol. 18, pp. 24-26, 2003.

[88] R. Bryant, K. Mossi, J. Robbins, and B. Bathel, "The correlation of electrical properties of prestressed unimorphs as a function of mechanical strain and displacement," *Integrated Ferroelectrics,* vol. 71, pp. 267-287, 2005.

[89] N. S. Goo, A. Haris, H. C. Park, and K. J. Yoon, "Validation of a laminated beam model of LIPCA piezoelectric actuators," *Journal of intelligent material systems and structures,* vol. 16, pp. 189-195, 2005.

[90] N. S. Goo, C. Kim, Y.-D. Kwon, and K. J. Yoon, "Behaviors and performance evaluation of a lightweight piezo-composite curved actuator," *Journal of intelligent material systems and structures,* vol. 12, pp. 639-646, 2001.

[91] A. Haris, N. S. Goo, H. C. Park, and K. J. Yoon, "Modeling and analysis for the development of Lightweight Piezoceramic Composite Actuators (LIPCA)," *Computational materials science,* vol. 30, pp. 474-481, 2004.

[92] C.-W. Kim and K.-J. Yoon, "Fatigue behavior degradation due to the interlaminar conditions in Lightweight Piezoelectric Composite Actuator (LIPCA)," *International Journal of Modern Physics B,* vol. 20, pp. 4365-4370, 2006.

[93] C. Li, P.-M. Wu, S. Lee, A. Gorton, M. J. Schulz, and C. H. Ahn, "Flexible dome and bump shape piezoelectric tactile sensors using PVDF-TrFE copolymer," *Microelectromechanical Systems, Journal of,* vol. 17, pp. 334-341, 2008.

[94] L. R. Pinto, J. Petrovic, P. Matavulj, D. K. Chambers, D. Qi, and S. Zivanovic Selmic, "Experimental and Theoretical Investigation of Photosensitive ITO/PEDOT: PSS/MEH-PPV/Al Detector," in *MRS Proceedings*, 2009, pp. 1190-NN11-01.

[95] L. APC International, "PHYSICAL AND PIEZOELECTRIC PROPERTIES OF APC MATERIALS."

[96] F. G. Garcia, B. G. Soares, V. J. Pita, R. Sánchez, and J. Rieumont, "Mechanical properties of epoxy networks based on DGEBA and aliphatic amines," *Journal of Applied Polymer Science,* vol. 106, pp. 2047-2055, 2007.

[97] F. Takeo, F. Koji, and F. Eiichi, "Electromechanical Properties in the Composites of Epoxy Resin and PZT Ceramics," *Japanese Journal of Applied Physics,* vol. 15, p. 2119, 1976.

[98] A. Seema, K. Dayas, and J. M. Varghese, "PVDF-PZT-5H composites prepared by hot press and tape casting techniques," *Journal of Applied Polymer Science,* vol. 106, pp. 146-151, 2007.

[99] B. Satish, K. Sridevi, and M. Vijaya, "Study of piezoelectric and dielectric properties of ferroelectric PZT-polymer composites prepared by hot-press technique," *Journal of Physics D: Applied Physics,* vol. 35, p. 2048, 2002.

[100] T. Furukawa, K. Ishida, and E. Fukada, "Piezoelectric properties in the composite systems of polymers and PZT ceramics," *Journal of Applied Physics,* vol. 50, pp. 4904-4912, 1979.